Weather influence on aviation NO_x climate impacts via ozone and methane

MSc Thesis

S.H. Rosanka

Faculty of Aerospace Engineering
Department of Control and Operations
Section: Aircraft Noise and Climate Effects

TU Delft

Weather influence on aviation NO_x climate impacts via ozone and methane

MSc Thesis

by

S.H. Rosanka

to obtain the degree of Master of Science
at the Delft University of Technology,
to be defended publicly on Tuesday August 1, 2017 at 10 a.m.

Student number:	4210107	
Project duration:	January 9, 2017 – August 1, 2017	
Thesis committee:	Prof. Dr. V. Grewe,	TU Delft (C&O - ANCE), DLR, supervisor
	Dr. A. Gangoli Rao,	TU Delft (FPP - PP)
	Dr. F. Yin,	TU Delft (C&O - ANCE)

An electronic version of this thesis is available at http://repository.tudelft.nl/.
Colours for plots by C. A. Brewer (http://colorbrewer2.org/).

TU Delft

Preface

This thesis is the final part to obtain my master's degree in Aerospace Engineering at the Delft University of Technology. My master track was Control and Operations with a main focus on Aircraft Noise and Climate Effects (ANCE). During this master I performed a three month internship at the German Aerospace Centre (DLR). Within this internship I focused on multiple aspects of the climate impact of aviation, by analysing data related to the REACT4C project. This increased my interest in the climate impact of NO_x emissions which lead to this thesis.

At this point I would like to thank Prof. dr. Volker Grewe for his intensive supervision and support throughout this thesis. If we would not have met, my career perspective would have been different. I would like to thank the German Climate Computing Centre (DKRZ) for hosting all REACT4C data, and providing me with the necessary server structure and support for this thesis. Further, I would like to thank Dr. Christine Frömming for providing in depth information on the different chemical reactions used by REACT4C. Thanks to Jesper for many effective and helpful discussions on the subject material and practical matters. Thanks to my girlfriend, friends, parents, brother, sisters and anyone else who supported me during this project.

S.H. Rosanka
Delft, July 2017

Abstract

Aviation activities contribute substantially to the anthropogenic climate impact. Due to an increasing demand on aviation transport, multiple mitigation strategies have been established to reduce the contribution to climate change by aviation. One promising strategy is to re-route aircraft, such that climate sensitive atmospheric areas are avoided. This mitigation strategy, depends on the scientific understanding of all processes involved. The European project REACT4C assessed the feasibility of such a mitigation technique by simulating the climate impact of NO_x, as well as other emissions and contrail formation for eight distinct weather pattern. For each weather pattern, unit emissions of NO_x are emitted in the North Atlantic flight sector. Each air parcel, containing the emitted NO_x, is tracked within the atmosphere. This unique model set-up allows to analyse concentration changes of O_3 and CH_4 along each trajectory. In general, due to the emitted NO_x, O_3 is produced and CH_4 is lost. Most recent results showed that by just increasing the operation cost by 1%, the climate impact can be reduced by about 10% (Grewe et al., 2017). By comparing climate cost functions (CCF), a metric of the climate impact per unit emission, to weather charts, a link between high pressure ridges and the total climate impact of NO_x is observed. Therefore, this research focuses on identifying weather influences on the temporal development of O_3 and CH_4 due to aviation attributed NO_x emission.

In this thesis, the NO_x chemistry, atmospheric transport processes and the model set-up of the REACT4C project is reviewed. The temporal development analysis of O_3 is split-up into two parts, the O_3 build-up and the O_3 depletion. First, all data from the climate model are re-gridded and chemical production and loss rates are isolated from all other loss terms (i.e. diffusion). Certain characteristics of the temporal concentration changes of O_3 are identified. A systematic analysis of the background chemical compounds and all important chemical reactions involved, provide insides to identify seasonal and emission altitude differences. With the help from literature and multiple statistical means, weather influences on those production and loss terms and thus the temporal development of O_3 and CH_4, are identified. In a final step, inter-seasonal variations are analysed.

In general, the chemical processes during the O_3 build-up are dominated by the emitted NO_x, whereas the chemical processes during the depletion of O_3 are dominated by the high O_3 concentration. Seasonal differences of the maximum O_3 concentration and the total CH_4 loss are caused by lower background concentrations of all chemicals involved during winter, which lead to lower production and loss rates of O_3 and CH_4. At the same time altitude differences in the production and loss of O_3 and CH_4 are caused by altitude variations in all chemicals involved.

The vertical transport within the atmosphere defines the time when the O_3 maximum is reached. If an air parcel containing the emitted NO_x, is transported fast to a lower altitude, the O_3 maximum occurs sooner. If however the same air parcel would stay for a longer time at a high altitude, a late O_3 maximum occurs. It could be identified that this downward motion is caused by the subsidence within a high pressure system. Air parcel with an earlier O_3 maxima, experience high subsidence, which leads to a higher chemical activity based on higher temperatures. During summer a high O_3 maximum can only be reached, if the background concentration of NO_x is low during the O_3 build-up. If the background NO_x concentration is high, only very low O_3 maxima occur. During winter the maximum O_3 concentration is limited by the background concentration of HO_2. Only high HO_2 background concentrations lead to high O_3 maxima. The temporal development of CH_4 is mainly influenced by the maximum O_3 concentration as well as specific humidity. High O_3 and H_2O concentrations lead to high OH productions, which lead to a high CH_4 losses. A high CH_4 loss only occurs, if the maximum O_3 concentrations and the specific humidity are high.

This study shows that the weather situation each air parcel, containing NO_x emissions, experiences has a direct influence on the resulting concentration changes of O_3 and CH_4. Therefore, weather has a direct impact on the climate impact of NO_x, since the concentration change of O_3 and CH_4 directly influences the resulting climate impact. The understanding of processes related to the climate impact of aviation attributed NO_x emission is increased. This improved understanding shows great potential to improve possibilities to forecast local climate impact resulting from aviation NO_x emissions, which is necessary for future re-routing mitigation strategies.

Contents

List of Figures

List of Tables

List of Abbreviations

Abbreviations

AEM	Advanced Emission Model
AIC	Aviation Induced Cloudiness
ANOVA	Analysis of Variance
AO	Arctic Oscillation
ATM	Air Traffic Management
ATM4E	Air Traffic Management for Environment
ATTILA	Atmospheric Tracer Transport In a LAgrangian model
COSMO	Consortium of Small-scale MOdels
DKRZ	German Climate Computing Centre
DLR	German Aerospace Centre
ECF	Environmental Change Functions
EMAC	ECHAM/MESSy Atmospheric Chemistry
HPR	High Pressure Ridge
HSD	Honest Significant Difference
IPCC	Intergovernmental Panel on Climate Change
IQR	Interquartile Range
IRF	Integrated Radiative Forcing
ITCZ	Intertropical Convergence Zone
KDE	Kernel Density Estimate
LOSU	Level of Scientific Understanding
MECCA	Module Efficiently Calculating the Chemistry of the Atmosphere
MESSy	Modular Earth Submodel System
NAO	North Atlantic Oscillation
PBL	Planetary Boundary Layer
PMO	Primary-Mode Ozone
RF	Radiative Forcing
SAAM	System for traffic Assigment and Analysis at a Macroscopic level
SP	Summer Pattern
SWV	Stratospheric Water Vapour

TKE	Turbulent Kinetic Energy
TREXP	Tracer Release EXperiments from Point sources
WeCare	Utilizing Weather information for Climate efficient and eco efficient future aviation
WP	Winter Pattern

Chemical Species

CH_2O	Formaldehyde
CH_3O_2	Methyldioxidanyl
CH_3O	Methhoxide
CH_3	Methyl Radical
CH_4	Methane
CO_2	Carbon Dioxide
CO	Carbon Monoxide
H_2O	Water, Water Vapour
H_2SO_4	Sulphuric Acid
HNO_3	Nitric Acid
HNO_4	Peroxynitric Acid
HO_2	Hydroperoxyl Radical
H	Hydrogen
M	M represents a gaseous third body
NO_2	Nitrogen Dioxide
NO_x	Nitrogen Oxides ($NO+NO_2$)
NO	Nitrogen Oxide
$O(^1D)$	Excited Oxygen Atom
$O(^3P)$	Excited Oxygen Atom
O_2	Molecular Oxygen
O_3	Ozone
OH	Hydroxyl Radical
$R^{'}CHO$	Aldehyde (where R is any organic group)
RH	Alkanes (where R is any organic group)
RO_2	Organic Peroxy Radicals (where R is any organic group)
ROOH	Carboxylic acid (where R is any organic group)
SO_2	Sulphur dioxide

1 Introduction

1.1. Thesis Background

In the past, present and future anthropogenic climate change is and will be a controversial topic, even though the overall scientific consensus is well established (Cook et al., 2013). It was estimated that aviation contributed about 3.5% to the total anthropogenic radiative forcing (RF) until 2005 relative to the pre-industrial time. This estimate increases to 4.9% if the relative uncertain impact of contrail induced cirrus are taken into account (Lee et al., 2009). Since aviation, as a mean of transportation, becomes more and more important, the contribution of aviation is expected to increase (Grewe et al., 2014a; Lee et al., 2009).

It becomes evident that reducing the climate impact of aviation is necessary to reduce the overall anthropogenic climate impact. Multiple different mitigation strategies have been developed to tackle this problem. Those include biofuels, taxes, advancements in engine technology and re-routing aircraft (Lee et al., 2010). The later one shows high potential. The climate impact of short-lived species like water vapour, NO_x and especially contrail formation is highly location dependent. If aircraft are re-routed such that they avoid those climate sensitive areas, the reduction of the climate impact for those species is higher than the additional climate impact caused by long-lived species due to more fuel burned (Matthes et al., 2012).

The European project, Reducing Emissions from Aviation by Changing Trajectories For the benefit of Climate (REACT4C) was set-up to investigate the feasibility of such an Air Traffic Management (ATM) measure. It combined a climate model, an emission model and an ATM model to assess the overall climate impact (Grewe et al., 2014a). The overall climate impact during summer and winter was calculated by simulating eight distinct weather situations which differ in the location and strength of the jet stream (Irvine et al., 2013). Based on atmospheric changes of chemical species, so called climate cost functions (CCF), a metric of the climate impact per unit emission, were obtained for carbon dioxide, water vapour and NO_x emissions. Additionally, CCFs are calculated for possible contrail formation (Grewe et al., 2014a).

For one winter pattern Grewe et al. (2014b) demonstrated that the overall climate impact for this weather pattern could be reduced by up to 25% by just increasing the operation costs by 0.5%. A more recent study showed that by combining the results of all weather pattern, a reduction of the climate impact by 10% is feasible if the operation costs are increased by 1% (Grewe et al., 2017). This difference shows that the weather situation itself seems to impact the resulting climate impact.

The overall REACT4C project was very computation intensive, since for each of the eight weather pattern 90 days needed to be simulated[1]. To use such a re-routing measure on a daily basis, the computation demand is too high. Understanding the processes involved and how they are influenced by atmospheric processes (i.e. weather), will provide crucial insides to reduce the computation time needed.

[1] http://delta.tudelft.nl/article/reduce-climate-impact-by-flying-more/30948

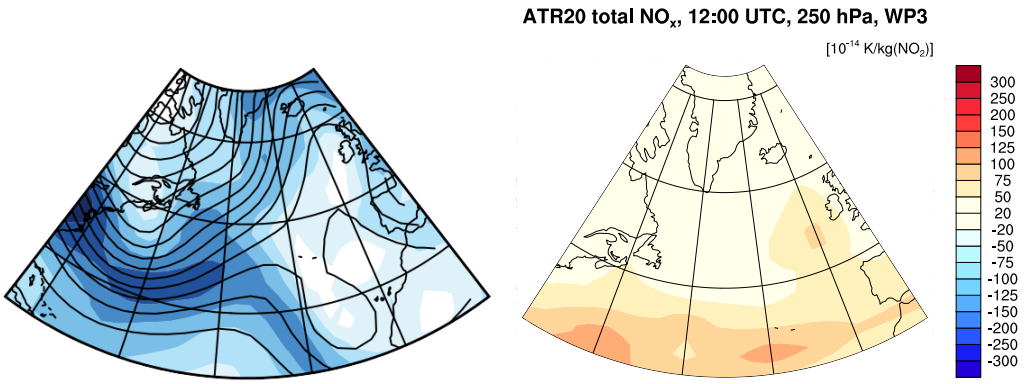

(a) Geopotential heigt & wind velocity (b) Climate Cost Function (CCF) of NO_x

Figure 1.1: Left: Geopotential height (black contours) and wind velocities (light to dark blue, starting at $10\,ms^{-1}$ with a 10 ms^{-1} interval) at 250 hPa. Right: Climate Cost Functions (CCF) for total NO_x (O_3 + CH_4 + PMO) at 250 hPa. Both valid for the third winter pattern as defined by Irvine et al. (2013). (Figures obtained from personal communication with Volker Grewe, 15th September 2016)

1.2. Research Objective

NO_x itself is considered to be transparent to longwave and shortwave radiation. However, NO_x influences the O_3 and CH_4 concentrations. Figure 1.1 shows the weather situation at the time of emission and the total CCF values for the third winter pattern. By closely examining the geopotential height (Figure 1.1a) it can be observed that their is a high pressure ridge (HPR) west of the British Isles and Spain. At the same time the CCF values of NO_x (Figure 1.1b) roughly coincide with the location of the HPR. This suggests that the climate impact is influenced by the weather situation. Since the climate impact is linked to the temporal concentration changes of O_3 and CH_4 (induced by the emitted NO_x), it is expected that those weather influences also influence the O_3 and CH_4 concentration.

Due to its model set-up, the REACT4C data set provides the unique opportunity to identify weather influences on the temporal development of O_3 and CH_4 along all 90 days of simulation. This leads to the following research objective: *"Identify relations between the local weather and the potential of aviation attributed NO_x emissions to increase the climate impact due to an enhancement in ozone and decrease the climate impact via methane depletion, by systematically comparing weather data to concentration changes of ozone and methane, along the tracer trajectories, obtained from the REACT4C project."*

For NO_x emissions, REACT4C takes the change of three chemical species into account. These are O_3, CH_4 and Primary-Mode Ozone (PMO). PMO denotes changes in O_3 resulting from changes in its precursor CH_4. In the case of PMO the results are obtained by linearly scaling the CCF results obtained for CH_4 (Grewe et al., 2014a). Therefore, PMO will not be taken into account within this thesis project. Since the other two chemical species differ significantly in their respective time scales and chemical mechanisms, both chemicals will be analysed separately.

1.3. Thesis Structure

Chapter 2 provides an introduction to the physics of climate change in general and in particular in relation to aviation . Chapter 3 and 4 provide background knowledge with respect to the atmospheric NO_x chemistry and the most important transport processes in the atmosphere. More in depth details on the REACT4C project are provided in Chapter 5. The methodology applied in this thesis is discussed in Chapter 6. Due to the methodology used, the result section is split-up into two separate chapters. First, the variability of the REACT4C data is assessed, with the main focus on the different production and loss terms (Chapter 7). Those insides are than used to identify weather influences on the temporal development of O_3 and CH_4 (Chapter 8). Each result chapter includes extensive discussions on the identified influences. Chapter 9 therefore only covers discussions related to the REACT4C project, the thesis design itself, future application possibilities as well as the results on a higher level. In a final step conclusions and recommendations for future studies are presented in Chapter 10.

2

Climate Physics and the Effects of Aviation

This chapter introduces the processes related to the climate impact of aviation. To achieve this the physics of climate change is reviewed. Afterwards, the aviation attributed climate effect is shortly discussed for each individual greenhouse gas and other aviation induced climate effects.

2.1. The Physics of Climate Change

Understanding the physics of climate change prior to the analysis performed in this study provides the basis to better understand the research question and objective. Climate change is based on Radiative Forcing (RF), which leads to a change in the near surface atmospheric temperature. Both concepts are shortly discussed.

2.1.1. Radiative Forcing

Radiation is one of the key physical concepts of heat transfer. The Earth's climate and temperature is defined by the radiation balance of the Earth and atmosphere. The Earth itself emits long wave radiation due to its low temperature and absorbs incoming short wave radiation from the sun. This results in a radiation equilibrium at the top of the atmosphere.

The Earth atmosphere contains certain gases and aerosols which may absorb, scatter and re-emit short and long wave radiation. Based on those effects the near surface atmospheric temperature is higher compared to the pure balance of incoming and emitted radiation. This concept is known as the greenhouse effect (Shine et al., 1990). If a greenhouse gas concentration changes (i.e. increases), more radiation is absorbed and remitted. This causes a radiation imbalance at the top of the atmosphere, which is known as radiative forcing (RF) (Hansen et al., 1997). The resulting RF depends on the radiation characteristics of the greenhouse gas and the atmospheric lifetime of the emission. This implies that a doubling of a specific greenhouse gas concentration, does not necessary lead to a doubling of the greenhouse effect.

2.1.2. Temperature Change

The radiative imbalance caused by a concentration change of a greenhouse gas will force the Earth system to adjust its outgoing radiation, to restore an equilibrium between incoming and outgoing radiation. Based on the Stefan–Boltzmann law, the emitted radiation is controlled by the temperature of the Earth. The temperature of the Earth will adapt to reach a new radiative equilibrium. A first approximation of the near surface atmospheric temperature change is calculated based on the induced RF (Equation 2.1). Here, λ indicates the climate sensitivity factor, which depends on the greenhouse gas, RF gives the radiative forcing and ΔT_s gives the change of the equilibrium near surface atmospheric temperature.

$$\Delta T_s \approx \lambda \cdot RF \tag{2.1}$$

2.2. Aviation Attributed Climate Effect

Air traffic emits carbon dioxide, nitrogen oxides, water vapour, carbon monoxide, unburned hydrocarbons and soot. These emissions lead to changes in greenhouse gas concentrations, such as carbon dioxide (CO_2), ozone (O_3), methane (CH_4) and water vapour (H_2O). Additionally, the formation of contrail-cirrus further influences the climate impact due to aviation (Lee et al., 2010). Climate impact due to aviation can be divided into CO_2 and non-CO_2 effects. The non-CO_2 effects are caused by all other emissions (NO_x, H_2O, Soot, SO_2 and HC), which additionally lead to changes in the atmospheric concentration of O_3, CH_4, aerosols and can induce cloudiness. The resulting climate impact for each of the components is shortly discussed in the following sections. Compared to CO_2 the lifetime of the various non-CO_2 species involved is rather short. Therefore, these species are globally less well mixed. This implies that the resulting climate impacts of those species depend on the time and location of the emission. The overview presented is mainly based on Lee et al. (2009) and Lee et al. (2010) since both give a good overview for all influencing factors. In some cases the results of more recent studies are included.

2.2.1. Carbon Dioxide Effects

CO_2 is a globally well mixed gas in the atmosphere associated with a very long lifetime. Therefore, CO_2 is mainly associated with long term climate impacts. The many involved natural CO_2 sinks introduce uncertainties while specifying the lifetime of CO_2. Archer (2005) suggests a mean lifetime in the order

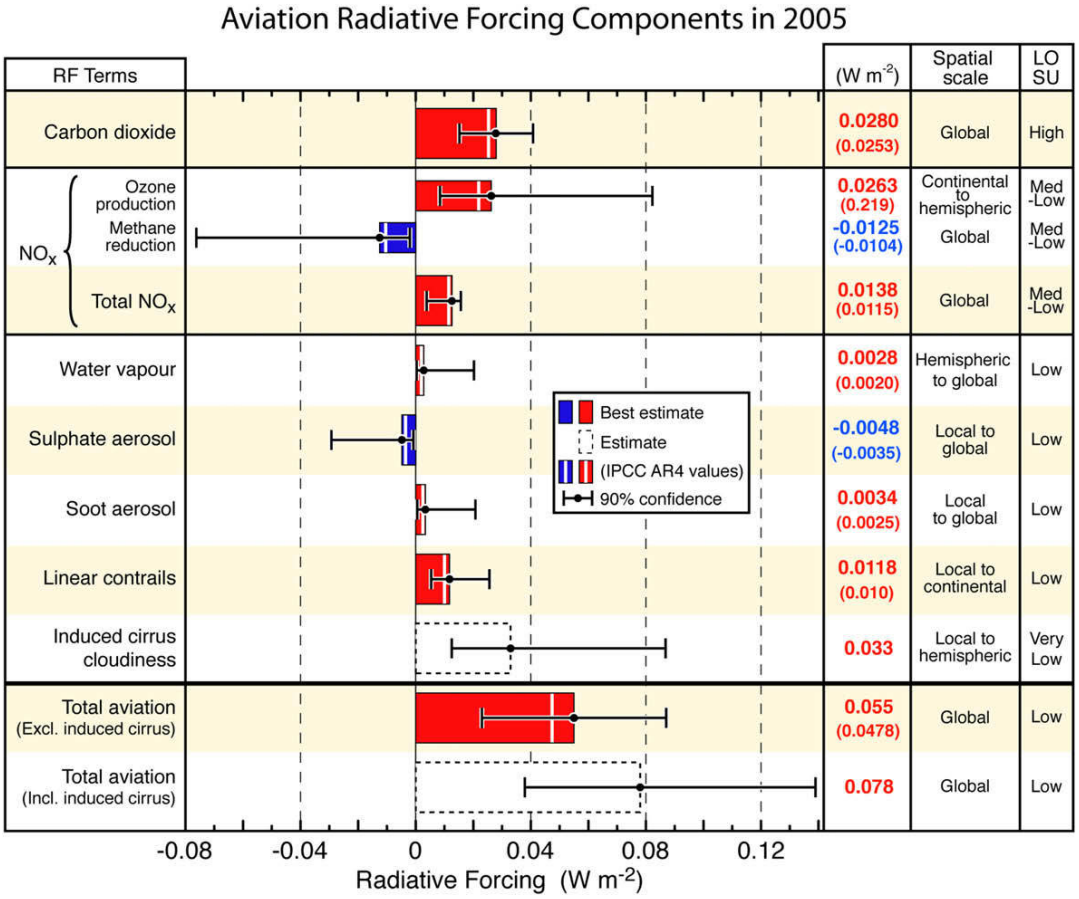

Figure 2.1: Radiative forcing (RF) components from global aviation as evaluated from preindustrial times until 2005 as reported by Lee et al. (2009). Bars represent best estimates or an estimate in the case of aviation induced cloudiness (AIC). IPCC values are indicated as reported by Forster et al. (2007). Numerical values are given for both IPCC (in parentheses) and updated values. The 90% likelihood range for each estimate, is indicated by the error bars. For each component the geographic spatial scale of the radiative forcing and the LOSU is indicated. (Figure obtained from Lee et al. (2009))

Table 2.1: Mean emission indices (mass of emissions per unit mass of burned fuel) for the fleet of aircraft in 2000. Ranges are indicates since the emission index of certain species depend on engine settings. In the case of NO_x, the emission index of NO_2 is given. (Table obtained from Lee et al. (2010))

Species	CO_2	H_2O	NO_x	Soot	SO_2	CO	HC
Emission index, [g/kg] (range)	3160	1240	14 g/kg(NO_2) (12-17)	0.025 (0.01-0.05)	0.8 (0.6-1.0)	3 (2-3)	0.4 (0.1-0.6)

of ten thousand years.

The mean emission index of CO_2 is well known. Table 2.1 gives the emission indices of all aviation related emissions based on the fleet of 2000 (Lee et al., 2010). The emission index indicates the amount of a substance emitted per kilogram fuel burned. For CO_2 the emission index is 3160 g/kg, which is the highest emission index given by Table 2.1. CO_2 mainly absorbs thermal radiation at around 15 µm. This has only a small impact on the incoming solar radiation. It absorbs longwave terrestrial radiation, which induces a warming of the atmosphere. Aviation attributed CO_2 emissions until the year 2005 induced a radiative forcing (RF) of 28 mWm^{-2} in 2005 (Figure 2.1). The current level of scientific understanding (LOSU) is highest for all known aviation induced climate effects. The LOSU indicates, how well the physical and chemical relations are understood and how the modelling spread and its uncertainties are.

2.2.2. Nitrogen Oxides Emissions

The mean emission index of nitrogen oxides is about 14 g/kg(NO_2) (Table 2.1) which is smaller compared to CO_2. The concentration of NO_x during combustion depends on the engine settings, i.e. the combustion temperature. Therefore, the emission index for NO_x differs for different flight phases (taxi, take off, cruise, approach, landing). This variation is indicated by the range given in Table 2.1. In the upper troposphere the emission of NO_x causes an increase in O_3 and a depletion of CH_4. The increase of O_3 induced a RF of about 26.3 mWm^{-2} until 2005, accompanied by an induced RF of about $-12.5\,mWm^{-2}$ by depleted CH_4 (Figure 2.1). As it is indicated in Figure 2.1, the LOSU is rather low but still higher than it is for other non-CO_2 emissions. If both atmospheric composition changes are taken into account, a total positive induced RF of about 13.8 mWm^{-2}, for all aviation attributed NO_x emissions until 2005 is obtained (Lee et al., 2009). More recent studies by Holmes et al. (2011) and Søvde et al. (2014) agree on the induced RF by the additional formed O_3. However, Søvde et al. (2014) found lower induced RF values for depleted CH_4.

A more detailed description and discussion of the different processes involved in the O_3 increase and the CH_4 depletion is provided in Chapter 4.

2.2.3. Water Vapour Emissions

The mean emission index for water vapour is 1240 g/kg (Table 2.1). Compared to NOx emissions, the emitted H_2O is independent of engine settings. Therefore, no range is indicated in Table 2.1.

In general, natural H_2O is considered to be the strongest greenhouse gas in the atmosphere. H_2O absorbs short wave and long wave radiation. Compared to NO_x, H_2O has a rather high emission index but the induced RF due to emitted H_2O until 2005 is only about 2.8 mWm^{-2} (Lee et al., 2009). Wilcox et al. (2012) even suggest a value below 1.0 mWm^{-2}. This rather low RF is based on the fact that the amount of background H_2O, present in the atmosphere, is very high. Compared to this high background concentration, aviation emits rather low concentrations of H_2O, leading to a low RF (Lee et al., 2010). The LOSU compared to all other species treated before is the lowest (Figure 2.1).

2.2.4. Aerosol Particle Emissions

All emissions treated so far are gaseous emissions. Additionally, aircraft emit solid aerosols (soot), organic compounds and sulphuric acid (H_2SO_4). These emissions cause direct RF. Soot aerosols absorb solar radiation and thus cause a positive RF, whereas sulphate aerosols backscatter solar radiation, causing a negative RF. The RF until 2005 due to aviation emissions of soot and sulphate aerosols is 3.4 mWm^{-2} and $-4.8\,mWm^{-2}$, respectively. Those RF's are almost one order of magnitude smaller compared to RF caused by other emission types. This can be linked to the very low emission indices

of soot and sulphate aerosols (Table 2.1). The LOSU of aerosols is low (Figure 2.1) (Lee et al., 2009).

In addition to this direct RF, emitted aerosols can act as a cloud condensation nuclei. This could cause additional formation of clouds which can further influence the climate impact. Further, those nuclei can influence the size and the amount of cloud particles in a given cloud. If more cloud particles are present, cloud particles tend to have a smaller size, since the same amount of water is distributed over more nuclei. The resulting change in the micro-physics of the cloud can extend the lifetime of a given cloud. Additionally, the chance of precipitation is reduced or precipitation events are delayed. Due to the fact that more cloud particles are present, the change of additional scattering increases, resulting in a higher cloud albedo. Reliable estimates of those effects are missing and the lifetime changes of clouds are generally not taken into account in current climate assessments (Lohmann and Feichter, 2005).

2.2.5. Contrails

Contrails are line shaped ice clouds which can form due to aviation activities. They are formed if the moist and hot exhaust of the engine is mixed with the cold and dry ambient air. Contrail formation, depends on the ambient conditions like ambient humidity, temperature and pressure. Further, it depends on exhaust conditions and engine properties like exhaust temperature, pressure, humidity, the water vapour emission index (dependent on the fuel used), as well as the overall propulsion efficiency. These are aircraft specific and therefore some aircraft are more prone to form contrails (Schumann, 1996). The relation if contrails are formed is known as the Schmidt-Appleman criteria, described by Schmidt (1941) and Appleman (1953). The lifetime of contrails highly varies and significantly depends on the surrounding atmospheric conditions (Gierens et al., 2008).

Additionally, persistent linear contrails can spread and form contrail cirrus if a significant wind shear exist. The climate impact due to those contrails cirrus can be more significant than for linear contrails, since they cover a larger area. Both, linear contrails and contrail cirrus can have a warming and cooling effect. On the one hand, they reflect sunlight back into space and therefore reduce the incoming shortwave radiation (cooling effect). On the other hand, they absorb terrestrial radiation, resulting in a positive RF (warming effect) (Fichter, 2009). The level of scientific understanding is low for linear contrails and very low for contrail cirrus (Figure 2.1) (Lee et al., 2009). In the last years the LOSU has been increased, due to results found by Burkhardt and Kärcher (2011). In general, the RF resulting from contrail cirrus is higher (33.3 mWm^{-2}) than it is for linear cirrus (11.8 mWm^{-2}). If both are combined, the contribution of the induced RF is highest (positive RF), compared to the other impacts (Lee et al., 2009).

2.3. Total Climate Effect due to Aviation

By combining all discussed climate effects by aviation activities, the total climate impact is evaluated. In total a positive climate impact (global warming) was and will be caused by aviation. The induced RF since preindustrial times till 2005 is summarised to about 55 mWm^{-2} (ranges from 23 to 87 mWm^{-2}), if induced cirrus are neglected. If they are taken into account, the RF increases to 78 mWm^{-2} (ranges from 38 to 139 mWm^{-2}) (Figure 2.1, ranges from Lee et al. (2009)). Further, it can be concluded that the LOSU varies form species to species. Some effects have a high level of understanding and others have a very low one, whereas the induced cirrus cloudiness has the lowest of all. Because of the low understanding the error bar is most significant for those impacts (Lee et al., 2009).

It can be concluded, that the LOSU should be increased to better evaluate the climate impact by aviation. Focus should be on non-CO_2 effects since for those groups, the understanding is lower than it is for CO_2 effects. The results obtained in this thesis project will contribute to the LOSU for aviation attributed NO_x climate impacts.

3

Tracer Transport in the Atmosphere

Understanding the processes involved in tracer transport is key for this study. In this chapter, the physical processes, typical circulation pattern and their time scales are reviewed. Throughout this chapter a differentiation between horizontal and vertical transport in the troposphere is kept. Afterwards, transport processes in different pressure systems are discussed. In a next step, exchange processes between troposphere and stratosphere are analysed. This chapter is concluded by discussing typical time scales of vertical and horizontal transport processes.

3.1. Vertical Transport in the Troposphere

In general, vertical mixing in the troposphere causes warm, moist air to be transported to higher altitudes and cold, dry air to be transported downwards. The vertical transport processes in the troposphere are based on temperature differences, incoming solar radiation, as well as latent and sensible heat. The efficiency of absorbing incoming solar radiation is higher for the Earth surface than for the atmosphere. Emitted infrared radiation from the Earth surface, heats the atmosphere from below. It is cooled by radiative cooling at higher altitudes. The lapse rate is increased and the atmosphere destabilises. Condensation in the troposphere releases latent heat, which can cause precipitation. Therefore, condensation enhances convection. Deep convection causes short lived trace gases like NO_x to be exchanged between the upper and lower troposphere in less time than their respectively lifetime. Thunderstorms can wash out trace gases by scavenging. Additionally, cyclones and anti-cyclones cause vertical exchange in the atmosphere (Brasseur et al., 1998; Ahrens, 2012). In the upper troposphere cirrus clouds can introduce radiative cooling. In addition with latent heat, the surrounding air cools, leading to mesoscale subsidence (Brasseur et al., 1998).

3.2. Horizontal Transport in the Troposphere

In the troposphere the redistribution of heat and trace components is governed by latitudinal differences in incoming solar radiation. This leads to large scale atmospheric motion, which causes latitudinal exchange of warm air into polar regions and cold air towards the tropics. The Coriolis force introduced by the Earth rotation deflects meridional motions. Those processes drive the Hadley circulation forming three mean flow cells, in exact the Hadley cell spanning from the Equator to the sub-tropics, the Ferrel cell spanning from the sub-tropics to about $60°$ and the polar cell spanning up to the poles. An idealized wind and surface-pressure distribution on the Earth is given in Figure 3.1. In the subtropical region, weather is influenced by easterly surface winds near the equator. In the tropics, deep convection clouds form. This areas is known as the intertropical convergence zone (ITCZ). Here, moist air is transported towards the ITCZ were the northeast trades converge with the southeast trades. In mid-latitudes westerlies are formed. These are formed base on the increasing Coriolis force towards higher latitudes, leading to a higher zonal wind component. Mid-latitudes are also dominated by transient synoptic weather systems which leads to a higher variability of weather in these regions. Those systems occur more often during winter due to a reduced latitudinal temperature difference. At lower latitudes the atmospheric motions are very persistent. (Brasseur et al., 1998; Ahrens, 2012)

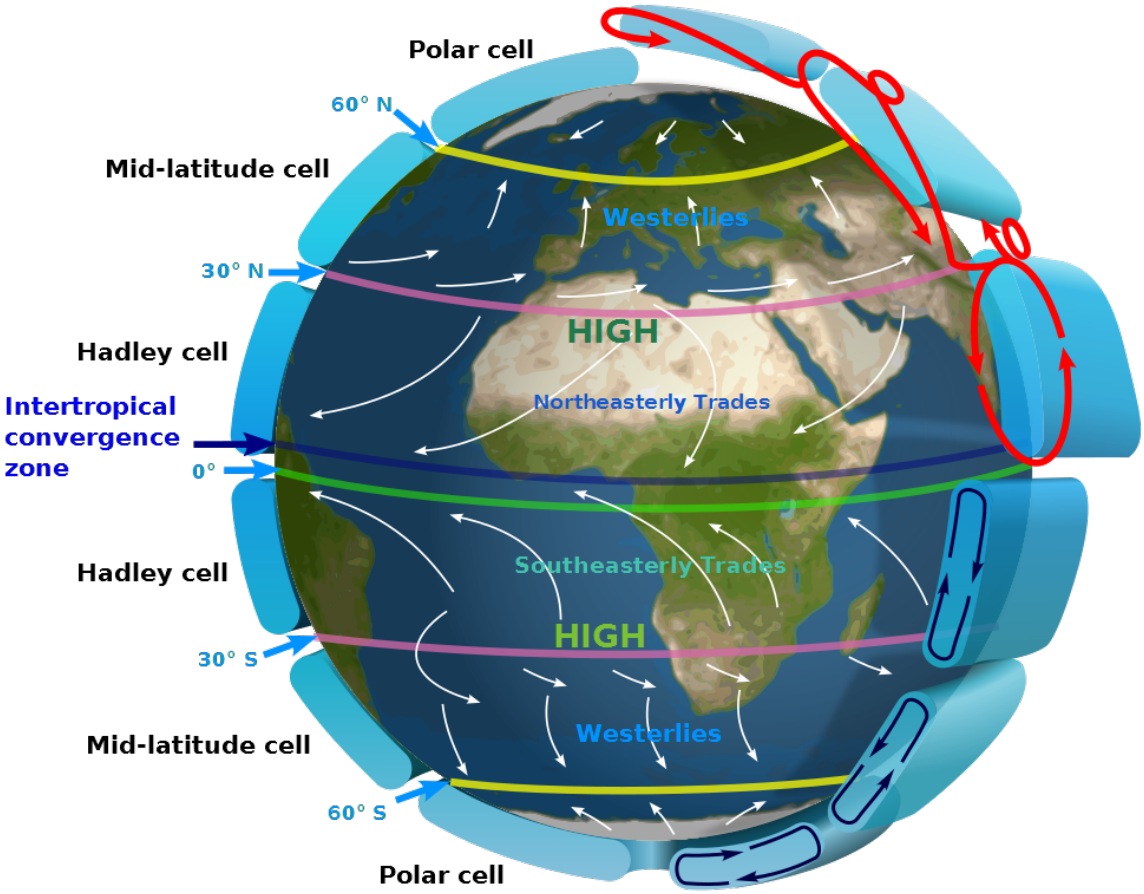

Figure 3.1: Idealized circulation pattern and wind distribution in the atmosphere. In this figure the mid-latitude cell indicates the Ferrel cell. Figure by Kaidor (Figure obtained on the 1st July 2017 from: `https://commons.wikimedia.org/wiki/User:Kaidor`).

3.2.1. Rossby Waves and Jet Streams

Cyclones and anticyclones in the upper and mid troposphere form planetary waves, also known as Rossby waves, which are dominated by eastward air motion. Warm air travels poleward and encounters cold air coming from the poles transported by polar easterlies. Both air masses do not rapidly mix and stay separated. They form the polar front associated with low pressures. Close to the tropopause wind speeds are persistent and high, which forms the jet stream. Air is warm at low latitudes and colder at higher latitudes. The horizontal temperature gradient causes a horizontal pressure gradient which results in high eastward wind velocities. Due to a lower densities at higher altitudes, a certain pressure gradient causes higher wind velocities than the same pressure gradient at lower altitudes. The direction of the jet stream is often governed by the planetary waves. Two different jet streams can be observed. The subtropical jet stream is a narrow band at $30°$, with high wind speeds up to or even exceeding $40\,\mathrm{ms}^{-1}$. The second jet stream occurs at $60°$ and is weaker, less persistent and sometimes discontinuous compared to the subtropical one. (Brasseur et al., 1998; Ahrens, 2012)

3.2.2. North Atlantic Oscillation (NAO)

Teleconnection pattern describe recurring, persistent, large-scale pressure and circulation pattern which span large geographical areas. In REACT4C the emissions are released above the North Atlantic (Grewe et al., 2014a). An important teleconnection pattern in this region is the North Atlantic Oscillation (NAO). It has two phases, a positive and a negative phase. In the positive phase the atmospheric pressure in the vicinity of the Icelandic low drops and pressure in the Bermuda-Azores increases. This

causes a high pressure gradient between both regions that strengthens the westerlies. Resulting from those strong westerlies, air masses and therefore storms will have a more northerly track into northern Europe. In the negative phase the opposite pressure behaviour occurs leading to weaker westerlies. Therefore, air masses are steered towards lower latitudes. The NAO mainly occurs during winter and varies from year to year. In the past 30 years a trend towards positive phases is observed. (Ahrens, 2012)

3.2.3. Arctic Oscillation (AO)

The Arctic Oscillation (AO) is another teleconnection pattern. It is closely related to the NAO and also effects tracer transport in the North Atlantic region. The AO is caused by changes of atmospheric pressure between the Arctic and southern regions. During its positive phase, a strong pressure difference exist, strengthening the westerlies and hinder Arctic air to be transported to lower latitudes. In addition to strong winds over the Atlantic, air masses are transported to northern parts of Europe. In the negative phase a small pressure difference exists. This leads to weak westerlies, allowing air masses to be transported from the pole, towards lower latitudes. Air masses from the Atlantic are transported to lower latitudes. (Ahrens, 2012)

3.3. Transport Processes within Pressure Systems

Transport processes in a low and high pressure system differ. The low surface pressure in a low pressure system, causes air to be transported towards the centre. This converging air is than transported upwards. At higher altitudes this rising air will diverge. In a high pressure system, air is moving away from the centre. Due to pressure gradient forces, aloft air is transported towards the surface. At higher altitudes (above the high pressure system), air converges to compensate air transported downwards (known as subsidence). If the diverging and converging air masses are in balance the surface pressure will not change, whereas an imbalance cause changes in surface pressure.

In general, clouds form due to moist air rising from the surface towards higher altitudes. Due to the subsidence in a high pressure system, clouds are uncommon. Since clouds are absence, the higher incoming solar radiation causes higher mean temperatures within the high pressure system. However, less clouds lead to less absorbed longwave radiation during night. Thus a higher temperature variation between day and night is observed. In a low pressure system air rises, which leads to the formation of clouds. Due to those calouds, low pressure system are associated with lower temperatures and less temperature variation between day and night.

3.4. Transport Between Troposphere and Stratosphere

The troposphere and the stratosphere are radiatively, chemically and and dynamically coupled. Generally, upward mass transport and therefore trace species, occurs close to the tropics. Downward mass transport between both layers occurs at the subtropics. The magnitude of the downward transport is about twice as high in the northern than in the southern hemisphere. In general, the transport between both layers is highest in late winter and spring. This is especially true for O_3 and can be related to the change in the tropopause height during winter (Brasseur et al., 1998). Based on the emission altitude and emission latitude a tracer might be emitted in the troposphere but transported into the stratosphere, which changes the chemical processes involved.

3.5. Time Scales of Vertical and Horizontal Transport

Atmospheric transport acts on different time scales. Downward transport from the upper troposphere to the surface takes on average one month (Jacob, 1999). Since NO_x has a short lifetime of about 14 days in the upper and of only a few days in the lower troposphere, the location of the emissions defines its impact on O_3 and CH_4. Transport from the stratosphere into the troposphere takes on average about one to two years. On the other hand, it takes about five to ten years for an air parcel to be transported from the troposphere to the stratosphere (Jacob, 1999). In general, this transport from the troposphere into the stratosphere occurs in the tropics and the reversed process at midlatitudes (Brasseur et al., 1998). Less important for this study but still worth to mention is the transport in the planetary boundary layer (PBL), which has a typical height of about one to two kilometre. Here, the mixing time scales are in the order of days and transport from the PBL to the middle of the troposphere takes about one

week (Jacob, 1999).

Compared to vertical transport, horizontal transport acts on synoptic scales. The wind speed in the longitudinal direction is higher than in latitudinal direction. Observation show, that to circumnavigate the whole globe, air needs only a few weeks. Since meridional wind speeds are lower, the meridional transport is slower and transport from the midlatitudes to the tropics or the poles takes on average about one to two month. Across the Equator, thermal forcing is lacking, leading to an even slower interhemispheric transport of about one year (Jacob, 1999).

It is important to notice that the mentioned values are only mean values. Compared to those values given above, a single air parcel might experience faster or slower transport processes.

4

Tropospheric Chemistry of Nitrogen Oxides

Tropospheric NO_x (NO_x = NO + NO_2) is considered to be transparent to radiation but still has a warming and a cooling effect, due to changes in O_3 and CH_4 concentrations. The aim of this research is to analyse relations between the climate impact of NO_x and the weather conditions along a trajectory. Therefore, it is key to fully understand all chemical processes involved in the O_3 and CH_4 changes. This chapter discusses those chemical reactions in detail. Here, the general chemistry of O_3 and CH_4 in the upper troposphere is based on Brasseur et al. (1998) and Seinfeld and Pandis (2016). All chemical compounds used in this chapter are listed in the List of Abbreviations. O_3, CH_4 and Hydroxyl Radical (OH) interact with each other due to additional NO_x. In a first step, those relations will be discussed, followed by discussing the lifetime of the different chemicals. Afterwards, an example of the temporal concentration change of emitted NO_x and resulting concentration changes of O_3 and CH_4 is elaborated. The chemical reaction rates involved depend on multiple factors which is discussed in a final step.

4.1. Ozone, Methane and Hydroxyl Radical Development

In the upper troposphere O_3 is mainly produced by catalytic productions including NO_x. Carbon monoxide (CO) oxidises by reacting with OH, which forms HO_2 (Reaction R1 - R2). The formed HO_2 reacts with NO leading to the formation of NO_2 and OH (Reaction R3). This NO_2 then forms $O(^3P)$ and NO by photodissociation (Reaction R4) of which the $O(^3P)$ further reacts with O_2 and a gaseous third body to form O_3. Radiation with a wavelength of 410 nm is needed for the photodissociation to take place. This wavelength is at the boarder of the visible spectrum. This reaction therefore only takes place if incoming solar radiation is present. Combining Reaction R1 - R5 results in the net reaction given by Reaction R6.

$$CO + OH \rightarrow CO_2 + H \quad \text{(R1)}$$

$$H + O_2 + M \rightarrow HO_2 + M \quad \text{(R2)}$$

$$NO + HO_2 \rightarrow NO_2 + OH \quad \text{(R3)}$$

$$NO_2 + h\nu(\lambda \leq 410\ nm) \rightarrow NO + O(^3P) \quad \text{(R4)}$$

$$O(^3P) + O_2 + M \rightarrow O_3 + M \quad \text{(R5)}$$

$$Net: \quad CO + 2O_2 + h\nu \rightarrow CO_2 + O_3 \quad \text{(R6)}$$

Additionally, O_3 is formed when CH_4 oxidises. This reaction process is described by Reaction R7 - R13, which results in the net Reaction R14. Here, CH_4 reacts with OH to form a methyl radical (CH_3) and H_2O. The methyl radical oxidises into methyldioxidanyl (CH_3O_2) forming methoxide (CH_3O) by

reacting with NO. From this HO_2 is produced. The final steps (Reaction R11 - R13) are equal to the ones presented in Reaction R3 - R5.

$$CH_4 + OH \rightarrow CH_3 + H_2O \quad \text{(R7)}$$
$$CH_3 + O_2 + M \rightarrow CH_3O_2 + M \quad \text{(R8)}$$
$$CH_3O_2 + NO \rightarrow CH_3O + NO_2 \quad \text{(R9)}$$
$$CH_3O + O_2 \rightarrow CH_2O + HO_2 \quad \text{(R10)}$$
$$NO + HO_2 \rightarrow NO_2 + OH \quad \text{(R11)}$$
$$NO_2 + h\nu(\lambda \leq 410\ nm) \rightarrow NO + O(^3P) \quad \text{(R12)}$$
$$O(^3P) + O_2 + M \rightarrow O_3 + M \quad \text{(R13)}$$

$$Net: \quad CH_4 + 4O_2 \rightarrow CH_2O + H_2O + 2O_3 \quad \text{(R14)}$$

Atmospheric O_3 is depleted if it reacts with NO_2 (Reaction R15). This reaction is dominating the depletion of O_3 within the stratosphere, where NO_2 concentrations tend to be higher than in the troposphere.

$$NO_2 + O_3 \rightarrow NO + 2O_2 \quad \text{(R15)}$$

If the concentration of OH is high enough, OH can deplete O_3 and produces HO_2 and O_2 (Reaction R16). Further, HO_2 reacts with O_3 as given in Reaction R17 to deplete O_3.

$$OH + O_3 \rightarrow HO_2 + O_2 \quad \text{(R16)}$$
$$HO_2 + O_3 \rightarrow OH + 2O_2 \quad \text{(R17)}$$

Most CH_4 is depleted by Reaction R7, which leads to a lower oxidising capacity of the upper troposphere and lower stratosphere. If more OH is present, more CH_4 will be depleted, which leads to an overall reduction of the CH_4 lifetime. Due to the depletion of CH_4 (caused by NO_x emission), less CH_4 is present, which leads to a lower O_3 production (Reaction R14). Further, concentration changes of OH and HO_x occur, which lead to a depletion of O_3 (Reaction R16 and R17). This reduction of O_3 is known as Primary-Mode Ozone (PMO) (Dahlmann, 2012). It is important to notice that this effect was not considered by Lee et al. (2009) (as discussed in Chapter 2). In addition to those changes, the oxidation of CH_4 leads to an increase of stratospheric water vapour (SWV). The oxidation of CH_4 is considered to be the main source of SWV in the stratosphere (Myhre et al., 2007).

Based on the discussion above, it becomes evident that the OH chemistry is influenced by NO_x. OH is mainly formed due to the photochemical depletion of O_3, which forms a highly reactive excited oxygen atom ($O(^1D)$). This oxygen atom then reacts with H_2O to form OH (Reaction R18 - R19). It can be noticed that the wavelength required to deplete O_3 photochemically is lower than the one needed in Reaction R4. From this it is concluded that a higher energy is needed to deplete O_3.

$$O_3 + h\nu(\lambda \leq 315\ nm) \rightarrow O(^1D) + O_2 \quad \text{(R18)}$$
$$O(^1D) + H_2O \rightarrow 2OH \quad \text{(R19)}$$

NO_x can also reduce the amount of OH. In this case, OH reacts with NO_2 and an additional gaseous third body to form nitric acid (HNO_3) (Reaction R20). Additionally, peroxynitric acid (HNO_4) is formed by Reaction R21.

$$OH + NO_2 + M \rightarrow HNO_3 + M \quad \text{(R20)}$$
$$HO_2 + NO_2 + M \rightarrow HNO_4 + M \quad \text{(R21)}$$

4.2. Lifetime of Important Chemical Species

Each chemical species has a different lifetime within the troposphere. An overview of typical lifetimes for the most important chemicals, is provided in Table 4.1. This table shows that the lifetime of different chemical species differs significantly. CH_4 has the longest lifetime (about 12 years) of all chemical species taken into account. Due to their high reactivity, OH has the shortest lifetime of a couple of seconds. OH is thus often refereed to as being the ”detergent” in the atmosphere (Isaksen and Dalsøren, 2011).

Table 4.1: Lifetime of the most important chemical compounds, influencing the tropospheric chemistry of NO_x.

Name	Formula	Lifetime	Reference
Nitrogen Oxides	NO_x = NO + NO_2	hours to weeks	(Ehhalt et al., 2001)
Ozone	O_3	days, weeks, month	(Ehhalt et al., 2001)
Methane	CH_4	about 12 year	(Ehhalt et al., 2001)
Hydroxyl Radical	OH	seconds	(Isaksen and Dalsøren, 2011)
Carbon Monoxide	CO	1-3 month	(Ehhalt et al., 2001)
Stratospheric Water	H_2O	1-6 years	(Ehhalt et al., 2001)
Hydoperoxyl Radical	HO_2	seconds	(Ehhalt et al., 2001)

4.3. The Temporal Development for Nitrogen Oxide Emissions

Based on the chemical reactions discussed above, the temporal influence of an additional aviation induced NO_x emission on the global atmospheric concentration of O_3 and CH_4 can be elaborated. Figure 4.1 shows an example of an additional NO_x emission obtained from the REACT4C project. Emission occurred at 06:00UTC on the 23rd December at 75°W, 30°N and 200 hPa (Grewe et al., 2014a). The induced NO_x is reduced almost exponentially and washed out after about a month. While the emitted NO_x mass decreases, the O_3 concentration increases due to the described O_3 production processes. When the emitted NO_x concentration is too low, no O_3 is produced and loss terms dominate the O_3 chemistry. The reduction of the additionally formed O_3 continuous and reaches zero after about

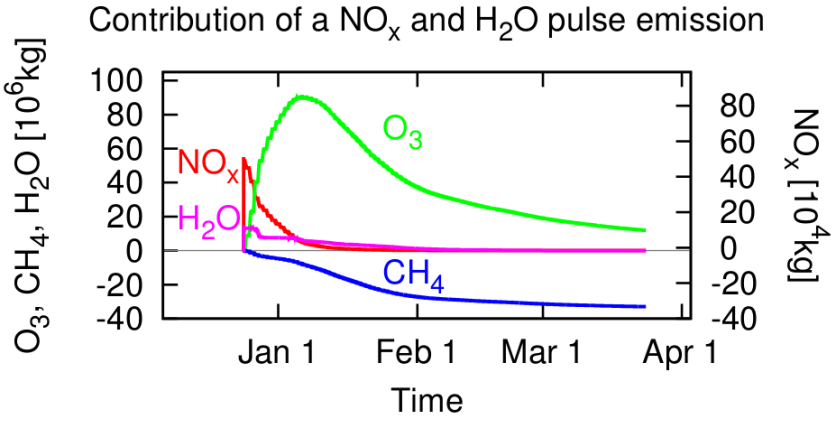

Figure 4.1: Contributions to the global atmospheric masses, due to additional NO_x and H_2O emission, at a given location (75°W, 30°N, 200 hPa, 23rd December, 06:00 UTC). Chemical compounds are indicated by colour: NO_x (red), H_2O (magenta), CH_4 (blue) and O_3 (green). (Figure obtained from Grewe et al. (2014a))

three month. At the same time the additional O_3 and NO_x increase the concentration of OH. This increase leads to a depletion of CH_4. This can be identified by a reduction of the CH_4 mass in Figure 4.1. A higher O_3 concentration leads to a higher oxidation of CH_4, after all NO_x is washed out. After a certain time, this negative CH_4 anomaly will start to decay and will reach its original values. This effect occurs after multiple years and is therefore not given in Figure 4.1, since here only the modelled three month of REACT4C are presented.

4.4. Chemical Reactions Rates

The reaction rate of a chemical reactions defines how fast a given reaction takes place. For many chemical reactions, the reaction rate is described by the power law. The power law is given by:

$$\frac{d[A]}{dt} = k \cdot [B]^n [C]^m \tag{4.1}$$

$[A]$ represents the concentrations of the product, whereas $[B]$ and $[C]$ represent the concentrations of the reactants of a given reaction. In case of Reaction R3, $[A]$, $[B]$ and $[C]$ represent the concentrations of NO_2, NO and HO_2, respectively. The exponents n and m give the partial reaction order. Those are usually obtained through experiments. The sum of both exponents $(n + m)$ is known as the overall reaction order (Kotz et al., 2008). The reaction rate coefficient is given by k. This coefficient may be influenced by multiple factors, like temperature, pressure and incoming solar radiation. Those impacts are discussed in the following sections. However, further factors exist, like the ionic strength and the surface area of an absorbent (Connors, 1990). Based on Equation 4.1, it is identified that the concentration of all species involved influences the reaction rate and therefore impacts the net production. The influence of the NO_x concentration on the production of O_3, is discussed in Section 4.4.4.

4.4.1. Temperature

Temperature has a significant impact on the reaction rate coefficient of many chemical reactions. This dependency can be based on two reasons. At a higher temperature the energy of the involved molecules increases. A higher energy state also increases the velocity of a molecule. This increases the chance of a collision between all molecules involved. Additionally, a higher energy state means that molecules will have a sufficient activation energy during a collision. The activation energy is needed to break up old and form new bonds in a reaction (Connors, 1990). The relation between the rate coefficient (k) and the temperature (T) was defined by Arrhenius (1889):

$$k = A \cdot \exp\left(\frac{-E_a}{R \cdot T}\right) \tag{4.2}$$

In this equation A represents a constant which is unique for each chemical reaction, E_a is the activation energy in joules and R is the universal gas constant (Connors, 1990). From the nature of this equation it is concluded that the reaction rate coefficient first increases exponentially but levels off at increasing temperature.

4.4.2. Pressure

The local pressure has an influence on gaseous reactions and the reaction rate coefficient may increase, if the local pressure increases. Pressure dependency of chemical reactions are rather complex and vary with each chemical. There are chemicals that highly depend on pressure and others where experiments showed that almost no pressure dependency exits. However, most reactions are only influenced if the pressure is higher than the atmospheric pressure at sea level. Thus pressure itself has most likely only little impact on the reactions discussed in Section 4.1 (Schettino et al., 2005).

4.4.3. Incoming Solar Radiation

Solar radiation is electromagnetic radiation, which is a form of energy. In general, solar radiation increases the energy of molecules. The required activation energy for some reactions can only be provided by solar radiation, below a certain wavelength, since the energy increases with decreasing wavelength. Reaction R4, R12 and R18 require solar radiation to destruct either NO_x or O_3. In this case, it means that their destruction is only possible, if solar radiation is present (i.e. during day time). This implies that those reactions do not occur during night. Therefore, a significant variation between

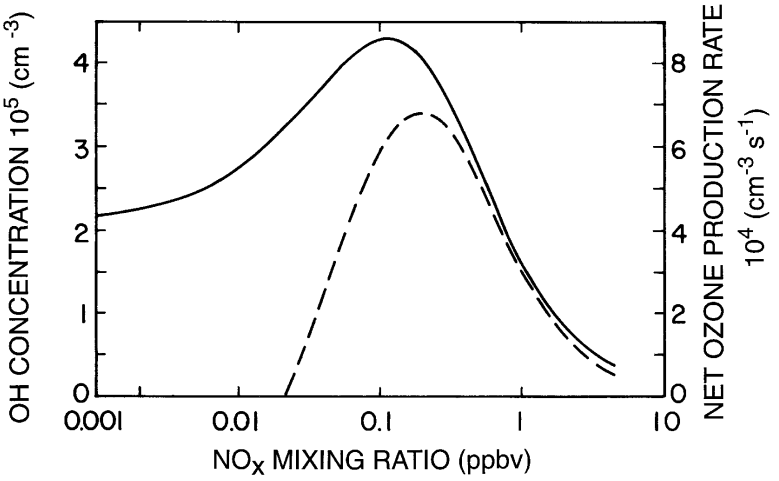

Figure 4.2: Net-O_3 production rate (dashed line) and OH concentration (solid line), as a function of the ambient NO_x concentration. Both relations are based on model results, given by Ehhalt and Rohrer (1995). Results are valid for the lower, mid-latitude troposphere during spring. (Figure obtained from Brasseur et al. (1998))

day and night is observed for those reactions. Additionally, these reaction rates will be significantly reduced during polar nights (polar night = night that last longer than 24 hours). This only occurs above the polar circle and therefore can only effect emissions which are emitted or transported into polar regions. A latitudinal dependency of the reaction rates exist, due to latitudinal changes of the incoming solar radiation. Those latitudinal changes are highest during winter (Warneck, 1999; Seinfeld and Pandis, 2016).

4.4.4. Background Concentrations

The reaction rate depends on the concentration of all chemicals involved (Equation 4.1). NO_x related reactions depend on the concentrations of CO, CH_4, H_2O and all other chemical species given in the reactions above. Further, the reaction rate is influenced by the background concentration of NO_x and HO_x.

Especially the background concentration of NO_x significantly influences the O_3 production rate as well as the OH concentration. This relation is given in Figure 4.2 which shows model results for the net-O_3 production and OH concentration depending on the NO_x mixing ratio. The model data are obtained at mid-latitude during spring and differ at other seasonal conditions (Ehhalt and Rohrer, 1995). It can be seen that at low NO_x mixing ratios, the net-O_3 production is negative. In this case, the depletion of O_3 dominates (Reaction R16 and R17). With increasing NO_x concentration the net-O_3 production becomes positive and increases until a certain NO_x concentration of about 0.2 ppbv is reached. After this the net-O_3 production rate decreases again, based on the higher losses of HO_2 (Reaction R20 and R21). Additionally, the OH concentration is reduced. This high concentration of NO_x can generally be observed in the lower stratosphere at high northern latitudes (Brasseur et al., 1998).

Nitrogen molecules have a very stable triple bound. In the upper troposphere lightning is the only natural process capable to break up those strong bond. Therefore, lightning can transform nitrogen gas (N_2) into highly reactive nitrogen species. Those reactive nitrogen species form natural NO_x. In the upper troposphere, lightning is therefore the only natural process that is capable to influence the background concentration of NO_x (Schumann and Huntrieser, 2007).

5

REACT4C - Model Description

This chapter comprises a description the REACT4C project. First, a general introduction of the REACT4C approach is given. Afterwards, a detailed description of the atmospheric model used and a selection of important submodels needed to simulate the effects of aviation NO_x emissions, is provided. Next the RF calculation for NO_x is elaborated. In a final step, the verification of REACT4C model set-up, is discussed. The calculation of the climate cost function (CCF), a specific climate metric measuring the climate impact per unit emission (Grewe et al., 2014a), is not provided. This is due to the fact that this study focuses on concentration changes, only. Throughout this chapter only steps related to NO_x are taken into account. Other impacts and emissions are neglected. The description of REACT4C is based on Grewe et al. (2014a).

5.1. REACT4C Objectives

Minimising the climate impact of aviation can be achieved by multiple means. Future aircraft could be redesigned such that emissions are reduced. This could be achieved by improving engines or optimising aircraft for operations at lower velocities (Lee et al., 2009). This strategy has a significant disadvantage since mainly future aircraft are effected. The impact on the current fleet is minimal. The impact of this measure will be recognisable in the far future, only. Another approach tries to reduce the climate impact by using the existing fleet. As suggested by Matthes et al. (2012), the climate impact can be reduced by re-routing aircraft to avoide climate sensitive areas. This concept is based on the fact that non-CO_2 climate impacts, highly depend on their emission location.

The European project REACT4C had two general objectives. It elaborated the feasibility of adopting flight routes and flight altitudes to minimise the climate impact of aviation and estimated the global effect of such air traffic management (ATM) measures (Grewe et al., 2014a). This mitigation option is assessed by using a modelling approach described by Grewe et al. (2014a) for the North Atlantic region. The general steps in this modelling approach are as follows: (1) select representative weather pattern, (2) define time-regions, (3) model atmospheric contribution for additional emissions in these time-regions, (4) calculate the adjusted radiative forcing (RF), (5) calculate the climate cost function (CCF) for each emission species and induced cloudiness, (6) optimize aircraft trajectories, based on the CCF results, by using an air traffic simulation (System for traffic Assigment and Analysis at a Macroscopic level, SAAM) which is coupled to an emission tool (Advanced Emission Model, AEM), and (7) calculate the resulting operation costs and the resulting climate impact reduction (Grewe et al., 2014a).

For the current study step 1 to 4 are most important. Only those steps are further discussed in this chapter. Step 5, 6 and 7 are neglected.

5.2. Weather Pattern Used in REACT4C

The significance of non-CO_2 climate effects are influenced by multiple factors. Especially contrail formation by aviation highly depends on the local weather situation (Lee et al., 2009). This suggests that different weather situations lead to different climate impacts of non-CO_2 emissions, which will ultimately influence the route adjustment to minimise the climate impact of a specific flight. Irvine et al. (2013)

Table 5.1: Characteristics of each weather pattern over the North Atlantic, used by REACT4C. Five different winter pattern (WP) and three different summer pattern (SP) are simulated. (Table obtained from Irvine et al. (2013))

Type	Jet Stream		Frequency (days/season)
	Position	Strength	
WP1	Zonal	Strong	17
WP2	Tilted	Strong	17
WP3	Tilted	Weak	15
WP4	Confined	Strong	15
WP5	Confined	Weak	26
SP1	Zonal	Strong	19
SP2	Weakly tilted	Weak	55
SP3	Strongly tilted	Weak	18

identified that by simulating frequently reoccurring weather situations within a season, the global seasonal effect of re-routing aircraft, is assessed. Therefore, eight different frequently occurring weather pattern are analysed by REACT4C. Based on the frequency of occurrence, the total climate impact due to each weather pattern is estimated. The weather patterns are divided into five winter pattern (WP) and three summer pattern (SP). Each weather pattern is defined by Irvine et al. (2013), which is based on the work performed by Woollings et al. (2010). Those typical weather pattern mainly vary in the strength and the position of the jet stream and the phase of the North Atlantic Oscillation (NAO) and the Arctic Oscillation (AO) (see Section 3.2.1, 3.2.2 and 3.2.3, respectively). During summer the variation of the jet stream, the NAO and AO is lower. Therefore, the global effect can be estimated by only analysing three different weather situations (Irvine et al., 2013). A summary of the frequency of each characteristic weather pattern and the position and strength of the jet stream is given in Table 5.1. Additionally, the geopotential height and the wind velocity for each weather pattern at 250 hPa, is given in Figure 5.1. By analysing these weather maps, the effect of the Arctic Oscillation (AO, see Section 3.2.3) in its positive phase becomes most evident in WP1.

Since those weather pattern represent frequently occurring weather situations, a representative day is selected during the REACT4C simulation. At this representative day all emissions occur (Grewe et al., 2014a).

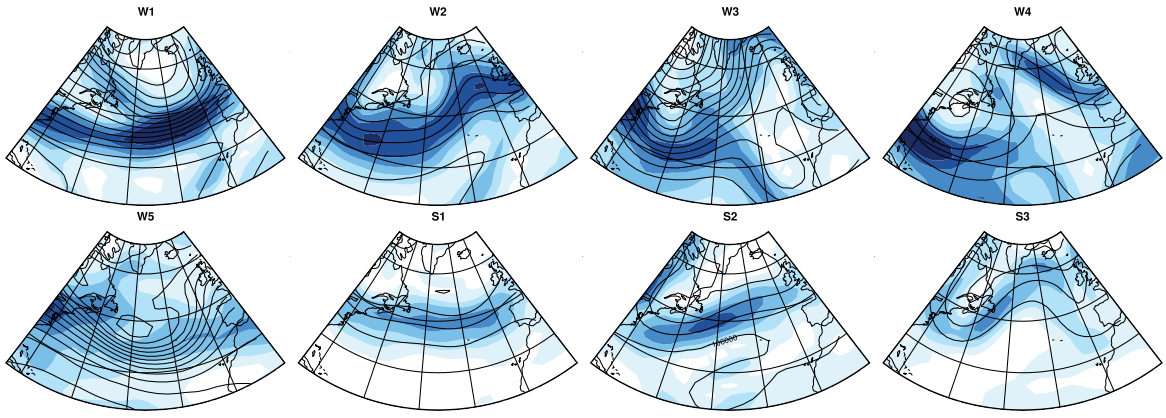

Figure 5.1: Weather maps for the five winter pattern (W1-W5) and the three summer pattern (S1-S3), used in REACT4C. Geopotential height (black contours) and wind velocities (light to dark blue, starting at 10 ms^{-1} with a 10 ms^{-1} interval) at 250 hPa, are indicated. Winter and summer pattern are defined by Irvine et al. (2013). (Figure obtained from personal communication with Volker Grewe, 15th September 2016)

Table 5.2: Definition of the time-region grid used by REACT4C (Table obtained from Grewe et al. (2014a))

Dimension	Number	Values	Unit
Longitude	6	75, 60, 45, 30, 15, 0	$°W$
Latitude	7	30, 35, 40, 45, 50, 60, 80	$°N$
Pressure	4	200, 250, 300, 400	hPa
Time	3	6, 12, 18	UTC

5.3. The Time-Region Grid

In a second step, the time-region grid is defined for each selected weather situation. This grid is further used to assess the climate impact of this representative day. Due to the modelling approach of REACT4C, two different grids are used. The atmospheric model ECHAM/MESSy Atmospheric Chemistry (EMAC) model, used to model all atmospheric processes, has a regular grid with a resolution of about 2.8° in longitude and latitude (for more details see Section 5.4). The routing model SAAM has an irregular grid, which differ from the EMAC grid. This means that the emission locations need to cover the area in which the routing optimisation is performed. In total 504 emission locations are defined for each weather pattern. The time-region grid has in total six longitudes and seven latitudes. It has been found, that by varying the flight altitude, the climate impact of aviation can be reduced (Köhler et al., 2008; Stordal et al., 2006; Fichter, 2009). Therefore, SAAM takes different altitudes into account and the time-region grid needs to cover those different altitudes. This leads to four different emission pressure altitudes between 400 hPa and 200 hPa, covering typical cruise altitudes. A summary of the defined time-region grid is given in Table 5.2. At each time-region grid point $5\,x\,10^{5}$ kg of NO (equals $2.33\,x\,10^{5}$ kg(N)) are emitted. The RF and the CCFs are calculated in the time-region grid and are interpolated onto the EMAC grid (Grewe et al., 2014a). This is done using a bilinear interpolation method (Volker Grewe, personal communication, 12th December 2016). Such a interpolation method does not assume linear relation but rather a quadratic relation between different sample points (Kirkland, 2010). This assumption needs to be taken into account while relating original data from EMAC to the interpolated values.

At each time-region grid point, the emission is distributed over 50 different emission location. This is performed by the EMAC submodel Tracer Release EXperiments from Point sources (TREXP). TREXP allows the release of tracer from point sources (Jöckel et al., 2010). Each emission is randomly located in the EMAC grid box at which the specific time-region grid point is located. 50 trajectories per grid box were selected based on a sensitivity study. In this sensitivity study, the number of emissions per grid point were varied. Sample emissions were released in selected grid boxes for 2 to 48 trajectories. Based on the mean of each trajectory and the mean of all trajectories at one time-region grid location, it was concluded that the deviation and standard deviation is smallest for 48 trajectories, reducing the noisiness of the model results. Therefore, it was decided that 50 trajectories were released (Grewe et al., 2014a).

Some of the chemical reactions resulting from NO_x emissions depend on the incoming solar radiation (see Section 4.4.3). A second sensitivity study for the emission times was performed. Here, an additional emission time of 09:00 UTC was added and compared to the interpolated values between the emission time of 06:00 UTC and 12:00 UTC. It became clear, that the temporal interpolation is less crucial than the horizontal interpolation. Further, it was identified that the variability of the climate impact of NO_x is higher than the possible interpolation error. Therefore, three different emission times (given in Table 5.2), each with a duration of 15 min, are considered to be sufficient. The simulation was performed for additional 90 days after emission (Grewe et al., 2014a).

5.4. The Atmospheric Chemistry Model: EMAC

REACT4C uses the ECHAM/MESSy Atmospheric Chemistry (EMAC) which consist of the Modular Earth Submodel System (MESSy) and the atmospheric general circulation model ECHAM5 (used as a base model) (Jöckel et al., 2006). In the MESSy concept, physical processes are coupled to the base model. The previous chapters showed that many processes are important while analysing the impact of NO_x emissions in the upper troposphere. In this section the most important submodels for this study are discussed, namely the atmospheric chemistry model MECCA, the atmospheric tracer

transport model ATTILA and the emission contribution model AIRTRAC (developed in the framework of REACT4C project).

5.4.1. The Base Model: ECHAM5

ECHAM5 is a global circulation model based on the global weather forecast model developed at the European Centre for Medium-Range Weather Forecasts (ECMWF). For climate studies, ECHAM5 was modified to allow longer time integrations. This is achieved by adapting the parametrisations used (Esch et al., 1996). A complete description of the model is given in Roeckner et al. (2003).

The tracer transport of ECHAM5 is based on a semi-Lagrangian approach and uses temperature, surface pressure, specific humidity, mixing ratio of total cloud water, vorticity and divergence as prognostic variables. In the REACT4C model set-up, those prognostic variables are represented by spherical harmonics with triangular truncation at wave number 42. A hybrid vertical presentation (hybrid sigma-pressure coordinate) with 41 layers is used (Grewe et al., 2014a). In hybrid sigma-pressure coordinates the layers close to the surface follow the terrain and the layers at the top of the model with continuous pressure fields are represented very smoothly (Roeckner et al., 2003).

5.4.2. The Atmospheric Chemistry Submodel: MECCA

EMAC uses the Module Efficiently Calculating the Chemistry of the Atmosphere (MECCA) submodel, to model all atmospheric chemistry processes. MECCA is capable to calculate the atmospheric chemistry in the troposphere and stratosphere. It models 116 different species and up to 295 different reactions. Those reactions are grouped as follows (Sander et al., 2005): (1) sulfur chemistry, (2) non-CH_4 hydrocarbon (NMHC) chemistry, (3) basic O_3, CH_4, HO_x and NO_x chemistry and (4) halogen (Cl, Br, I) chemistry.

In the scope of this research, the chemical reactions involved in the NO_x climate impact are most important. As already noticed before, the background concentration of NO_x highly influences the O_3 production. These background processes (ass discussed in Chapter 4) are well modelled in MECCA (Supplement of Sander et al. (2005)) and also selected in REACT4C (Christine Frömming, personal communication, October 2016).

MECCA is highly flexible in terms of the chemical reactions used and its numerical integration methods. The user can select which chemical reaction shall be taken into account and which numerical integration method shall be used. With respect to the numerical integration method, the user can choose to optimise the integration method for either efficiency, stability, accuracy or precision. This factor is handy since MECCA can be used in simple box models or in GCMs. Additionally, the user can add individual chemical reactions if required to the ones predefined in MECCA (Sander et al., 2005).

5.4.3. The Atmospheric Tracer Transport Submodel: ATTILA

In REACT4C, the Atmospheric Tracer Transport In a LAgrangian model (ATTILA) is used to model the transport of the air parcels, containing the emitted species. In general, ATTILA is used to model the global-scale transport of passive trace species by using a Lagrangian approach (Reithmeier and Sausen, 2002). A complete description of ATTILA is given by Reithmeier and Sausen (2002).

ATTILA models on average two parcels for each grid box and uses the wind field calculated by the base model EACHM5 to advect the centroids of each parcel. Those parcels have a constant mass and the mixing ratios of the different species are defined on the parcels centroid. Here, it is assumed that the centroid is representative for the whole air parcel. In a Lagrangian approach, the computational cost is independent of the number of air parcels transported, since the advection of all air parcels occurs simultaneously. This leads to an significant advantage if many trace species are involved (Reithmeier and Sausen, 2002). The Lagrangian approach is also favourable in the REACT4C modelling approach of emissions, since it allows to track the emitted species along their trajectories.

Some disadvantages need to be taken into account. To calculate the interactions between the tracer and the background concentration, the parcel concentration is needed. However, in this approach, the concentration is defined on the parcel centroid. Secondly, the grid box concentration might be over- or underestimated. This depends on the number of parcels taken into account. Finally, it is important to keep in mind that the resolution depends on the initial distribution of the air parcels (Reithmeier and Sausen, 2002).

5.4.4. The Emission Contribution Submodel: AIRTRAC

The submodel AIRTRAC is used to calculate the contribution of the additional emissions at each time-region grid point. In general, two different contribution calculation methods can be used. The first method is the so called ”sensitivity method”. In this method, two different simulations are performed, one base case and one simulation in which one emission category is changed by a certain factor. Based on the concentration changes of important chemicals in the atmosphere, between both simulations, the climate impact due to that specific emission is assessed. As one can imagine this approach would require many simulation and would be very computational and time intensive. The sensitivity method has another significant disadvantage. It assumes that a linear relation between two species exist which in reality is most often non the case (Grewe et al., 2010).

The second method is the ”tagging approach”. In this method, a species is tagged and all chemical reactions are doubled. In REACT4C the tagging approach described by Grewe et al. (2010) is used (Grewe et al., 2014a). An example is given in Reaction R22 and R23. In this case, Reaction R22 is doubled for the additional NO_x emission introduced at each time-region grid point. However, this additional tagging of certain species and the additional modelling of each chemical reactions involved, leads to an increase of processing power needed (Grewe et al., 2010).

$$NO_2 + OH \rightarrow HNO_3 \tag{R22}$$

$$NO_2^{\text{aviation}} + OH \rightarrow HNO_3^{\text{aviation}} \tag{R23}$$

The next step is to calculate the production and loss of O_3 and CH_4, due to the emitted NO_x. This is necessary to calculate the RF and CCFs. Therefore, two emission categories are defined, one including the extra emission (e) and the other the background concentration (b). The background concentrations are obtained from the base model EMAC and are calculated by MECCA. The concentration changes calculated by AIRTRAC are not fed back into EMAC. This isolates the effect due to the emissions. This means that no compensation effects due to the contribution of other emission sectors takes places. This compensations are due to chemical saturation effects (most often non-linear). The tagging approach in REACT4C is implemented such that the calculation of the contribution by the emitted species is less detailed then other processes modelled by EMAC (Grewe et al., 2014a).

Based on Grewe et al. (2010), the production and loss terms for O_3 is described. For better illustration two examples are provided, one for the O_3 production and one for depletion of O_3. Reaction R3 influences the production rate of O_3. Its corresponding production rate can be calculated using Equation 5.1. In this equation $P^e_{O_3}$ and $P^b_{O_3}$ represent the production rate due to the additional NO_x emission and due to the background concentration. A representative loss rate calculation is given by Equation 5.2. This loss term is based on Reaction R16.

$$P^e_{O_3} = \frac{1}{2} \cdot P^b_{O_3} \cdot \left(\frac{HO_2^e}{HO_2^b} + \frac{NO^e}{NO^b} \right) \tag{5.1}$$

$$L^e_{O_3} = \frac{1}{2} \cdot L^b_{O_3} \cdot \left(\frac{OH^e}{OH^b} + \frac{O_3^e}{O_3^b} \right) \tag{5.2}$$

AIRTRAC takes two simplifications into account. First, it is assumed that the O_3 production due to aviation is only caused by NO_x emissions. This is consistent with the results obtained by Brasseur et al. (1998) (see Chapter 4). Further, O_3 depletion is split into two parts. The first is based on the additional NO_x (Reaction R15) and the second on all other loss reactions (referred to as non-NO_x loss reactions). Additionally, background nitrogen is combined into one group from which the contribution to the additional emission is calculated. This group does not include NO, NO_2 and HNO_3. In this calculation, it is assumed that the emissions are small and no change in the reaction rate occurs. Combining this simplifications, the O_3^e change with time is calculated by (Grewe et al., 2014a):

$$\frac{dO_3^e}{dt} = \frac{P^b_{O_3}}{NO_x^e} - \frac{1}{2} D^b_{O_3,1} \left(\frac{NO_x^e}{NO_x^b} + \frac{O_3^e}{O_3^b} \right) - D^b_{O_3,2} \frac{O_3^e}{O_3^b} \tag{5.3}$$

The CH_4 loss rate is calculated using the same approach. As described in Chapter 4, the CH_4 concentration change depends on the OH concentration (Reaction R7). Therefore, it is key to model

the OH production and loss as accurate as possible. The OH production is based on Reaction R3, R17 and R18-R19. Using the same methodology as given for O_3, the OH production rate can be calculated by:

$$P_{OH}^{e} = P_{R18-R19}^{b}\frac{O_3^e}{O_3^b} + \frac{1}{2}P_{R17}^{b}\left(\frac{HO_2^e}{HO_2^b} + \frac{O_3^e}{O_3^b}\right) + \frac{1}{2}P_{R3}^{b}\left(\frac{HO_2^e}{HO_2^b} + \frac{NO_x^e}{NO_x^b}\right) \tag{5.4}$$

The OH loss is based on Reaction R1-R2, R7-R8 and R16 (see Section 4.1). Additionally, the loss of OH due to RH and HO_2 is taken into account by considering the following two reactions:

$$OH + RH \xrightarrow{O_2} RO_2 + H_2O \tag{R24}$$

$$OH + HO_2 \rightarrow H_2O + O_2 \tag{R25}$$

Combining all these reactions, the OH loss is calculated by:

$$L_{OH}^{e} = \frac{1}{2}L_{R16}^{b}\left(\frac{OH^e}{OH^b} + \frac{O_3^e}{O_3^b}\right) + L_{R1-R2}^{b}\frac{OH^e}{OH^b} + L_{R24}^{b}\frac{OH^e}{OH^b} + L_{R7-R8}^{b}\frac{OH^e}{OH^b} + \frac{1}{2}L_{R25}^{b}\left(\frac{OH^e}{OH^b} + \frac{HO_2^e}{HO_2^b}\right) \tag{5.5}$$

It is important to note that in Equation 5.4 and 5.5, the contributions due to H_2O, CO, RH and CH_4 emissions from aircraft are neglected, since their contribution is considered to be small. The HO_2 concentration influences the OH concentration and thus the CH_4 loss. The HO_2 production and loss are calculated using the same methodology as for OH, with the additional contribution of Reaction R26 to the HO_2 production, and Reaction R27 and R28 to additional HO_2 losses (Grewe et al., 2014a).

$$RO_2 + NO \xrightarrow{O_2} HO_2 + R'CHO + NO_2 \tag{R26}$$

$$RO_2 + HO_2 \rightarrow ROOH + O_2 \tag{R27}$$

$$HO_2 + HO_2 \rightarrow H_2O_2 + O_2 \tag{R28}$$

Finally, the CH_4 depletion due to changes in OH (from aviation NO_x), is combined to Equation 5.6 (based on the Reactions R7-R8) (Grewe et al., 2014a; Frömming et al., 2013):

$$L_{CH_4}^{e} = L_{R7-R8}^{b}\frac{OH^e}{OH^b} \tag{5.6}$$

5.5. Radiative Forcing (RF) Calculations

In Section 2.1.1 the general concept of radiative forcing (RF) is introduced. In the scope of REACT4C, the calculation of the CCF of O_3 and CH_4 is based on RF. In this study, neither RF data nor CCF data are used. However, by understanding the RF calculation the climate impact of a certain concentration change can be understood in a better manner. The RF for O_3, CH_4 and PMO are shortly discussed separately.

5.5.1. RF Calculation for O_3

The mass changes of O_3 are feed into the radiation submodel RAD4ALL. RAD4ALL calculates the instantaneous RF for O_3. It is based on the global mean radiation flux changes F at the tropopause and calculated by Equation 5.7, where T is given to be one year (Grewe et al., 2014a).

$$RF_{inst.} = \frac{1}{T}\int_{t_0}^{t_0+T} F(t)dt \tag{5.7}$$

The instantaneous RF of O_3 is considered to be a non-perfect metric to assess the near surface atmospheric temperature change. Instead the adjusted RF is considered to be a better quantification.

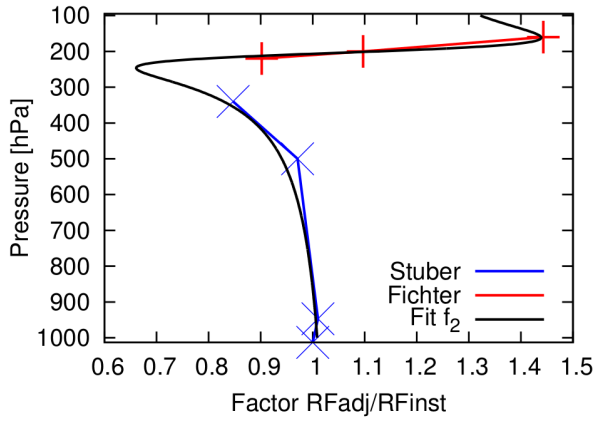

Figure 5.2: Relation between adjusted and instantaneous RF with altitude. RF values are mean RF due to additional O_3 induced by NO_x emissions. Data are based on Fichter (2009) and Stuber (2003). (Figure obtained from Grewe et al. (2014a))

In the scope of REACT4C, pulse emissions are considered that are part of the total climate impact of aviation. In reality, a sequence of flights will each emit a pulse emission. This leads to sustained emissions and induces a stratospheric temperature adjustment. This will then reduce the adjusted RF with respect to the instantaneous RF. This needs to be taken into account if a single emission is assessed as part of a sequence of emissions. The adjusted RF for O_3 is calculated using Equation 5.8 in which function $f_1(t)$ and $f_2(t)$ represents the adjustment due to the seasonal cycle and the emission height, respectively (Grewe et al., 2014a).

$$RF_{adj} = f_1(t) \cdot f_2(t) \cdot RF_{inst} \tag{5.8}$$

To assess seasonal and height variation, a simulation was performed based on the work and data provided by Fichter (2009) and Stuber (2003). In this simulation, the adjusted and instantaneous RF are simulated using EMAC over a one year period. Here, each month is considered to be a pulse emission. Based on the output from EMAC, the relation between the adjusted and the instantaneous RF was assessed for each month. The simulation is performed at a pressure altitude of 200 hPa, 160 hPa and 130 hPa in the Northern Hemisphere (NH) (Fichter, 2009).

The seasonal cycle is considered to be independent of the emission altitude. Only magnitude differences exist, for different altitudes. The seasonal variation is based on the varying seasonal isolation, effecting the shortwave influence on the RF (Grewe et al., 2014a). During summer (July) the relative difference between the adjusted and the instantaneous RF is zero and becomes -15% during winter (February). The seasonal variation is approximated by the equation provided by Grewe et al. (2014a).

The altitude dependency (Figure 5.2) is also derived from the three pressure levels given in Fichter (2009). Additionally, five data points were added from Stuber (2003) for lower altitudes. It is important to notice that both experiments differ significantly in the O_3 pattern used (Grewe et al., 2014a). A mathematical fit is provided by (Frömming et al., 2013). The difference between instantaneous and adjusted RF is insignificant for pressure levels between 1000-500 hPa. Afterwards, the fraction between both RF decreases but increases again and becomes higher than 1 above 200 hPa. A lower adjusted RF in the lower troposphere implies a cooling. As soon as the emissions are close or above the tropopause the adjusted RF becomes higher than the instantaneous RF, causing warming in the lower stratosphere.

Other studies from Hansen et al. (1997) and Stuber et al. (2001) concluded that the instantaneous RF becomes negative at very high altitude between 150 hPa and 50 hPa but still have a positive adjusted RF. The negative instantaneous RF is based on the fact that shortwave radiation dominates the instantaneous longwave cooling. This relation is not well modelled by the mathematical fit provided by Frömming et al. (2013) (Grewe et al., 2014a). This could lead to inaccurate results of the adjusted RF for O_3 at high altitudes and needs to be considered in further discussions (van Manen, 2017).

5.5.2. RF Calculation for CH_4

The RF calculation of CH_4 is based on the IPCC formula described by Wigley (1987) (Shine et al., 1990) and is given in Equation 5.9. The terms M_0 and N_0 represent the background concentration of CH_4 and N_2O, respectively. The overlap Equation 5.10, is defined by Hansen et al. (1988). In this equation, M represents the CH_4 concentration and N the N_2O concentration in ppbv. Both equations are only valid for concentrations of CH_4 below 5 ppmv (Wigley, 1987; Hansen et al., 1988).

$$RF = 0.036\left(\sqrt{M} - \sqrt{M_0}\right) - (f(M, N_0) - f(M_0, N_0)) \tag{5.9}$$

$$f(M, N) = 0.47 \ln\left[1 + 2.01 \cdot 10^{-5}(MN)^{0.75} + 5.31 \cdot 10^{-15} M(MN)^{1.52}\right] \tag{5.10}$$

The background concentration for CH_4 and the depletion of CH_4 due to the emitted NO_x are calculated by MECCA and AIRTRAC (Equation 5.6), respectively. The value of N_2O are based on measurements and do not vary in the simulation (Volker Grewe, personal communication, 18th November 2016).

It is important to notice, that the calculation of the CH_4 RF is based on a formula that is more than 25 years old. Additionally, the paper by Wigley (1987) was not available during this thesis, making it hard to assess how Equation 5.9 was obtained.

5.5.3. RF Calculation for PMO

Due to its long lifetime, modelling PMO is rather computational intensive. In REACT4C, the RF of PMO is based on the same calculation used by Dahlmann (2012). PMO is calculated by applying a constant factor of 0.29 to the RF of CH_4. This factor was obtained by using the ”sensitivity method” (described in Section 5.4.4). Based on the resulting net-O_3 RF and the RF due to short lived O_3, the contribution due to PMO was calculated (Dahlmann, 2012). It can be argued that this factor is only half of the value found by Köhler et al. (2008). However, it is still in an acceptable range compared to other studies by Wild et al. (2001), Stevenson et al. (2004) and Hoor et al. (2009).

5.6. REACT4C - Verification

Verifying such a complex simulation set-up is complicated. Measuring variation in the atmospheric chemistry, due to additional NO_x emissions in the upper troposphere above the North Atlantic, is currently not feasible. To track an emission along its trajectory over three month (as it is done in REACT4C), is in reality impossible. Further, the long term temperature effect due to such emissions is in principle not measurable. The verification of REACT4C is based on a sanity check by comparing model results with previous studies. Previous studies differ significantly in their approach and model set-up. Additionally, most studies assess the global impact of aviation and not the local effects as done by REACT4C.

The performed sanity check found that the lifetime of NO_x and O_3 are comparable to results found by other studies. The same is true for O_3 mass changes due to NO_x and the induced RF. Only the total O_3 column change differs to other studies. This can be linked to the fact that this study only considers higher altitudes. Other studies also took lower flight levels into account (Grewe et al., 2014a).

A sanity check is also used for all CCFs. Here, CCF results were compared to results from Fuglestvedt et al. (2010). Compared to Fuglestvedt et al. (2010) the results obtained by REACT4C are in the same range. The considered time-region grid is in the upper troposphere, which results in a higher CH_4 depletion. This leads to lower CCF results, if compared to Fuglestvedt et al. (2010) (Grewe et al., 2014a).

6 Methodology

This chapter elaborates on the methodology used during this master thesis. Figure 6.1 gives a graphical representation of all steps taken. First, a general overview of each step is presented in Section 6.1. Afterwards, each step is elaborated in more detail. Data limitations and data preparations are discussed in Section 6.2 and 6.3. Section 6.4 presents all steps taken in the main analysis. Section 6.5 provides a summary of all factors taken into account during the main analysis. Afterwards, each method used within the main analysis is presented (Section 6.6). In a last step, a few practical notes are presented (Section 6.7). The terminology used is the same as the on used by Grewe et al. (2014a). Differentiation is made between foreground and background. Foreground refers to the additional emissions which are given in the Lagrangian grid. Background refers to the general circulation and chemistry model data provided in the regular Eulerian grid.

6.1. General Approach

Figure 6.1 gives a graphical representation of the methodology used in this thesis. This section shortly present each step taken to provide a general overview. More detailed description of each step are presented in the follow-up sections. Prior to this thesis a literature study was performed, which covered all topics discussed in Chapter 2 to 5. All data used within this study were stored on a server of the German Climate Computing Centre (DKRZ). Due to the data structure used, each data set needs to be modified and prepared for analysis (Section 6.2 and 6.3). In a next step the temporal development of O_3 and CH_4 is analysed to identify important characteristics. In Section 4.4 and 5.4.4 it became evident that the foreground and background chemical concentrations influence the production and loss terms

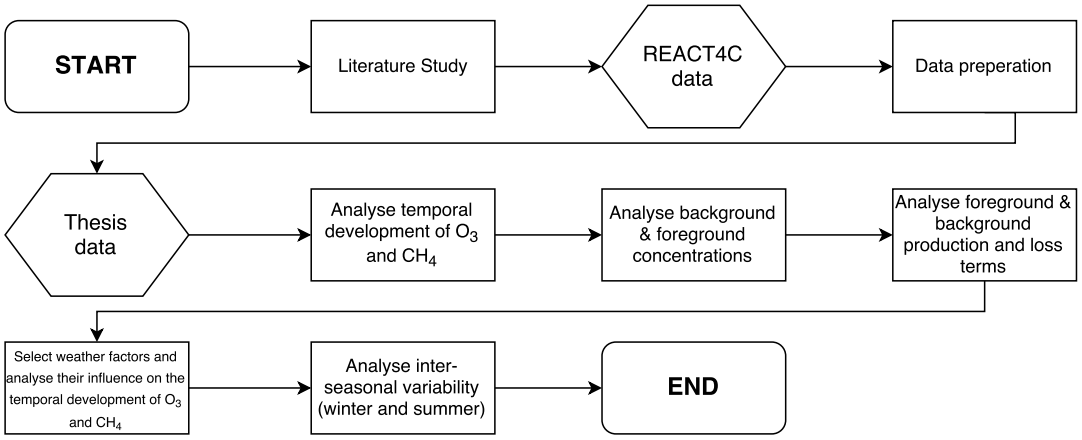

Figure 6.1: Flow chart of all steps taken to identify weather influences on the temporal development of O_3 and CH_4 due to NO_x emissions. Additional steps that do not directly influence the results obtained are omitted.

in the foreground and background. Therefore, each chemical concentration and all chemical reaction rates are analysed in the background and foreground. Weather factors are selected and analysed to identify their influence on the temporal development of O_3 and CH_4. Throughout the performed analysis only seasonal differences are considered. In a last step, the inter-seasonal variability is assessed.

6.2. Data Limitations

Since REACT4C is a rather large and complex project, missing or in correct data are common. Those data can not be taken into account. Otherwise the obtained result might be inconclusive or incorrect. All incorrect data are caused by two problems: (1) missing data and (2) wrong initialised tracer. This section elaborates both topics separately. Table 6.1 provides an overview of all data that are ignored in this thesis, based on the before mentioned causes.

6.2.1. Missing Data

Grewe et al. (2014a) analysed the temporal and horizontal resolution. Here, it became evident that the horizontal interpolation is more important than the temporal interpolation. For the first winter pattern (WP1) all three emission times were simulated (6:00, 12:00 and 18:00 UTC). For all other weather situations (winter and summer), only one emission time was simulated (12:00 UTC). This is due to the high computation amount needed to simulate each emission time. All data related to the other emission times (6:00 UTC and 18:00 UTC) are missing for all weather pattern, except WP1. Therefore, this study only takes data related to emissions occurring at 12:00 UTC into account.

While analysing the second winter pattern (WP2), it became evident that only the first 30 days after emission were correctly saved on the DKRZ server. In this study, the main focus is on the whole temporal development over all 90 days. Since no single tracer for WP2 is complete, the entire weather pattern is not be taken into account.

Some weather pattern have additional missing data for selected emission location. The first 30 days are missing for three emission locations of WP4 at 400 hPa. In the case of WP5, twelve days in March are missing for fifteen emission locations. For the same winter pattern, the last 30 days of all background data are missing, for all emission locations. Thus weather influences for the last 30 days can not be analysed for WP5. For this winter pattern, all foreground data (90 days) are still present and will be taken into account.

6.2.2. Wrong Tracer Initialisation

Individual tracers have been initialised incorrectly. For SP2, all tracers were wrongly initialised at 35°N 30°W at 250 hPa. Here, the total NO_x emission was emitted on a single tracer and not distributed over all 50 tracers. Additionally, a different mass of NO_x was emitted (not the intended $5\,x\,10^{5}$ kg(NO) (Grewe et al., 2014a)). The influence of such a higher emitted mass on a single tracer is unknown. Therefore, this single emission location will not be taken into account, since the introduced uncertainties can not be assessed.

All weather pattern have six emission locations that have been initialised incorrectly. For the first three emission locations (80°N 75°W, 80°N 60°W, 80°N 45°W at 250 hPa), no NO_x was emitted. For other three emission locations (30°N 30°W, 30°N 15°W, 30°N 0°W at 400 hPa), the emission occurred at different locations and time. This makes it impossible to attribute concentration changes to one emission location. Those tracer introduce uncertainties that can not be neglected. Thus they are not taken into account.

Due to the wrong tracer initialisation the temporal development of O_3 and CH_4 differ, which leads to a wrong RF and CCF value. In the case of the three emission location were no NO_x has been emitted the CCF value is going to be low (tracer can still gain O_3 by diffusion) or even zero. This will most likely make those areas favourable for re-routing measures. This might impact the overall global climate reduction. It should be evaluated if the re-routing results obtained (i.e. Grewe et al. (2014b)) are influenced by the identified wrong tracer initialisations.

6.3. Data Preparation

All data used are stored in Network Common Data Form (netCDF) files on the server of the DKRZ. In general two different array structures are used. All foreground data (e.g. O_3 concentration) are present

Table 6.1: Overview of all data not taken into account, due to missing data or incorrect tracer initialisations.

Weather Pattern(s)	Emission Location	Emission Altitude	Time
WP2	All	All	After 90 days
WP4	30°N 30°W, 30°N 15°W, 30°N 0°W 40°N 75°W, 40°N 60°W, 40°N 45°W, 40°N 30°W, 40°N 15°W, 40°N 0°W,	400 hPa	First 30 days after emission
WP5	35°N 75°W, 35°N 60°W, 35°N 45°W, 35°N 30°W, 35°N 15°W, 35°N 0°W, 30°N 75°W, 30°N 60°W, 30°N 45°W	400hPa	12 days in March
SP2	35°N 30°W	250hPa	All 90 days after emission
WP1-WP5, SP1-SP3	80°N 75°W, 80°N 60°W, 80°N 45°W	250 hPa	All 90 days after emission
WP1-WP5, SP1-SP3	30°N 30°W, 30°N 15°W, 30°N 0°W	400 hPa	All 90 days after emission

on the tracer grid with two dimensions (tracer id and time). The background data (e.g. temperature) are stored on the original EMAC grid, which has four dimensions (longitude, latitude, level and time). To use all given data in an efficient manner, the necessary data need to be transformed onto the same grid. For some specific applications (i.e. certain weather analysis techniques) additional manipulations are necessary. Each manipulation is explained in the following sections. Before a certain data set is taken into account, it is analysed to ensure correct data integrity. Each of these steps is performed before the actual analysis.

6.3.1. Data Regriding

In Chapter 5 it became clear that two different grids were used in REACT4C. This thesis does not focus on climate metrics but rather on concentration changes. The time-region grid contains all the information related to each tracer. Even though the time-region grid contributions are less detailed, it is of most interest in this thesis. Analysing everything within this grid allows to isolate each tracer. This results a more detailed analysis. If the analysis would be performed on the regular EMAC grid, the degree of complexity would increase. The data on the EMAC grid contain information for each grid cell. If no tracer is within a specific grid cell, the data provided within the cell is of no interest. Thus each data-file (in the EMAC grid) contains information which do not add any information to the analysis and only increase the size of each netCDF file. This results in a higher amount of data that need to be loaded. This results in longer computation times, which is considered to be a disadvantage.

Based on those reasons it is necessary to regrid all background process information from the EMAC grid on the tracer grid. To accomplish this, it is assumed that as soon as a tracer is within a grid box of EMAC, the background information are valid for this tracer.

6.3.2. Concentrations to Production Rates

Even though the simulation was performed with a time resolution of 15 minutes (Grewe et al., 2014a), most data obtained only contain information with a time resolution of six hours. This is done to reduce the amount of data that need to be stored. Only data related to contrail information exist in a time resolution of 15 minutes. If those data are relevant for this analysis, the time resolution is reduced to six hours and all other information are neglected. Additionally, the background loss and production terms of each reaction calculated within MECCA are given in concentrations ([mol mol^{-1}]) and not in concentration changes ([mol mol^{-1} 6 h^{-1}]). Therefore, the concentration change for each time step is added to the concentration of the previous time step. However, in this analysis concentration changes are of interest. Those concentration changes are estimated by calculating the central derivative. The central derivative is given in Equation 6.1. Here, Δt is the time step, of six hours.

$$f'(x) \approx \frac{f(x+\Delta t) - f(x-\Delta t)}{2\Delta t} \tag{6.1}$$

6.3.3. Isolate Loss and Production Terms

To analyse weather influences on the temporal development of O_3 and CH_4, each production and loss rates are needed. The given data only contain the current concentration of the different chemical species in each air parcel. This includes the loss and gain due to diffusion from mass exchange between different air parcels.

In general, concentration changes of O_3 can be summarised by Equation 6.2 (in this model set-up). Here, the production of O_3 (due to the additional NO_x) is given by $P^F_{O_3}$, the loss of O_3 within the air parcel is given by $L^F_{O_3}$. The production of O_3 by other terms is not taken into account. Additionally, O_3 is lost by other factors (i.e. diffusion) indicated by $L^D_{O_3}$.

$$\frac{d}{dt}O_3 = P^F_{O_3} - L^F_{O_3} - L^D_{O_3} \tag{6.2}$$

It is necessary to isolate the diffusion terms of O_3 and CH_4. This can be done by two different approaches. In a first approach, the diffusion term can be recalculated based on the total mass of all air parcels. The other approach recalculates the different production and loss terms, based on the approach discussed by Grewe et al. (2010) and Grewe et al. (2014a) (see also Section 5.4.4). The first approach introduces unpredictable uncertainties which might influence the accuracy of the reaction rates. The main uncertainty introduced by the second approach is due to the derivative calculation discussed in Section 6.3. This uncertainty can be better predicted than the one introduced by recalculating the loss of all chemicals by diffusion (based on global data). Therefore, the second approach is used in this thesis.

6.3.4. Calculate Data at Constant Pressure Altitude

Some meteorological methods used within this study require a certain variable at a constant pressure altitude. For example the geopotential at a given pressure altitude is analysed to identify high pressure ridges. EMAC uses sigma-pressure coordinates (see Section 5.4.1). At each sigma level the pressure is different for each location. Thus it is not possible to obtain certain weather variables at a constant pressure altitude from the EMAC data directly. In this case, the weather variable is approximated by assuming a linear relation ship for each variable between two sigma levels. This introduces an uncertainty of the variable at the constant pressure altitude.

6.4. Main Analysis

Identifying weather influences without analysing the different reaction rates increases the chance of insufficient results. Additionally, by analysing those reactions, important insides to improve the LOSU, are obtained. The main analysis is split up into six parts:

1. Split-up temporal development of O_3 into O_3 build-up and O_3 depletion
2. Analyse the temporal development of O_3 and CH_4
3. Assess the variability of all important chemical species (identified in Chapter 4)
4. Analyse and identify seasonal and location influences of all production and loss terms
5. Identify and analyse different weather influences on the temporal development of O_3 and CH_4
6. Identify inter-seasonal differences for each season

O_3 and CH_4 will be analysed using the same approach. Additionally, they will be analysed at the same time. This increases the chance to find links between them and reduce the amount of tasks that need to be performed repeatedly (i.e. data preparation).

6.4.1. Split-up Between O_3 Gain and O_3 Loss

Figure 6.2 gives the temporal development of global mean masses of O_3 and CH_4, due to the emitted NO_x. This shows that their is a high variability in the temporal development of O_3 and CH_4 for different emission location. By taking this variability and the high amount of data into account, a systematic

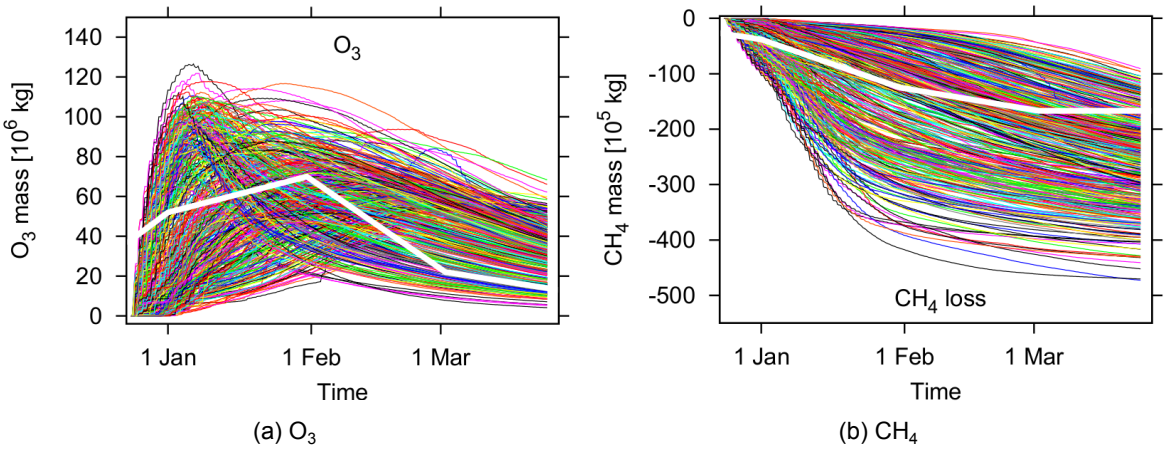

(a) O_3 (b) CH_4

Figure 6.2: Temporal evolution of global mean masses of O_3 and CH_4. The global mean over all 50 tracer released at each emission location is given (Table 5.2). In total 504 coloured lines are presented. (Figure obtained from Grewe et al. (2014a))

analysis is key to find sufficient results. It is assumed that similar developments are also influenced by similar weather factors.

Since the O_3 build-up depends on other chemical reactions and chemical species than the O_3 depletion, differentiation is made between both processes. This leads to two main analysis areas (O_3 build-up and O_3 depletion). The CH_4 loss is split up in the same groups (since the OH chemistry is also influenced in different manners). Figure 6.3 provides a graphical representation of the defined split-up.

In addition to the main split-up, further typical behaviour are observed. Each typical behaviour will be analysed separately, to identify which weather factor causes this behaviour.

There are tracer that have an O_3 maximum at the end of simulation. The O_3 production is always higher than the O_3 loss. Even though they reach a maximum at the end of simulation, this does not mean that if the simulation would continue, the O_3 loss would dominate. The O_3 build-up can still continue if the foreground concentration of NO_x is high.

The second typical development that is identified, is a constant concentration of O_3 for at least four days. It is unclear what causes this behaviour. Two different reasons will be analysed. First, this behaviour could be caused since no O_3 is produced or depleted, based on a reduced chemical activity. Secondly, it could be that the loss and production rates of O_3 have the same magnitude. Since the

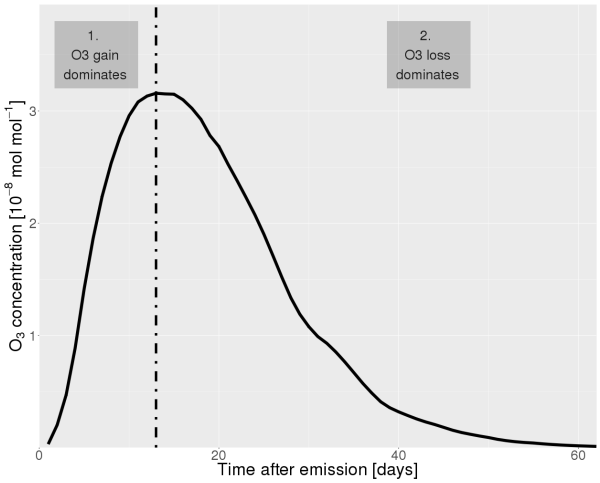

Figure 6.3: Graphical representation of both main analysis areas (O_3 build-up and O_3 depletion). In the first main analysis area, the O_3 gain dominates, leading to a increasing O_3 concentration. In the second main analysis area, the O_3 depletion dominates, leading to a decreasing O_3 concentration. The temporal development of CH_4 is split-up into the same groups.

concentration is constant for four or more days, a sensitivity study will be performed to identify if the same weather factor influences air parcels with a constant concentration for less than four days.

6.4.2. Temporal Development of O_3 and CH_4

Due to the high variability in the temporal development of O_3 and CH_4, certain characteristics of each temporal development are analysed. Those characteristics include the time and magnitude of the O_3 maximum, an approximation of the instantaneous RF as well as a location analysis (longitude, latitude and altitude). The later one includes the location of the O_3 maximum as well as the location of the air parcels when the O_3 loss dominates.

6.4.3. Variability of Important Chemical Species

In order to identify what influences each production and loss rate in the atmosphere, the most important influencing chemicals are analysed. This will provide insides in seasonal and location effects on the climate impact of CH_4 and O_3, due to emitted NO_x. Both, foreground and background concentrations are analysed.

6.4.4. Analysing Production and Loss Terms

Based on the insides gained by analysing the different chemical species concentrations, each production and loss rate is analysed. Each foreground production or loss rate is directly influenced by the following factors:

1. The background concentrations of all chemical species involved
2. The background production/loss rate (also influenced by item 1)
3. The foreground concentrations of all chemical species involved

Each of these factors will be analysed separately, to identify its influence on the temporal development of O_3 and CH_4.

6.4.5. Analyse Weather Factors

In a next step, weather influences on the temporal development of O_3 and CH_4 are analysed. Here, different weather analysis techniques are applied on the given data set. All weather factors given in Section 6.5 are taken into account.

From literature multiple weather factors that have an influence on the climate impact of NO_x, could be identified. It will be analysed if the similar influences exist within the REACT4C simulation. If this is the case, those factors will be elaborated in detail. If no influence can be identifies, a short discussion of the related reason, is provided.

Within this analysis mean values will be provided. Different tracer have different times after emission when the O_3 maximum occurs. Thus taking the mean over seven or 90 days of simulation, might result in a biased comparison due to the chaotic behaviour of the atmosphere. The first O_3 maxima occurs around the seventh day after emission. For better comparison, the mean will also be analysed for the first seven days. This is done to identify if the same trend and observation is made for the same time span for each air parcel.

6.4.6. Analyse Inter-Seasonal Differences

Due to space and time limitations within this thesis, both seasons will be analysed as a whole throughout the performed analysis. To identify if inter-seasonal difference, each relation identified is tested on each separate weather pattern. In this part of the analysis, the Spearman rank coefficient for each weather pattern, is compared. In some cases visually representation of relations are provided.

6.5. Factors Taken into Account

All variables taken into account were obtained based on data integrity and an extensive literature study. All variables taken into account can be split up into the following six groups:

- Background and foreground chemical concentrations

- Background and foreground reaction rates
- General weather factors
- Specific weather factors related to lightning
- Specific weather factors related to convection
- Specific weather factors related to clouds

Table 6.2 provides an overview of all variables taken into account. A complete list of all reactions included in each production and loss term is given in Table A.1 (see Appendix A). Foreground and background reaction rates are named in a similar manner. In the cased of the O_3 production, ProdO3N refers to the background, whereas airProdO3N refers to the foreground reaction rate.

Table 6.2: Overview of all variables taken into account. The column ”source” indicates from which data archive those data are obtained. Additional variables are taken into account but not listed. Most variables are grouped by their respective submodel. A complete list of all reactions included in each production and loss term is given in Table A.1 (see Appendix A).

Name	Description	Source	Unit
	Background Chemical Species:		
N_2O	Nitrous Oxide	Tracer	$[\mathrm{mol\,mol^{-1}}]$
PAN	Peroxyacyl Nitrates	Tracer	$[\mathrm{mol\,mol^{-1}}]$
CO	Carbon Monoxide	Tracer	$[\mathrm{mol\,mol^{-1}}]$
HNO_3	Nitric Acid	Tracer	$[\mathrm{mol\,mol^{-1}}]$
HNO_4	Peroxynitric Acid	Tracer	$[\mathrm{mol\,mol^{-1}}]$
CH_4	Methane	Tracer	$[\mathrm{mol\,mol^{-1}}]$
O_3	Ozone	Tracer	$[\mathrm{mol\,mol^{-1}}]$
NO	Nitrogen Oxide	Tracer	$[\mathrm{mol\,mol^{-1}}]$
NO_2	Nitrogen Dioxide	Tracer	$[\mathrm{mol\,mol^{-1}}]$
HO_2	Hydroperoxyl Radical	Tracer	$[\mathrm{mol\,mol^{-1}}]$
OH	Hydroxyl Radical	Tracer	$[\mathrm{mol\,mol^{-1}}]$
H_2O	Water, Water Vapour	Tracer	$[\mathrm{mol\,mol^{-1}}]$
	Foreground Chemical Species:		
airO_3	Ozone	Tracer	$[\mathrm{mol\,mol^{-1}}]$
airCH_4	Methane	Tracer	$[\mathrm{mol\,mol^{-1}}]$
airHO_2	Hydroperoxyl Radical	Tracer	$[\mathrm{mol\,mol^{-1}}]$
airOH	Hydroxyl Radical	Tracer	$[\mathrm{mol\,mol^{-1}}]$
airHNO_3	Nitric Acid	Tracer	$[\mathrm{mol\,mol^{-1}}]$
airNO_x	Nitrogen Oxides (NO+NO_2)	Tracer	$[\mathrm{mol\,mol^{-1}}]$
airH_2O	Water, Water Vapour	Tracer	$[\mathrm{mol\,mol^{-1}}]$
	Foreground/Background Production Rates:		
(air-) ProdO3N	O_3 produced due to NO_x: $HO_2 + NO \longrightarrow OH + NO_2$	Tracer	$[\mathrm{mol\,mol^{-1}\,6\,h^{-1}}]$
(air-) LossO3N	O_3 lost due to NO_x: $NO_2 + O_3 \longrightarrow NO + 2\,O_2$	Tracer	$[\mathrm{mol\,mol^{-1}\,6\,h^{-1}}]$
(air-) LossO3Y	All other loss terms of O_3 (in total 61 reactions)	Tracer	$[\mathrm{mol\,mol^{-1}\,6\,h^{-1}}]$
(air-) LossCH4	CH_4 loss due to NO_x: $OH + CH_4 \xrightarrow{O_2} CH_3O_2 + H_2O$	Tracer	$[\mathrm{mol\,mol^{-1}\,6\,h^{-1}}]$
(air-) LossNOx	NO_x loss through HNO_3: $NO_2 + OH \longrightarrow HNO_3$	Tracer	$[\mathrm{mol\,mol^{-1}\,6\,h^{-1}}]$

(air-) ProdOH1	OH produced by: $H_2O + O(^1D) \longrightarrow 2\,OH$	Tracer	$[mol\,mol^{-1}\,6\,h^{-1}]$
(air-) ProdOH2	OH produced by: $HO_2 + O_3 \longrightarrow OH + 2\,O_2$	Tracer	$[mol\,mol^{-1}\,6\,h^{-1}]$
(air-) ProdOH3	OH produced by: $HO_2 + NO \longrightarrow OH + NO_2$	Tracer	$[mol\,mol^{-1}\,6\,h^{-1}]$
(air-) LossOH1	OH lost by: $OH + O_3 \longrightarrow HO_2 + O_2$	Tracer	$[mol\,mol^{-1}\,6\,h^{-1}]$
(air-) LossOH2	OH lost by: $OH + CO \xrightarrow{O_2} HO_2 + CO_2$	Tracer	$[mol\,mol^{-1}\,6\,h^{-1}]$
(air-) LossOH3	OH lost by: $OH + RH \xrightarrow{O_2} RO_2 + H_2O$	Tracer	$[mol\,mol^{-1}\,6\,h^{-1}]$
(air-) LossOH4	OH lost by: $OH + CH_4 \xrightarrow{O_2} CH_3O_2 + H_2O$	Tracer	$[mol\,mol^{-1}\,6\,h^{-1}]$
(air-) LossOH5	OH lost by: $OH + HO_2 \longrightarrow H_2O + O_2$	Tracer	$[mol\,mol^{-1}\,6\,h^{-1}]$
(air-) ProdHO21	HO_2 produced by: $RO_2 + NO \xrightarrow{O_2} HO_2 + R'CHO + NO_2$	Tracer	$[mol\,mol^{-1}\,6\,h^{-1}]$
(air-) LossHO21	HO_2 lost by: $RO_2 + HO_2 \longrightarrow ROOH + O_2$	Tracer	$[mol\,mol^{-1}\,6\,h^{-1}]$
(air-) LossHO22	HO_2 lost by: $HO_2 + HO_2 \longrightarrow H_2O_2 + O_2$	Tracer	$[mol\,mol^{-1}\,6\,h^{-1}]$
(air-) LossHNO3	HNO_3 lost by: $HNO_3 + OH \longrightarrow H_2O + NO_3$	Tracer	$[mol\,mol^{-1}\,6\,h^{-1}]$
	General Weather Factors:		
geopot	Geopotential height	ECHAM5	$[m^2\,s^{-2}]$
tm1	Dry air temperature	ECHAM5	[K]
tpot	Potential temperature	ECHAM5	[K]
tvirt	Virtual temperature	ECHAM5	[°C]
tte	Dry air temperature tendency	ECHAM5	$[K\,s^{-1}]$
rhum	Relative humidity	ECHAM5	[%]
aps	Surface Pressure	ECHAM5	[Pa]
um1	Longitudinal wind velocity	ECHAM5	$[m\,s^{-1}]$
vm1	Latitudinal wind velocity	ECHAM5	$[m\,s^{-1}]$
xlm1	Cloud water	ECHAM5	$[kg\,kg^{-1}]$
lim1	Cloud ice	ECHAM5	$[kg\,kg^{-1}]$
xite	Cloud ice tendency	ECHAM5	$[kg\,kg^{-1}\,s^{-1}]$
xlte	Cloud water tendency	EACHM5	$[kg\,kg^{-1}\,s^{-1}]$
tke	Turbulent kinetic energy	g3b	$[m^2\,s^{-2}]$
q	Specific humidity	g3b	$[kg\,kg^{-1}]$
qte	Specific humidity tendency	g3b	$[kg\,kg^{-1}\,s^{-1}]$
vervel	Vertical velocity	g3b	$[m\,s^{-1}]$
pblh	Planetary boundary layer height	tropo	[m]
tp_{clim}	Climatological tropopause pressure	tropo	[Pa]
tp_{PV}	PV tropopause pressure	tropo	[Pa]
tp_{WMO}	WMO tropopause pressure	tropo	[Pa]
PV	Potential vorticity	tropo	[PVU]
	Lightning:		
xnox	Lightning NO_x emission	lnox	$[kg(N)\,s^{-1}\,m^{-3}]$
fpscg	Cloud-to-ground (CG) flash frequency	lnox	$[s^{-1}]$
fpsic	Intra-cloud (IC) flash frequency	lnox	$[s^{-1}]$
fpsm2cg	CG flash frequency	lnox	$[s^{-1}\,m^{-2}]$
fpsm2ic	IC flash frequency	lnox	$[s^{-1}\,m^{-2}]$
npcanz	Number of lightning events	lnox	[-]
NOxcg	CG NO_x lightning emission	lnox	[kg(N)]
NOxic	IC NO_x lightning emission	lnox	[kg(N)]
telnox	Lightning NO_x emission tendency	lnox	$[mol\,mol^{-1}\,s^{-1}]$

	Convection:		
$conv_{type}$	Type of convection	convect	[-]
$conv_{top}$	Top level of convection	convect	[-]
$conv_{bot}$	Bottom level of convection	convect	[-]
massfu	Updraft mass flux	convect	$[kg\,m^{-2}\,s^{-1}]$
massfd	Downward mass flux	convect	$[kg\,m^{-2}\,s^{-1}]$
cv_{cover}	Estimated convective cloud cover	convect	[-]
cth	Convective cloud top height	convect	[m]
CAPE	Convective available potential energy	convect	$[m^2\,s^{-2}]$
	Cloud:		
$prec_{cover}$	Large scale precipitation cloud cover	cloud	[-]
aclc	Large scale cloud cover	cloud	[-]
condensation	Condensate in cloud covered part of gridbox	cloud	$[kg\,kg^{-1}]$
iwc	Large scale cloud snow/ice content	cloud	$[kg\,kg^{-1}]$
lwc	Large scale cloud liquid water content	cloud	$[kg\,kg^{-1}]$
mimelt	Large scale frozen precipitation melting	cloud	$[kg\,m^{-2}\,s^{-1}]$
misedi	Large scale ice sedimentation	cloud	$[kg\,kg^{-1}]$
$rain_{evap}$	Large scale rain evaporation	cloud	$[kg\,kg^{-1}]$
$rain_{form}$	Large scale rain formation inside cloud	cloud	$[kg\,kg^{-1}]$
rainflux	Large scale rain precipitation flux	cloud	$[kg\,m^{-2}\,s^{-1}]$
rhc	Critical relative humidity for natural clouds	cloud	[%]
$snow_{form}$	Large scale snow formation inside cloud	cloud	$[kg\,kg^{-1}]$
$snow_{subl}$	Large scale snow sublimation	cloud	$[kg\,kg^{-1}]$
snowflux	Large scale snow precipitation flux	cloud	$[kg\,m^{-2}\,s^{-1}]$

6.6. Methods Used

Throughout the main analysis multiple different analysis methods are used. This section shortly elaborates each of those analysing methods and their application.

6.6.1. Box Plots

The number of data points used within this study is very high (up to 21'226'800 points per variable if all weather pattern and time steps are taken into account). Box plots can be used to visualise the variability of those data in a compact way. Box plots do not assume any underlying distribution, which is an advantage over other statistical methods. Within this study so called Tukey box plots are used. The bottom and top of the box represent the first and third quartiles. The line within the box represents the median (i.e. the second quartile). In addition to the median, the mean is indicated by a black circle. The whiskers extend to the 1.5 time the Interquartile Range (IQR). If the minimum and maximum would result in a shorter whisker, the whisker would extend until those locations. Outlier are indicated by black crosses. Those points indicate observations which are either higher or lower than 1.5 times the first or third IQR, respectively. If a correlation or influence of a certain factor is expected or identified, the generated box plots will represent that factor along one dimension. In most cases, those factors are emission latitude, longitude, altitude, season or each weather pattern.

Box plots are mainly used when relations between two different variables are compared and one of both variables has discrete values (e.g. days after emission). If box plots are presented with respect to the time after emission, when the O_3 maximum is reached, those box plots will be merge to box plots containing information of six days. Otherwise 90 different box plots would need to be compared.

6.6.2. Statistical Significance Test: T-Test

While comparing two data subsets, a parametric test is applied to identify if both data sets are significantly different from each other or if both populations have an equal mean. This is known as hypothe-

sises testing, were the null hypothesis (H_0) and the alternative hypothesis (H_1) are denoted as:

- H_0: The samples are from the same population (equal mean)
- H_1: The means of two samples are different

The most famous significance test is the ”Student’s t-test”. This test assumes that both populations are normally distributed and have the same variance (Student, 1908). In this study, the variance and sample size is not always the same. Thus the ”Welch’s t-test” is applied in most cases. This test is designed for unequal variance and unequal sample size (Welch, 1947). In reality most observed data are non-normal distributed which generally limits the applicability of both test. Each weather pattern has 3’032’400 data points (for each variable), which results in 21’226’800 data points if all seven weather pattern are considered. Due to the high number of observations, the distribution of the sample means is most likely normal distributed, even though the sampling population is strongly non-normal. This concept is known as the central limit theorem and is applied in this study. It even applies if only a subset of the total population is considered.

Within this study the null hypothesis is rejected if the probability of faulty rejecting the null hypothesis is below 5%. The probability value (p-value) is only stated if the null hypothesis is not rejected. If the p-value is not indicated, the reader may assume that the p-value is below 0.05 and that the null hypothesis is rejected. In most cases the t-test is used to compare both seasons.

6.6.3. Statistical Significance Test: One-Way ANOVA & Tukey HSD

In many cases more than two populations are compared (e.g. different emission altitudes from the same season). If a combination of multiple t-test would be applied to test if all samples are significantly different, the likelihood of a type I error increases. A type I error indicates an incorrect rejection of a true null hypothesis (”false positive”). A type II error means that a false null hypothesis is incorrectly retained (”false negative”). To overcomes the increasing chance of a type I error, an one-way analysis of variance (ANOVA) is applied instead of multiple t-tests.

For the one-way ANOVA test the sample size does not need to be the same but needs to be normally distributed. However, this test is rather robust against non-normality. Again the central limit theorem is applied to overcomes this limitation. Theoretically, the samples should all have the same standard deviation. It is generally assumed that this test is robust, if the standard deviation differs. The Welch modification is used to overcome unequal variance (Welch, 1951).

The one-way ANOVA test is combined with the Tukey’s honest significant difference (HSD), to identify if all mean values that are significant difference from each other (Tukey, 1949). The null hypothesis is rejected if the probability of faulty rejecting the null hypothesis is below 5%. Again the p-value is not indicated if the null hypothesis is rejected.

6.6.4. Correlation Matrices

Many weather factors used in this study correlate with each other or location parameters (altitude, longitude or latitude). One example is specific humidity, which indicates the ratio between water vapour mass and the total air mass of an particle (Ahrens, 2012). It is well known that with increasing altitude water vapour decreases. This leads to a decrease of specific humidity. Additionally, higher temperatures at low latitudes allow higher water vapour masses to be stored in the same air parcel without condensation. Thus specific humidity correlates with temperature but also location parameters.

Correlation coefficients are used to assess the correlation between different weather factors. In general no perfect correlation coefficient exist. Two different correlation coefficients are used within this study, both focusing on different aspects of a correlation. The Pearson correlation coefficient analysis if a linear relation exists, whereas the Spearman rank coefficient gives high values if a monotonous relation exist. Both factors return values between -1 and 1. A high value indicates a strong correlation. A positive correlation is indicated by a positive correlation factors, whereas a negative value indicates a negative correlation.

Due to the high number of variables, correlation matrices are used. They provide a convenient visualisation method to quickly analyse the correlation between multiple variables. Scatter matrices provide an alternative method to visualise those correlations. They have the advantage that the correlation can be inspected visually. Due to the high number of data points, this method is to computational

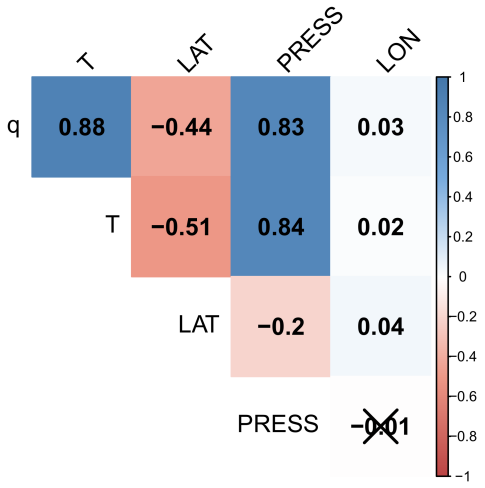

Figure 6.4: Correlation matrix for specific humidity (q), dry air temperature (T), latitude (LAT), pressure (PRESS) and longitude (LON). Within this matrix the Spearman rank coefficient is used.

intensive and therefore not used. Correlation matrices are always applied for each factor analysed. If a correlation is identified, a scatter plot (Section 6.6.5) is used to visually inspect the correlation.

As an example the correlation between specific humidity (q), dry air temperature (T) and location variables (LAT, LON, PRESS) is given in Figure 6.4. Here, the Spearman rank coefficient is used. The coefficient clearly indicates a strong correlation between specific humidity and dry air temperature. Both factors show similar correlation with pressure due to the dependency explained before. A weaker correlation exist for both factors with latitude. No correlation can be observed for any of those factors with longitude. There is no correlation between longitude and pressure. For those two location variables (pressure and longitude), the significance test indicates that the null hypothesis can not be reject.

6.6.5. Scatter Plots

To illustrate identified relations, scatter plots may be provided. If applicable a fitting function may be applied. In the most extreme case (if all weather pattern and time steps are taken into account), 21'226'800 different points will be plotted. When plotting this high number of points, over-plotting occurs. Over plotting of multiple points results in the loss of the information about the number of points at a certain location, within the scatter plot. To overcome this problem, density contours may be plotted above the scatter plot. In all cases the density is colour coded. A high density is indicated by red and a low by green. For better readability the points are slightly illuminated. This density adjustment is only applied if it adds information to the scatter plot. In some cases the range of the axis are selected such that the main area of interest is displayed. Similarly to box plots, scatter plots are used if the relation between two variables needs to be graphically represented. The main difference here is that both variables have continuous data values.

6.6.6. Weather Analysis and Forecasting Techniques

This study focuses on weather influences. Regular use is made of weather analysis techniques, typically used for weather analysis and forecasting. For example pressure systems are often identified by analysing the geopotential height at 500 hPa. If such a method is used, this method and its use is shortly elaborated prior to presenting the obtained results (in Chapter 8).

6.6.7. The Location Problem

Within the literature part of this thesis it became evident that many atmospheric conditions, chemical species or weather factors are location depended. Due to this dependency it is always complicated to attribute a certain influence to the weather factors itself, since other influences could still be present. Even though the correlation matrices indicate such a relation, a more sophisticated method is required to overcome this location problem. Most weather factors depend on latitude and altitude. No factor used within this study is known to depend on longitude. From this location problem, the following two

main question arise: (1) Is a certain relation behaving in the same manner independent of altitude and latitude? and (2) How does a specific value compare to standard (mean) values at a certain location?

For each of these area of interest, a specific method is applied. In most cases, due to space limitations within this thesis, no graphical representation is presented. Those methods are applied if the variable analysed has a high location dependency (identified by using correlation matrices, see Section 6.6.4). It is indicated if such a method is applied to obtain certain results.

Method 1
In the first method the atmosphere will be split up into regular bands along the dimension of interest. Temperature decreases with increasing altitude within the troposphere. As an example the atmosphere will be split up into bands of 50 hPa to assess the altitude influence. In each band, the mean production of O_3 in relation to the temperature will be calculated. Each of those relations will be compared between all different bands. If the comparison reveals a similarity for all bands, an independence of the altitude is assumed.

Method 2
The second method uses a similar approach. Again the atmosphere is split up into regular bands. Each value is compared to typical values (i.e. the mean) at the given location (i.e. by calculating the difference). It is expected that this method is used mainly for latitude (resulting in the latitude anomaly), whereas the first method is more interesting for altitude dependencies.

6.6.8. Verification
Verifying the results obtained is complicated due to the complex modelling scheme used. It is not an option and generally not possible to verify those relations by performing field measurement campaigns or something similar. Within this study no other simulation results are available which could be used to assess if the same relation exist for different model set-ups. Therefore, the results obtained are verified by comparing the obtain relation to earlier studies and are revisited based on reasoning.

6.7. A Few Practical Notes
- Due to the high number of analyses performed within this study, not all figures can be shown within this report. It will be indicated, if no graphical representation is provided (”not shown”).
- To reduce the number of points within a scatter plot, daily mean data are analysed. If a relation is identified, the same correlation is checked based on the original data (six hour resolution).
- By modelling convention, loss rates and loss concentrations are defined positive. The same methodology is used within this study.
- This report contains many different analyses. For better readability a short discussion is performed at the end of each analysis.
- During the analysis it turned out that air parcel with an O_3 maximum after the 33 day after emission are influenced by the same factors. If box plots are used in relation to the time of the O_3 maximum, those air parcel are grouped into a single box plot.
- The atmosphere is a highly dynamic system which has to some degree a chaotic behaviour. Further uncertainties and limitations are introduced by the methodology used within this thesis (e.g. by approximating certain weather factors at constant pressure altitudes). The main interest is on identifying trends of certain behaviours and their relations. Focus is on the mean or in the case of box plots on the first, second and third quartile.
- In the following chapters, the word ”tracer” refers the trace gas itself, whereas ”air parcel” refers to the air parcel in which the emission occurred. In the analysis, all data are obtained along the air parcel trajectory.

7

Variability of the REACT4C Data

Following the methodology (Chapter 6), this chapter analysis the variability of the REACT4C data. The O_3 maximum is analysed first, since the magnitude and time of the O_3 maximum impacts the resulting RF. Chemical reactions depend on the concentrations of all chemicals involved. To be able to analyse the different production and loss rates, the background and foreground chemical concentrations are analysed (Section 7.2). Afterwards, each production and loss rate is analysed (Section 7.3). The last analysis step, elaborates on the relation between O_3 and CH_4. In a final step, the most important results obtained in this chapter are summarised.

7.1. Variability of the O_3 maximum

This section analyses the variability of the O_3 maximum with the main focus on: (1) the time after emission when the O_3 maximum occurs, (2) the relation of the O_3 maximum and the instantaneous RF, (3) the location of the O_3 maximum. Additionally, the identified characteristics of the O_3 maximum are compared to previous studies.

7.1.1. Time of O_3 maximum after emission

Figure 7.1 shows the relative number of tracers in relation to the time after emission when the O_3 maximum is reached. Most air parcels reach their O_3 maximum within the first 21 days after emission. During winter about 47.5% (of the total 32400) and during summer more than 72% (of the total 24250) of all air parcels have an O_3 maximum within the first 21 days. A tracer emitted during summer has a higher chance to reach its maximum earlier after emission. It can be observed that during winter about 2.5% of the tracer have their maximum at the end of simulation. During summer this number reduced to 1%.

Each of the three summer pattern has a similar number of tracer at each time after emission, when the O_3 maximum is reached. The same observation holds for winter. Only the amount of tracer having an O_3 maximum within the first nine days is higher for WP3. Here, about 40% of those tracers, are emitted during WP3.

There is a significant altitude variability for both seasons. All emission altitudes have air parcels that have an O_3 maximum within the first 27th days. Afterwards, only tracers emitted at a high altitude reach an O_3 maximum. In this case, highest emission altitude (200 hPa) contributes the most tracers. At the same time the two highest emission altitudes (200 and 250 hPa) contribute the least to the number of tracers with an early O_3 maximum. Here, most tracers originate from the lower two emission altitudes (300 hPa, 400 hPa). This implies that the chance that an early O_3 maximum is reached, is higher for low emission altitudes.

The influence of the emission latitude is different (not shown). Air parcels which have their O_3 maximum at the same time after emission, originate from all seven emission latitudes. During winter the amount of air parcels reaching their O_3 maximum early, is higher for lower latitudes. After 21 days the amount of air parcels from higher latitudes increases. After 60 days, the number from each emission latitude becomes constant. A different tendency can be observed during summer (not shown). Even

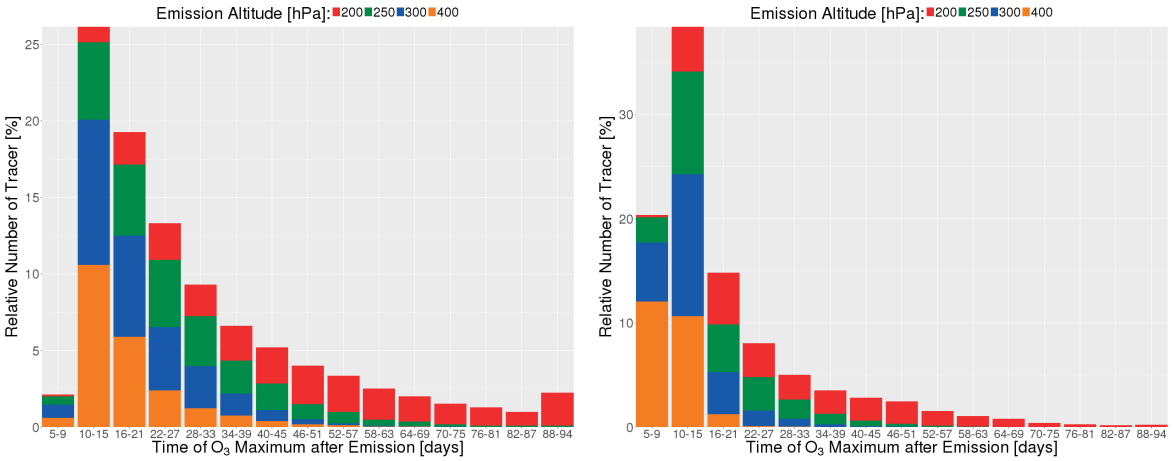

(a) Winter (b) Summer

Figure 7.1: Relative number of tracers in relation to the time after emission, when the O_3 maximum is reached.

though a similar trend for late O_3 maxima exists, the trend for early ones is not the same. Here, most air parcels originate from mid-latitudes (35°N, 40°N, 45°N).

No clear trend for the emission longitude can be observed (not shown).

7.1.2. Radiative Forcing (RF) vs O_3 maximum

In Section 2.1.1 the general concept of radiative forcing is introduced. From Equation 2.1 one can concluded that a higher concentration change of O_3, leads to a higher near surface temperature adjustment. However, from Section 5.5 it became evident that the calculation of the RF as well as the total climate impact is rather complicated, within REACT4C. Calculating the adjusted RF for O_3 is out of the scope of this thesis project. An estimation of the RF needs to be obtained, to identify a relation between concentration changes of O_3 and the resulting RF.

From the REACT4C (i.e. the rad4all submodel data) the net radiation flux change at the tropopause is calculated using the following relation:

$$F = (SW_p - SW) + (LW_p - LW) \tag{7.1}$$

Here, SW and LW give the net shortwave and longwave radiation flux at the tropopause SW_p and LW_p indicate the net shortwave and longwave radiation flux at the tropopause, perturbed due to the additional O_3 formed. In a second step, the resulting radiative flux change is integrated over the total simulation time (90 days). This calculation is therefore an estimate of the instantaneous RF. This approximation is considered to be sufficient within this study.

Figure 7.2 gives the total net radiation flux change at the troposphere, integrated over the 90 days of simulation, in relation to the maximum O_3 concentration (Figure 7.2a). Additionally, this instantaneous RF estimate is provided in relation to the time after emission when the O_3 maximum occurs (Figure 7.2b). Those results are valid for winter but a similar relations exist for summer. From Figure 7.2a it can be obtained that a higher O_3 concentration change most likely results in a higher net radiation flux which leads to a higher RF. The Spearman correlation factor is given to be 0.74. Figure 7.2b indicates that early O_3 maximum, most likely leads to higher instantaneous RF values. If the O_3 maximum is reached late, the approximate instantaneous RF is rather low which most likely results in a low CCF value.

Lacis et al. (1990) demonstrated that the climate impact for the same O_3 concentration change, differs with altitude. If the concentration change occurs in the lower troposphere the warming effect is lowest. It increases towards the upper troposphere and is highest close to the tropopause (in their study at 12 km). Above the tropopause, the warming effect decreases again. A cooling effect occurs if the concentration change occurs above 30 km. If the approximate RF (Equation 7.1) is normalised by the maximum O_3 concentration (not shown), a similar altitude behaviour exists. The normalised RF

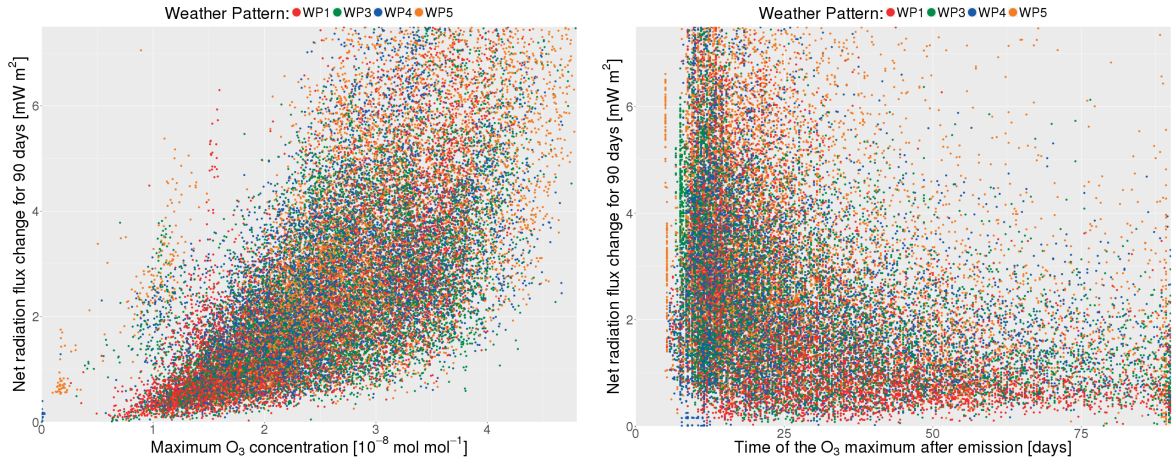

(a) O_3 maximum (b) Time of O_3 maximum

Figure 7.2: The net radiation flux at the tropopause, integrated over all 90 days of simulation. Results for each air parcel are indicated. Left: In relation to the maximum O_3 concentration. Right: In relation to the time of the O_3 maximum. In each figure the emission altitude is colour coded. Results valid for winter.

approximation is highest for the highest emission altitude and lowest for emissions occurring at 400 hPa. The decreasing effect at higher altitudes (as identified by Lacis et al. (1990)) is not identified. This is most likely caused by the fact, that most emissions occur below the tropopause. The results obtained in this thesis therefore represent the results of Lacis et al. (1990).

It is important to keep in mind that the calculation of climate impact by Equation 7.1 is only an approximation. The resulting CCF value can be different. Especially due to the altitude adjustment between the instantaneous and adjusted RF (see Figure 5.2). Still this approximation provides important insides that steers the following analysis in a certain direction. The resulting three most important questions are: (1) *"Which weather factor causes a higher O_3 maximum?"*, (2) *"Which weather factor causes an early O_3 maximum?"* and (3) *"Which weather factor causes a higher total CH_4 loss?"*.

Due to the long lifetime of CH_4, the RF for CH_4 is considered to be proportional to the total CH_4 loss. Therefore, the total CH_4 loss is only of interest.

7.1.3. Location of the O_3 Maximum: Altitude

Figure 7.3a gives the kernel density estimate (KDE) for the pressure location of the O_3 maximum. Most air parcel have an O_3 maxima below their emission altitude. A seasonal difference exist. During winter the O_3 maxima occurs at lower altitudes than during summer. For the lowest emission altitude during winter, most tracer have an O_3 maximum close to the surface. The KDE for summer indicates that no O_3 maximum occurs at the surface. This is most likely related to the fact that during summer tracer have the tendency to have an earlier O_3 maximum.

7.1.4. Location of the O_3 Maximum: Latitude

Most O_3 maxima occur at a latitude around 30°N. Figure 7.3b gives the KDE for the latitudinal location of the O_3 maximum. Additionally, most air parcel originating from higher latitudes, are transported to lower latitudes. Only a slight seasonal difference can be observed. During summer more O_3 maxima occur at higher latitudes, independent of the emission altitude. Changes in the solar zenith angle cause seasonal differences in the incoming solar radiation. The absence of O_3 maxima at high latitudes during winter is most likely related to a reduction of incoming solar radiation and the complete absence of incoming solar radiation at high latitudes (polar night). The incoming solar radiation influences the reaction rates involved in the tropospheric NO_x chemistry (see Section 4.4.3). Due to the absence of incoming solar radiation during a polar night, all reaction rates are reduced, which leads to less O_3 being produced or depleted. Therefore, no O_3 maxima occurs at very high latitudes during winter. During summer midnight sun occurs at high latitudes in the NH. Due to a higher incoming solar radiation and therefore higher reaction rates, O_3 maxima can occur also at higher latitudes.

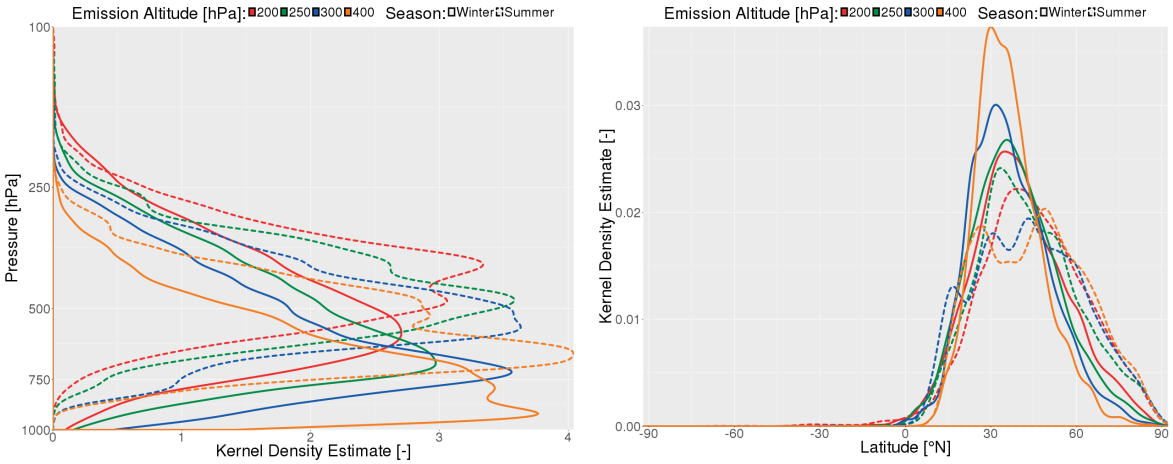

(a) Pressure Altitude (b) Latitude

Figure 7.3: Left: KDE of the pressure location of the O_3 maximum. Right: KDE of the latitudinal location of the O_3 maximum. The emission altitude is colour coded. Seasonal difference are indicated.

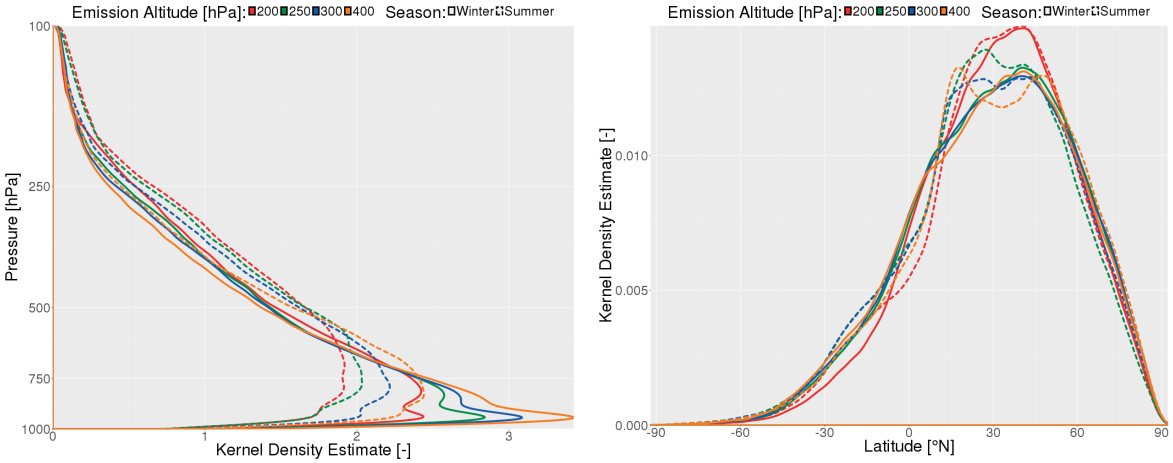

(a) Pressure Altitude (b) Latitude

Figure 7.4: Left:KDE of the pressure location of all air parcel after the O_3 maximum. Right: KDE of the latitudinal location of all air parcel after the O_3 maximum. The emission altitude is colour coded. Seasonal difference are indicated.

7.1.5. Location of the Tracer after the O_3 Maximum

In the time period from emission until the O_3 maximum, no air parcel reaches an altitude that is below the altitude of the O_3 maximum. After the O_3 maximum is reached, all emission altitudes have similar distributions in the atmosphere. Figure 7.4 illustrates this situation by providing the KDE for pressure altitude and latitude. Most air parcel stay close to the surface, whereas during summer air parcels stay at slightly higher altitudes. Most air parcel stay around an latitude of 30°N. After the O_3 maximum is reached, a substantial amount of air parcels is transported into the SH.

7.1.6. Discussion

Most air parcels have an O_3 maximum before the 22nd day after emission (see Figure 7.1). When the O_3 maximum is reached, the depletion rates of O_3 become higher than the production rate. This indicates that the production rate is low, which is most likely caused by low concentrations of NO_x (Equation 4.1, Section 4.4). It is assumed that almost all emitted NO_x is reduce (also found in Section 7.2.2). This indicates that most air parcels have a NO_x emission lifetime of about 22 days. This findings roughly agree with the lifetimes found by Stevenson et al. (2004) and the ones concluded by Grewe

et al. (2014a), while verifying the REACT4C data. A seasonal difference exist which is not mentioned by Grewe et al. (2014a), since only a single winter pattern is analysed. However, the performed analysis shows that during summer the NO_x emission lifetimes seems to be shorter.

In general, an air parcel is transported to a lower altitude to reach its O_3 maximum. Additionally, most O_3 maxima occur at lower latitudes. This suggests that at higher altitudes the production of O_3 dominates, whereas at lower altitudes the loss of O_3 dominates. The fact that most air parcel stay at low altitudes after the O_3 maximum, further indicates that loss processes dominate at lower altitudes. Further, the O_3 build-up is higher at lower latitudes. This roughly agrees with the results found by Köhler et al. (2008) and Köhler et al. (2013).

After the O_3 maximum occurred, all emission altitudes are similarly distributed in the atmosphere (Figure 7.4). Therefore, less variation of chemical background concentrations, weather situations and weather influences is expected (after the O_3 maximum occurred). Due to this lower variation mainly seasonal differences might be observed. This also indicates that the emission location has no impact on weather influences, which influence the depletion of O_3 and CH_4, after the O_3 maximum occurred. This means that the time between the O_3 maximum and the end of the simulation is of less interest. Therefore, the following analysis focuses on the time between emission and the O_3 maximum.

7.2. Variability of Chemical Background and Foreground Concentrations

Most chemical concentrations differ in the atmosphere. For example the concentration of NO_x tends to be very low in the lower troposphere but high in the upper troposphere and stratosphere. Additionally, seasonal differences exist. Foreground and background concentrations influence the production and loss rates (Section 4.4 and 5.4.4). Analysing those chemical species with respect to the time of the O_3 maximum, the season and the emission altitude and latitude, will provide the necessary basis to analyse important reaction rates. This section is intended to assess the variability of the chemical species. Main focus is on foreground concentrations. The explanation what causes the foreground variability is provided in Section 7.3. For completeness and due to the fact that background concentrations influence the background and foreground reaction rates, background concentration are discussed as well. For each emission, background concentrations are obtained along the air parcels trajectory, based on the location of the air parcel (see Section 6.3.1). Before assessing the variability of the most important chemical species, the relation between foreground and background concentrations and reaction rates is demonstrated (Section 7.2.1).

7.2.1. Relation Between Foreground and Background Concentrations

The background temporal concentration change of a chemical species is influenced by two factors (Section 4.4). Those two factors are the reaction rate coefficient and the concentrations of the chemical species involved. The foreground temporal concentration change is influenced by three different factors (Section 5.4.4): the background temporal concentration change, the foreground concentration and background concentration of all chemical species involved. Therefore, a link exist between the background and foreground. This section illustrates this link by analysing the foreground and background relation of the CH_4 depletion (Reaction R7), as an example.

The temporal concentration change of Reaction R7 depends on the background concentration of OH and CH_4. Equation 7.2 gives the temporal concentration change for this reaction, based on Equation 4.1. Here, k is the reaction rate coefficient given by Equation 7.3 (Atkinson, 2003). To simplify this equation for the following discussion, the overall reaction order is assumed to be two (i.e. $n = 1$ and $m = 1$).

$$\frac{d\mathrm{CH_4}}{dt} = k \cdot \mathrm{OH}^n \cdot \mathrm{CH_4}^m \tag{7.2}$$

$$k = 1.85 \cdot 10^{-20} \cdot \exp\left(2.82 \cdot \ln(T) - \frac{987}{T}\right) \tag{7.3}$$

Figure 7.5a illustrates the background depletion of CH_4. The reaction rate coefficient depends on the surrounding temperature and will be higher at higher temperatures. The reaction rate coefficient is

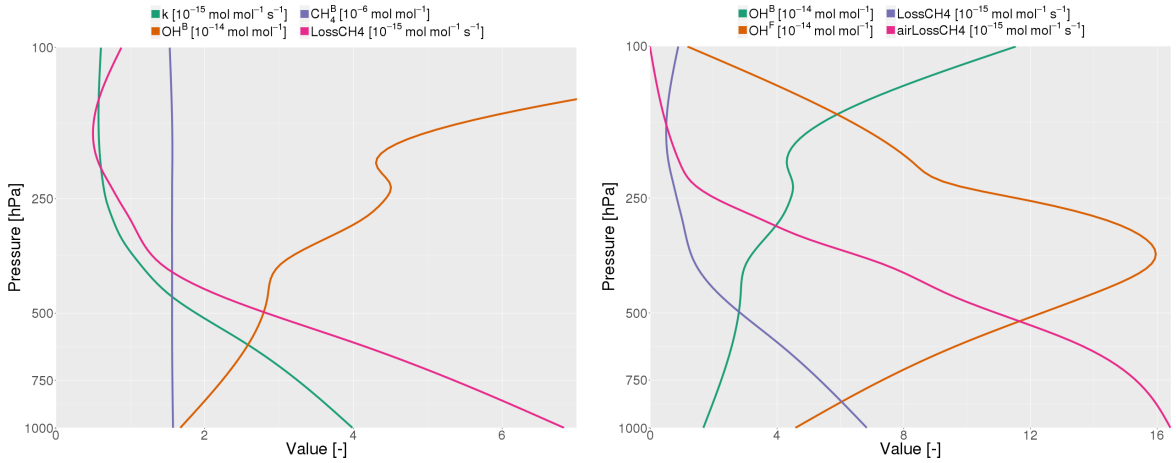

(a) Background (b) Foreground

Figure 7.5: Left: Mean values of all contributing factors that influences the background depletion of CH_4, in relation to altitude. The reaction rate coefficient (Equation 7.3) is given by k. Right: Mean values of all contributing factors, influencing the foreground depletion of CH_4, in relation to altitude. Both figures are valid for the time until the O_3 maximum is reached and are valid for winter. Superscript B and F denote background and foreground concentrations, respectively.

highest at the surface an decreases with increasing altitude, since the temperature decreases with increasing altitude in the troposphere. Close to the tropopause the reaction rate becomes rather constant with increasing altitude. The background concentration of CH_4 is constant with altitude and has only little impact on the altitude behaviour of the background CH_4 depletion rate. The background OH concentration increases with increasing altitude. This directly impacts the background depletion of CH_4. In the lower troposphere the reaction rate coefficient defines the reaction rate altitude behaviour. Above the tropopause the OH concentration increases exponentially which leads to an increasing reaction rate, even though the reaction rate coefficient tends to be low in the upper stratosphere.

Figure 7.5b illustrates the altitude behaviour of the foreground CH_4 depletion. Since aircraft emissions of CH_4 are neglected (Grewe et al., 2014a), only the foreground and background OH concentrations are the two chemical concentrations directly influencing the foreground CH_4 depletion. In the troposphere the foreground OH concentration tends to be higher than the background concentration. This results in higher foreground than background depletion rates of CH_4. However, above the tropopause the background concentration of OH tends to be higher than the foreground concentrations. This leads to lower foreground than background CH_4 depletion rates.

This example illustrates why analysing the variability of the foreground and background concentrations of the most important chemical species, is necessary to assess and understand the foreground production and loss of O_3, CH_4, OH and HO_2.

Figure 7.5 shows the mean vertical profiles of each factor influencing the foreground CH_4 depletion. However, this figures does not show the variability of each factor at each altitude. This variability can be high for certain chemicals. The trajectory of each air parcel also differs. If only mean vertical profiles would be analysed, information of each individual air parcel would be lost. Further, influences of the emission location and season are harder to identify. The following analysis therefore focuses on relations with emission altitude and season. This means that figures presented in the following sections will show relations with respect to season, emission altitude and the time when the O_3 maximum occurs.

7.2.2. Foreground NO_x Concentration at O_3 maximum

At the time of the O_3 maximum, the foreground NO_x concentration is non-zero. This indicates that O_3 will still be produced after the O_3 maximum occurs. The O_3 loss becomes dominate if the foreground NO_x concentration is reduced by about 90%. The mean concentration of foreground NO_x at the time of the O_3 maximum, in relation to the emitted NO_x concentration, is about 10% during winter and 9% during summer. Additionally, the mean tends to be slightly higher for earlier O_3 maxima and is only 6% if the O_3 maximum occurs at the end of simulation. Early O_3 maxima have a higher foreground NO_x

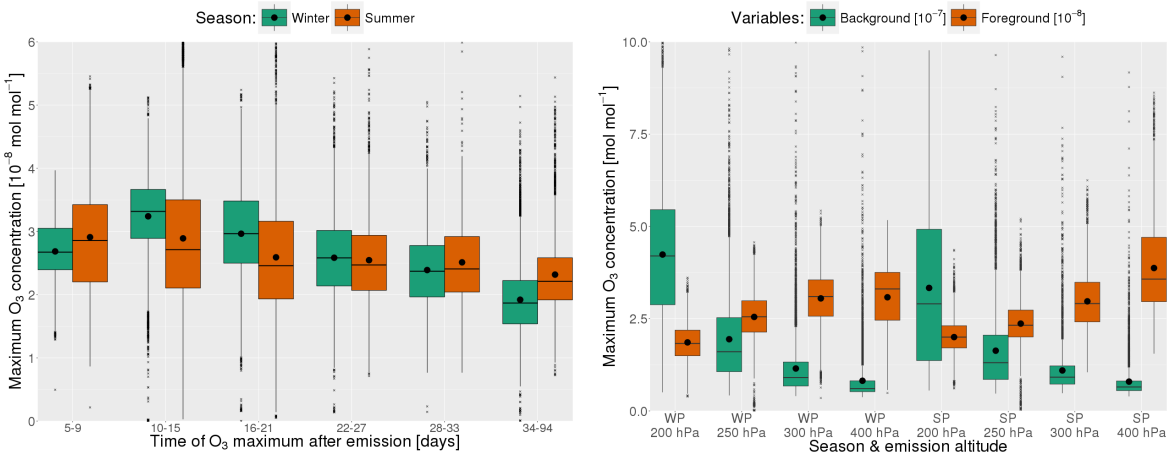

(a) Foreground (b) Foreground & Background

Figure 7.6: Left: Maximum O_3 concentration in relation to the time when the O_3 maximum is reached. The season is colour coded. Right: Maximum foreground and background concentration of O_3 in relation to the emission altitude and season. Background and foreground values are colour coded.

concentrations, when the O_3 depletion dominates. This indicates that the O_3 loss rates can dominate, even if their is still a substantial production of O_3.

7.2.3. Foreground O_3 Concentration

Figure 7.6a shows the maximum concentration of O_3 in relation to the time when the O_3 maximum occurs. A seasonal difference exist. During summer the difference in the mean is minimal for different times of the O_3 maximum. Additionally, the variability within the data is larger. The variability is generally lowest for late O_3 maxima. It is highest if the O_3 maximum occurs between the tenth and fifteens day after emission. Winter behaves differently. The lowest mean O_3 concentrations are given for late O_3 maxima. The mean increases the earlier the O_3 maximum occurs. However, it decreases if the O_3 maximum occurs before the tenth day after emission. Therefore, the time of the O_3 maxima has only little impact on the maximum O_3 concentration (for air parcel with an O_3 maximum before the 34th day after emission).

The emission altitude has a more significant impact on the maximum O_3 concentration (Figure 7.6b). For both season, the mean of the maximum O_3 concentration is higher if the emission occurs at lower

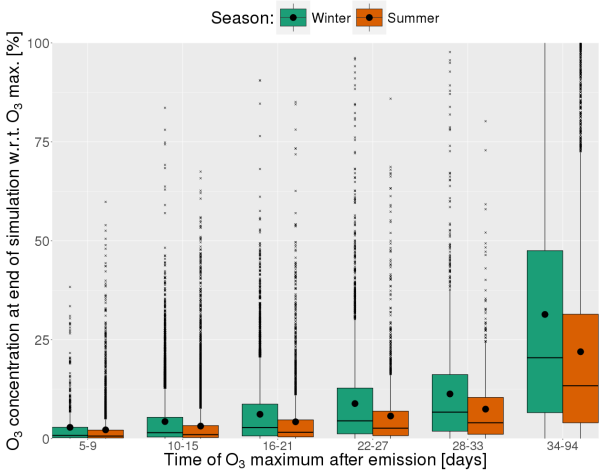

Figure 7.7: Concentration of O_3 at the end of simulation scaled by the maximum O_3 concentration of the given air parcel.

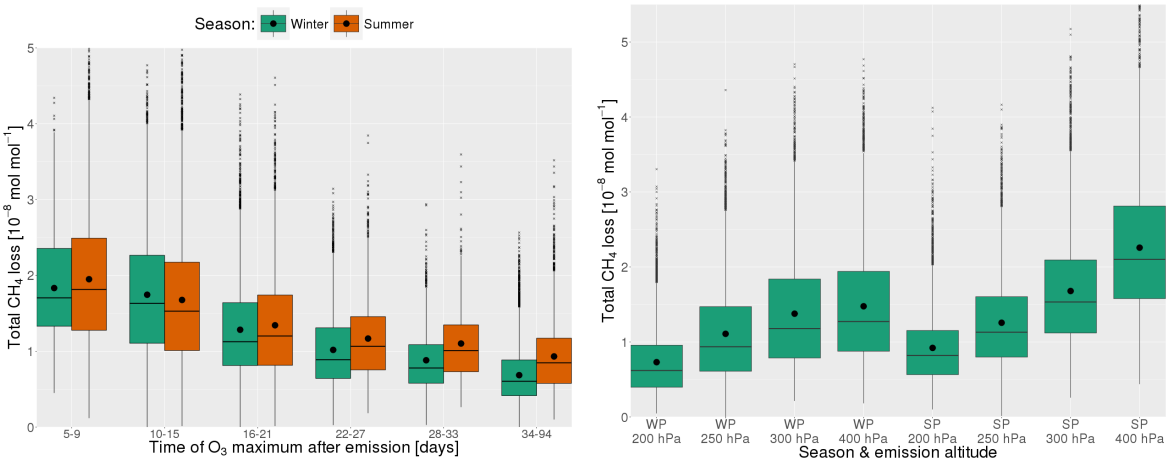

(a) Time of O_3 maximum

(b) Season & emission altitude

Figure 7.8: Left: Total foreground CH_4 loss in relation to the time after emission when the O_3 maximum is reached. The season is colour coded. Right: Total foreground and background loss in relation to emission altitude and season.

altitudes. The variability increases with decreasing emission altitude. Again seasonal differences are minimal. The main difference is that the mean value increases linearly with decreasing emission altitude during summer. During winter the mean increases linearly as well. However, the lower two emission altitudes have a mean with a similar magnitude (still the null hypothesis is rejected).

During winter the mean of the maximum O_3 concentration decreases monotonically with increasing latitude (not shown). The variability of the maximum O_3 concentration does not vary with emission latitude. No monotonic increase with increasing latitude is observed during summer. Only a small differences in the mean value exist. At the highest emission latitude, the mean O_3 maximum is slightly higher. The variability on the other hand increases with increasing emission latitude. During summer the highest concentration of O_3 occurs at the highest emission latitude for a tracer that originates from 400 hPa.

In Figure 7.7, the O_3 concentration at the end of the simulation is given, scaled to the maximum O_3 concentration. The mean increases in an exponential manner the later the O_3 maximum is reached. Higher O_3 concentrations are still present if the O_3 maximum occurs late. Additionally, the variability is lower for air parcels with an early O_3 maximum. There are tracers with a late O_3 maximum were all of the build up O_3 is lost again. Of course if the O_3 maximum is reached shortly before the end of simulation, the O_3 concentration tends to be high at the end of simulation.

7.2.4. Background O_3 Concentration

Generally, it is known that the O_3 concentration inside the troposphere is low. Close to and inside the stratosphere, the O_3 concentration increases rapidly (see Figure 7.6b). For tracer emitted at low altitudes, the O_3 concentration is low, whereas at high emission altitudes, the background O_3 concentration is higher. During summer the background O_3 concentration tends to be slightly lower than during winter. The background concentration of O_3 is always higher than the foreground concentration.

7.2.5. Foreground CH_4 Loss

Figure 7.8 shows the total CH_4 loss in relation to the time after emission when the O_3 maximum is reached. Compared to the maximum O_3 concentration, the seasonal differences are minimal. The mean value is highest for tracer with an O_3 maximum within the first fifteen days. For later O_3 maxima the total CH_4 loss is lower. The lowest mean value occurs if the O_3 maxima is between 34 and 94 days after emission. At the same time the variability is lowest for late O_3 maxima. Thus the total CH_4 loss tends to be higher, the earlier the O_3 maximum is reached.

Figure 7.8b shows the total CH_4 loss in relation to the emission altitude and season. Again the seasonal difference is minimal and only slightly lower magnitudes occur during winter. The following description is thus independent of season. If a tracer is emitted at higher altitude, the total CH_4 loss is

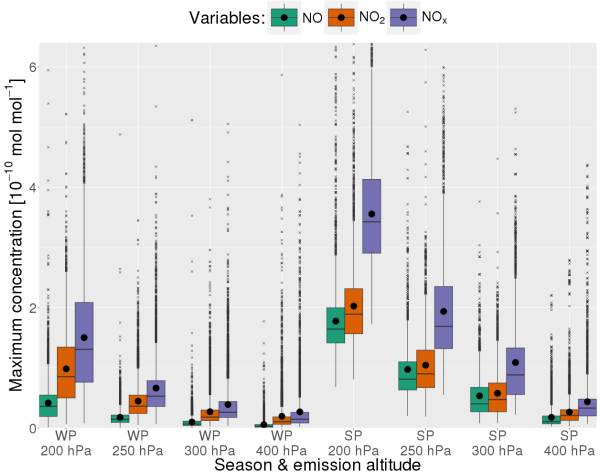

Figure 7.9: Maximum background NO_x (= NO + NO_2) concentration during the O_3 build-up, in relation to emission altitude and season. Different chemical species are colour coded.

lowest. The mean increases with lower emission altitudes. At the same time the variability increases. Therefore, a lower emission altitude favours a higher CH_4 loss. Due to the long perturbation lifetime of CH_4, a higher total loss leads to a higher negative RF. This results in a higher cooling effect by CH_4, for lower emission altitudes.

During winter about 35% (range between 23% and 56%) and during summer about 43% (range between 24% and 62%) of the total CH_4 loss is reached, when the O_3 maximum occurs. The mean value is independent of the time when the O_3 maximum occurs. Only for very late O_3 maxima, this value increases (O_3 maximum at 76-94 days after emission).

On average, the total CH_4 loss is reached 19 (during winter) and 21 (during summer) days after the O_3 maximum occurred. This value is again independent of the time when the O_3 maximum occurs. If the O_3 maximum is reached at a late stage, this value differs (not shown). In those cases the total CH_4 loss occurs at the end of simulation.

During summer the total CH_4 loss seems to be independent of the emission latitude (not shown). Here the mean value and the variability is constant with emission latitude. During winter the total CH_4 loss monotonically increases with decreasing latitude. The variability is highest at the lowest emission latitude.

7.2.6. Background CH_4 Concentration

CH_4 is a well mixed gas in the troposphere (see Figure 7.5a). No altitude difference below the tropopause exists. Above the tropopause the mixing ratio decreases slightly. A clear seasonal difference exist. During winter the global mean is $1.55 \cdot 10^{-6}\,\mathrm{mol\,mol^{-1}}$, which is lower than the global mean during summer ($1.61 \cdot 10^{-6}\,\mathrm{mol\,mol^{-1}}$). The seasonal differences are caused by varying surface emissions. Due to higher temperatures during summer, more CH_4 is emitted from the permafrost (Wuebbles and Hayhoe, 2002). The one-way ANOVA test and the Tukey HSD indicate that the null hypothesis for most combinations, can not be rejected. This indicates that the mean is most likely the same for all population and that only little inter-seasonal variability of the background CH_4 concentration exist. Therefore, the background CH_4 concentration is assumed to be constant for each season.

7.2.7. Background NO_x (= NO + NO_2) Concentration

Figure 7.9 gives an overview on the maximum background NO_x concentrations. The background concentration of NO_x differs with altitude and season. Independent of emission altitude, the mean NO_x concentration is always lower during winter, compared to the same emission altitude during summer. The NO_x concentration decreases with altitude in a heteroskedastic manner. At the time of emission about $3.1 \cdot 10^{-10}\,\mathrm{mol\,mol^{-1}}$ are emitted in each air parcel. This means that during winter the foreground concentration is always higher than the background concentration. At the highest emission altitude during summer, the mean background concentration is higher than emitted NO_x. This might

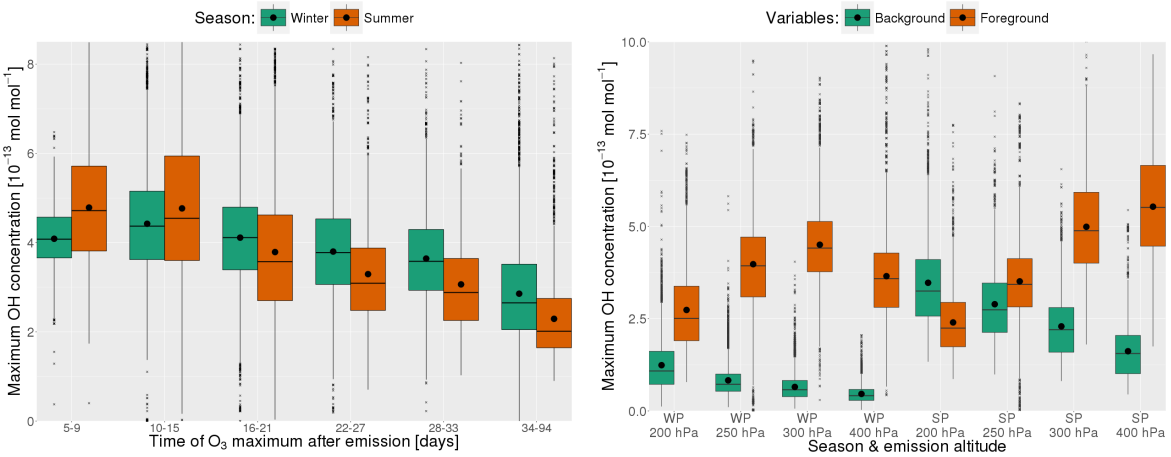

(a) Foreground (b) Foreground & Background

Figure 7.10: Left: Maximum foreground OH concentration until the O_3 maximum is reached. The season is colour coded. Right: Maximum foreground and background concentration of OH, until the O_3 maximum is reached. Background and foreground values are colour coded.

influence the foreground reaction rates during summer at this emission altitude.

7.2.8. Foreground OH Concentration

Figure 7.10b provides the maximum OH concentration in relation to the time of the O_3 maximum. The maximum OH concentration has a similar trend as the total CH_4 loss. This link is caused by the fact that CH_4 is only depleted by reacting with OH (Reaction R7). Based on Equation 7.2 a higher OH concentration leads to higher CH_4 loss rates. If the O_3 maximum occurs early, the mean of the maximum OH concentrations is highest. If the O_3 maxima occur within the first nine days, the foreground OH concentration has a slightly lower mean value, compared to air parcel with an O_3 maximum between the tenth and fifteenth day after emission. The mean value decreases the later the O_3 maximum occurs. Additionally, the variability is lower. Only little seasonal difference exist. For early O_3 maxima, the mean is higher during summer, whereas for late O_3 maxima the mean is higher during winter. The overall difference between early and late O_3 maxima is thus higher during summer.

The emission altitude influences the maximum OH concentration (Figure 7.10b). The lowest mean of the maximum OH concentration is given at the highest emission altitude (200 hPa). The mean value increases towards lower altitudes. Here, only the lowest emission altitude (400 hPa) differs during winter. In this case, the mean is lower compared to the two next higher emission locations (300 and 250 hPa). For other chemical species the variability changed with emission altitude. This is not the case for OH. The variability between different emission location is similar. Only the lowest emission altitude has a higher variability during summer. For all emission altitudes, the mean is slightly higher during summer.

7.2.9. Background OH Concentration

The background OH concentration behaves different with altitude than the foreground concentration (Figure 7.10b). The mean of the maximum OH concentration decreases with decreasing emission altitude, independent of season. Furthermore, the variability decreases with decreasing emission altitude. The global mean is higher during summer. During summer the mean value is more than twice as high (in magnitude), compared to the same emission altitude during winter. During winter the mean of the maximum background concentration is always lower than the mean of the maximum foreground concentration. The opposite is true for the highest emission altitude during summer. In this case the background concentration is higher than the foreground concentration.

7.2.10. Foreground HO_2 Concentration

Figure 7.11a gives the maximum foreground HO_2 concentration in relation to the time of the O_3 maximum. Compared to other chemical species, a clear seasonal difference exists. During winter the

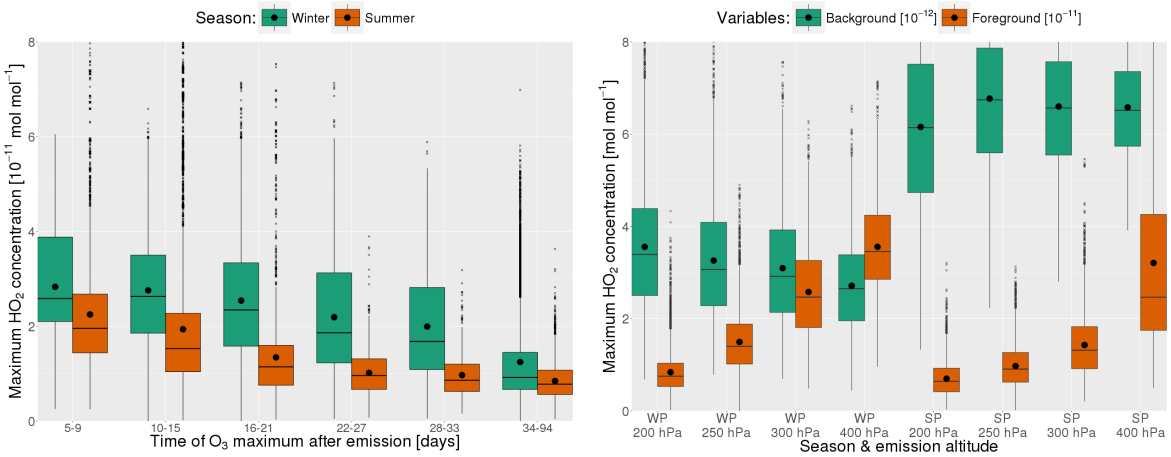

(a) Foreground (b) Foreground & Background

Figure 7.11: Left: Maximum foreground HO_2 concentration until the O_3 maximum is reached. The season is colour coded. Right: Maximum foreground and background concentration of HO_2, until the O_3 maximum is reached. Background and foreground values are colour coded.

mean foreground concentration is always higher. Additionally, the variability is higher during winter. In general, the mean of the maximum concentration is higher the earlier the O_3 maximum occurs. This concentration decreases with later O_3 maxima. The decreasing mean value is more dominant during summer.

Figure 7.11b give the same value in relation to the emission altitude. Overall, the mean of the maximum foreground HO_2 concentration and the variability increase with decreasing emission altitude. The global mean is higher during winter. This also explains the seasonal difference in Figure 7.11a. During winter the mean increases linearly with decreasing emission altitude, whereas during summer the mean increases in an exponential manner.

7.2.11. Background HO_2 Concentration

The background concentration of HO_2 is rather independent of emission altitude (Figure 7.11b). Only a seasonal difference exists. During summer the mean value is higher than during winter. During winter the HO_2 concentration slightly decreases towards lower emission altitudes. The variability is similar for each emission altitude. During winter the foreground mean of the maximum concentration is always higher than the background concentration. By definition this will result in high foreground production and loss rates (if HO_2 is involved). During summer the mean foreground concentration is also higher for the lower two emission altitudes. At the highest emission altitude the foreground mean is very close to the background mean. At this emission altitude the foreground production and loss rates will have lower values. The populations for each season seems to be very similar for all emission altitudes (Figure 7.11b). Still the one-way ANOVA test in combination with the Tukey HSD indicates that the null hypothesis is always rejected.

7.2.12. Discussion

The performed analysis showed that many chemical species have a high variability within the atmosphere. This holds for foreground and background concentrations. Seasonal difference exist which most likely cause the seasonal difference in the temporal development of O_3 and CH_4. The following discussion focuses on the foreground concentration changes of O_3 and CH_4. Background concentrations will not be discussed. Most comparable studies analysed the induced RF due to aviation attributed NO_x emissions. Within this discussion it is assumed that for both O_3 and CH_4, a higher concentration change always leads to a higher RF (see Figure 7.2a).

For lower emission altitudes Köhler et al. (2008) found a monotonic increase of the O_3 RF with increasing emission altitude. However, a non monotonic relation ship is given for NO_x emissions occurring from emission altitudes similar to the emission altitudes used within REACT4C. Those results are obtained by simulating global emissions within 16 different altitude bands. Köhler et al. (2008) emit-

ted different amounts of NO_x for each band. Therefore, this change from monotonic to non-monotonic behaviour is most likely caused by non-linearity within the tropospheric NO_x chemistry. Stordal et al. (2006), Grewe and Stenke (2008) and Fichter (2009) found a slightly decreasing global O_3 RF with decreasing emission altitude. The fuel consumption varies at different altitudes, due to different flight characteristics. Therefore, Stordal et al. (2006) and Fichter (2009) adjust the emitted NO_x for different emission altitudes. Those different emissions influence the resulting RF values.

Within this thesis the mean of the maximum O_3 concentration increases monotonically with decreasing emission altitude, which results in an increasing instantaneous RF with decreasing emission altitude. Still lower O_3 maxima at the highest emission altitude most likely lead to higher instantaneous RF than the same maximum O_3 concentration at a lower emission altitude would induce (see Section 7.1.2 and Lacis et al. (1990)). The relation between the instantaneous RF and the adjusted RF is altitude dependent (see Section 5.5.1). The ratio between both RF is always below one for emission altitudes below 200 hPa, whereas the lowest ratio is given at 250 hPa. At 200 hPa the ratio is higher than one resulting in a higher adjusted RF. Due to the monotonic behaviour of the maximum O_3 concentration, it is expected that the adjusted RF is higher at 200 hPa than at 250 hPa, even though higher concentration changes occur at 250 hPa. Due to low difference in the maximum O_3 concentration between the lower two emission altitudes during winter, it is expected that adjusted RF stays within a similar range. Thus the results obtained within this thesis appear to not agree well with the results found by Stordal et al. (2006), Grewe and Stenke (2008) and Fichter (2009). However, comparison of those results is limited since only concentration changes (of this study) are compared to RF results (from other studies).

During winter the maximum O_3 concentration decreases towards higher latitudes. However, during summer this concentration is relatively constant with latitude. Köhler et al. (2013) found a similar relation for the O_3 RF resulting from NO_x emissions within the REACT4C domain. Those results were obtained by emitting a constant of NO_x within latitudinal bands of 20°. Other studies performed by Grewe and Stenke (2008), Fichter (2009) and Dahlmann et al. (2016) show similar trends.

Seasonal differences for the maximum O_3 concentration were observed. In general, higher values are possible during summer. This indicates a higher chemical activity during summer. Gilmore et al. (2013) investigated the seasonal effect on the O_3 production efficiency, based on actual aircraft movements within the NH. During summer the production rate of O_3 due to aviation attributed NO_x, is about 20% higher and 15% lower during winter compared to the yearly mean. Stevenson et al. (2004) performed a similar study which resulted in similar observation. Therefore, both studies show similar trends, as found in this thesis.

The total CH_4 loss increases monotonically with decreasing emission altitude. Grewe and Stenke (2008) and Fichter (2009) found similar relations for the CH_4 lifetime change with altitude. Köhler et al. (2008) however found no real altitude difference for the RF of CH_4. As discussed before, this might be caused by non-linearity of the tropospheric chemistry.

Köhler et al. (2013), Grewe and Stenke (2008) and Fichter (2009) found decreasing CH_4 RF with increasing latitude. Within this thesis the same observation could be made during winter. However, during summer almost no difference could be observed. Therefore, findings in this thesis only partially agree with previous studies. Hoor et al. (2009) found seasonal dependent changes of OH due to aviation attributed NO_x. Here, the higher concentration changes occur during summer. Within this study a similar observation is made. Due to higher changes of OH, more CH_4 is lost. This indicates that the overall lower foreground concentration change of OH causes the lower CH_4 loss during winter. A seasonal difference was also found by Stevenson et al. (2004). During summer the same NO_x emission lead to higher negative RF values and thus to a higher cooling effect due to changes of the CH_4 lifetime. This seasonal difference is also observed in this thesis. The latitudinal dependency during winter is most likely caused due generally to lower incoming solar radiation and thus lower chemical activities at high latitudes (in the most extreme case: polar night). During summer however this effect is absent (midnight sun) which reduces the latitudinal dependency.

7.3. Production and Loss Rates

The previous analysis of the different chemical concentrations in the atmosphere allows to analyse the production and loss rates (see Figure 7.5). This is done by systematically analysing foreground and background reaction rates. For each emission, reaction rates are obtained along the air parcels

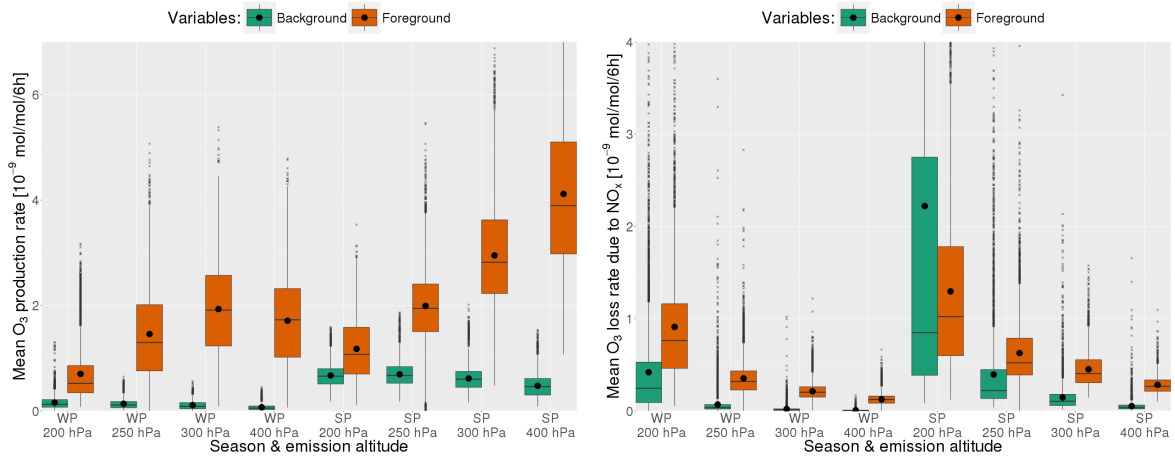

(a) Mean O_3 production rate due to NO_x

(b) Mean O_3 depletion rate due to NO_x

Figure 7.12: Left: Mean foreground and background O_3 production rate, during the O_3 build-up. Left: Mean foreground and background loss rate of O_3 by NO_x, during the O_3 build-up. In both figures: foreground and background values are colour coded.

trajectory, based on the location of the air parcel (see Section 6.3.1). If a reaction influences multiple important chemicals (O_3, OH and HO_2), this reaction is only discussed once.

7.3.1. O_3 Production Rate due to NO_x

Figure 7.12a shows the mean foreground and background O_3 production rate (Reaction R3), during the O_3 build-up. The production rate depend on the emission altitude. Higher emission altitudes have lower mean production values and thus do not allow high O_3 maxima. A heteroskedastic behaviour exist for the different emission altitudes within a season. Again the lowest emission altitude during winter has a lower mean than the next highest emission altitude. The background production rate is always lower than the foreground production rate. The global mean is higher during summer. Additionally, the mean decreases with increasing emission altitude.

The O_3 production depends on foreground and background HO_2 and NO concentration, which differ with altitude and season. Both chemical species have lower values during winter. During winter those lower concentration lead to lower O_3 production rates in the background.

For the tagging approach used, the ratio of the foreground and background concentration of both chemical species is crucial (Section 5.4.4 and 7.2.1). Based on the concentration analysis performed before, it becomes evident that the foreground to background ratio of NO tends to be higher during winter. The same is true for the ratio of HO_2. This means that if the background reaction rate would be the same for both seasons, more foreground O_3 would be produced during winter. Therefore, the higher background reaction rates during summer lead to higher foreground reaction rates, even though the foreground to background concentration ratios are lower.

The mean background production rate during winter at the lowest emission altitude is not smaller than at the next higher emission altitude. Additionally, the mean background of NO differs only slightly. Therefore, the foreground production rate is similar for the lower two emission altitudes, even though the HO_2 foreground value differs.

After the O_3 maximum is reached, the background O_3 production rate is higher than the foreground production rate (not shown). This is the case for all emission altitudes. Both production rates are slightly higher during summer. This shows that the O_3 production is low, when O_3 depletion dominates.

7.3.2. O_3 Loss Rate due to NO_x

Figure 7.12b shows the mean loss rate due to Reaction R15. The O_3 loss due to NO_x is significantly lower than the O_3 produced. An opposite altitude dependency, if compared to the O_3 production rate, is observed. The mean value increases with increasing altitude for both, background and foreground. The loss rate increases exponentially above the tropopause and tends to be lower within the troposphere. In general the O_3 loss is higher in the foreground than in the background.

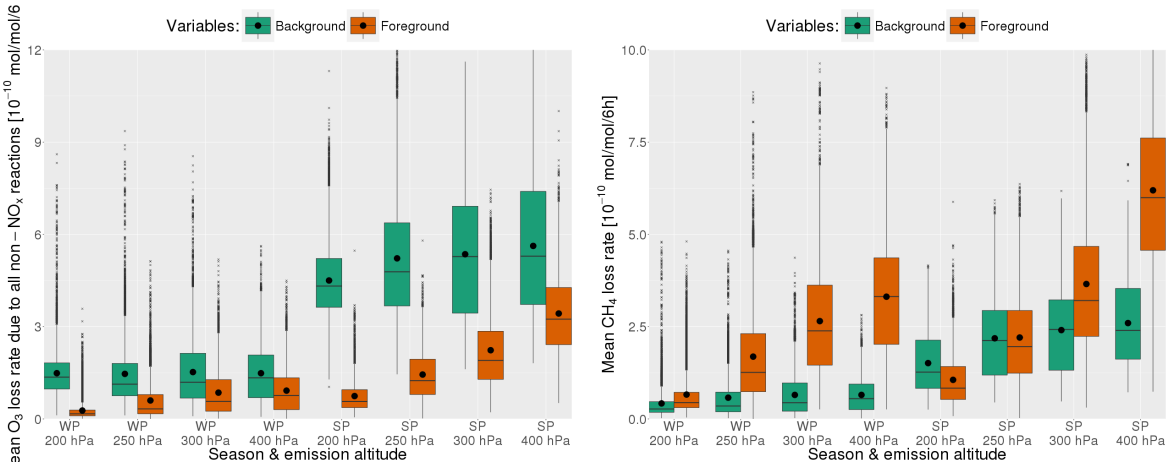

(a) O_3 loss rate due to all non-NO_x reactions (b) CH_4 loss rate

Figure 7.13: left: Mean foreground and background loss rate of O_3 due to all non-NO_x reactions during the O_3 build-up. Left: Mean foreground and background CH_4 depletion rate, until the O_3 maximum is reached. In both figures: background and foreground reaction rates are colour coded.

Even though the background O_3 concentration tends to be higher during winter, the loss rate tends to be lower. This is due to a seasonal difference of the background NO_2 concentration. Therefore, the lower background loss rates during winter can be related to lower NO_2 background concentrations.

The foreground to background ratio of the loss rate itself is higher during winter. The foreground to background ratio of O_3 is similar for both seasons. The ratio of NO_2 is higher during winter. Therefore, more foreground O_3 would be depleted during winter than during summer, if the background loss rate would be the same. Still due to higher background loss rates in summer, more foreground O_3 is lost in this season.

After the O_3 maximum is reached, the background loss rate of O_3 due to NO_x is higher, than the foreground loss rate (not shown). The mean value is the same for all emission altitudes and both seasons.

7.3.3. O_3 Loss Rate due to all non-NO_x Reactions

Figure 7.13a shows the mean O_3 loss rate due to all non-NO_x reactions, until the O_3 maximum is reached. A heteroskedastic behaviour exists for the foreground loss rate. For both seasons, the mean and the variability increases with decreasing emission altitude. Generally, the mean O_3 loss rate is higher during summer. At the same time the mean background O_3 loss rate is three times as high in magnitude, during summer. In the background the mean loss rate is rather independent of emission altitude.

In total, 61 reactions are combined in this loss term (see Table A.1, Appendix A). Thus it is impossible to analyse each background and foreground chemical species concentration involved. However, most of those reactions include OH. The background OH concentration is generally higher during summer, which explains the higher background reaction rate. The altitude difference in the foreground is caused due to higher O_3 values in the foreground and lower O_3 values in the background, at lower emission altitudes. This increases the foreground loss rate of O_3. The lower loss rates during winter are based on lower background loss rates. At the lowest emission altitude, the loss rate is similar to the next higher one. This is caused by the similar behaviour of the foreground O_3.

After the O_3 maximum is reached the background O_3 loss is higher, whereas the overall foreground loss rate is only slightly increased (not shown). The background loss rate is always higher than the foreground loss rate. Both are independent of emission altitude and season. Even though the mean loss rate of O_3 is very similar, more O_3 is lost after the O_3 maximum.

7.3.4. CH_4 Loss Rate

Figure 7.13b gives the foreground and background loss rate of CH_4 until the O_3 maximum is reached. The mean foreground loss rate is almost always higher than the mean background loss rate. Only

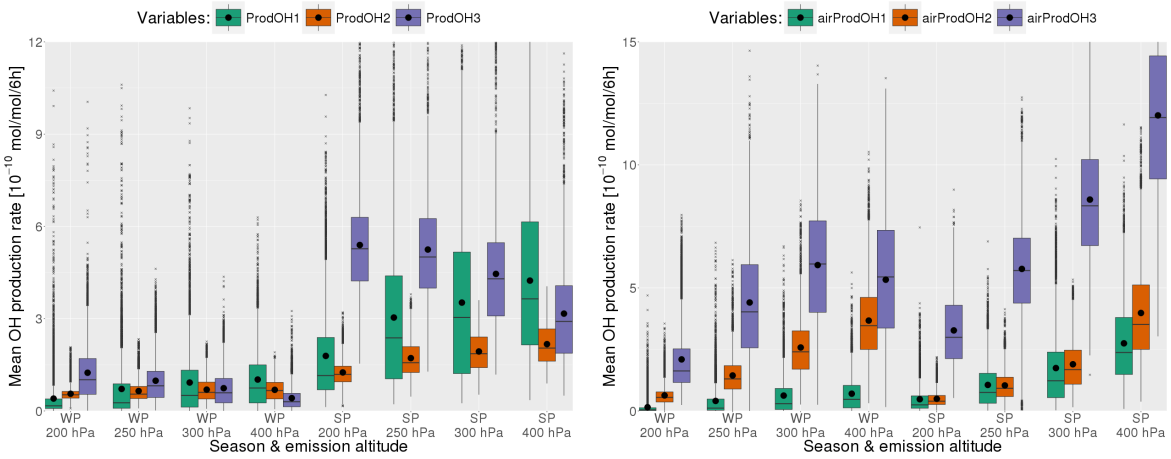

(a) Background (b) Foreground

Figure 7.14: Left: Mean background OH production rates during the O_3 build-up. Right: Mean foreground OH production rates during the O_3 build-up. In both figures: different OH production rates are colour coded.

during summer at the highest emission altitude is the background loss rate higher than the foreground loss rate. During summer more CH_4 is lost in the background. This is based on higher background concentration of CH_4. In the background the CH_4 loss rate slightly increases with decreasing emission altitude. However, the foreground loss rate increases with altitude. This is based on the foreground to background ratio of OH. This ratio increases with decreasing emission altitude (see Figure 7.10b). Thus more CH_4 is lost in the foreground at lower emission altitudes.

During winter the OH ratio at the lowest emission altitude is similar to the ratio of the next higher emission altitude. One would expect that therefore the CH_4 tends to be the same. However, the mean background loss rate is slightly higher, which has a higher influence on the foreground CH_4 loss. Thus more CH_4 is lost at the lowest emission altitude.

The lower foreground CH_4 loss at the highest summer emission altitude is caused by the fact that the background OH is higher than the foreground OH concentration. This leads to lover CH_4 losses in the foreground than in the background.

After the O_3 maximum is reached, the background CH_4 loss rate increases (not shown). Generally, more CH_4 is lost during the O_3 depletion (see Section 7.2.5). However, the mean foreground CH_4 loss rate decreases slightly after the O_3 maximum and is always lower than the background loss rate (not shown). The higher total CH_4 loss is caused by the fact that the time between the O_3 maximum and the time when the total CH_4 loss is reached, is longer than the time between emission and the O_3 maximum. Therefore, lower foreground loss rates still leads to higher CH_4 losses. Both, the mean foreground and background loss rate are similar for each emission altitude and season, after the O_3 maximum occurred.

7.3.5. OH Production Rate

Figure 7.14 provides the foreground and background production rates of OH, during the O_3 build-up. In the background the production rates are lower during winter. This is caused by lower background concentrations of all chemicals involved. The relative contribution of each reaction differs between foreground and background. This is most evident if HO_2 reacts with NO to form OH and NO_2 (airProdOH3, Reaction R3). In the background the reaction rate decreases with decreasing emission altitude, whereas in the foreground the production rate increases with decreasing emission altitude. The decreasing background production rate with emission altitude is based on the decreasing background NO concentration, with decreasing altitude. At the same time this lower background concentration leads to a higher foreground production rate, since the foreground NO concentration is fairly constant with emission altitude.

The contribution due to Reaction R19 (airProdOH1) is lower in the foreground than in the background. In the background the reaction rate increases with decreasing emission altitude, due to higher background H_2O concentration. The lower foreground production rate is based on higher background

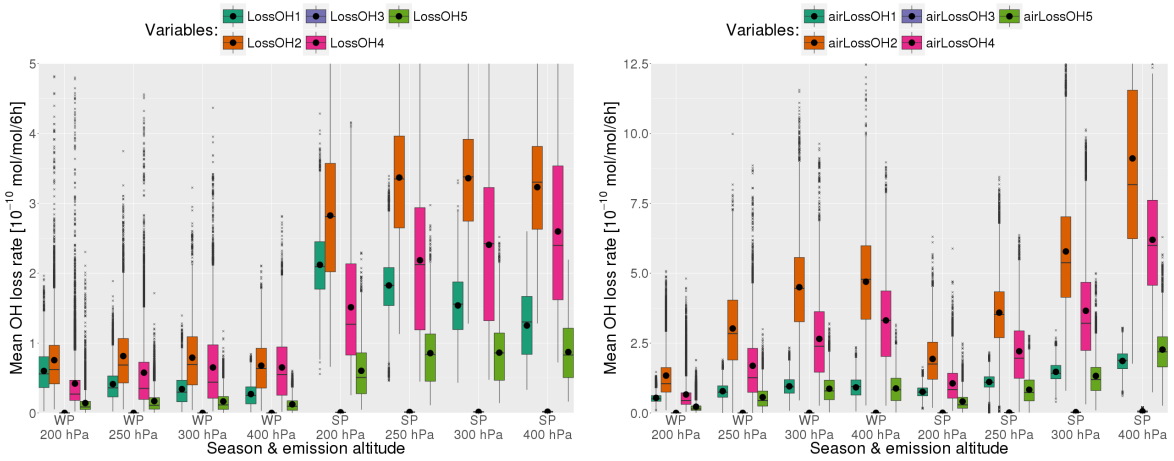

(a) Background (b) Foreground

Figure 7.15: Left: Mean background OH loss rates during the O_3 build-up. Right: Mean foreground OH loss rates during the O_3 build-up. In both figures: different OH loss rates are colour coded.

than foreground O_3 concentration. Thus less OH can be produced due to O_3.

The background concentration of HO_2 is rather constant with emission altitude (Figure 7.11b). The O_3 background concentration is higher at high emission location. One would expect that the background OH production rate by Reaction R17 (airProdOH2) would decrease with emission altitude. The opposite effect can be observed during summer. Therefore, the reaction rate coefficient of this reaction needs to be altitude dependent or influenced in another manner. The more pronounced emission altitude dependency in the foreground is based on higher foreground concentrations of HO_2, with decreasing emission altitude.

After the O_3 maximum is reached, the overall foreground OH production rate is lower and similar for each emission altitude (not shown). Since the foreground NO_x concentration is low during the O_3 depletion, almost no OH is produced due to Reaction R3. The production rate due to Reaction R17 is reduced due to lower HO_2 concentrations as well as decreasing O_3 concentrations in the foreground. Most air parcel stay at low altitudes were the H_2O concentration is high. This leads to most OH being produced due to Reaction R19, which at the same time reduces the foreground O_3 concentration.

7.3.6. OH Loss Rate

Figure 7.15 provides the foreground and background loss rate of OH, during the O_3 build-up. Overall the loss is higher in the foreground. This is due to higher foreground than background OH concentrations. The seasonal difference is higher in the background than in the foreground. In the background and foreground almost no OH is lost by Reaction R24 (airLossOH3). This is based on very low background concentrations of all chemicals involved. Since the contribution is so low, no further discussion is provided.

In the foreground and background most OH is lost by Reaction R1 (airLossOH2). The background loss rate is rather independent of the emission altitude. This is due to increasing OH but decreasing CO concentration with increasing emission altitude. The foreground loss rate increases with decreasing emission altitude, due to higher OH concentrations at lower altitudes.

The second highest contribution to the OH loss, is due to the depletion of CH_4 (airLossOH4). Due to increasing foreground OH concentrations with decreasing emission altitudes, more CH_4 is depleted at lower emission altitudes.

In the foreground, the OH loss due to Reaction R16 (airLossOH1) increase with decreasing emission altitude, whereas in the background the mean decreases. The decreasing trend in the background is based on lower O_3 concentrations at lower emission altitudes. In the foreground, the O_3 concentration is higher at low emission altitudes. This results in an opposite trend between foreground and background.

The second lowest foreground and background contribution is caused by Reaction R25 (airLossOH5). The altitude variation is higher in the foreground, due to increasing foreground OH and HO_2 concentrations and lower OH background concentrations, with decreasing emission altitude.The mean

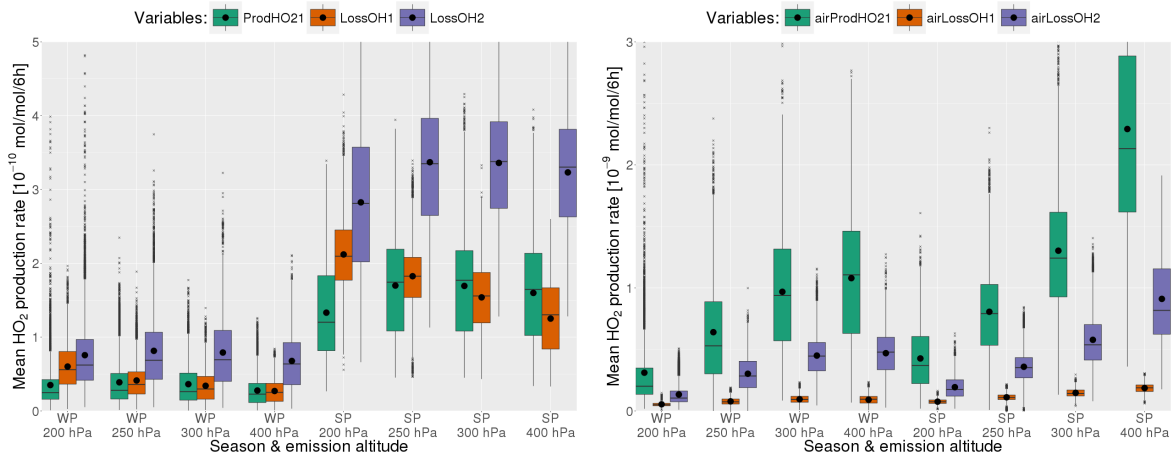

(a) Background (b) Foreground

Figure 7.16: Left: Mean background HO_2 production rates during the O_3 build-up. Right: Mean foreground HO_2 production rates during the O_3 build-up. In both figures: different HO_2 production rates are colour coded.

loss rate is similar to the next higher emission altitude, for the lowest emission altitude during winter. This is due to similar OH concentration at both emission altitudes.

After the O_3 maximum is reached, the contribution of the different OH loss rates differs and is independent of emission altitude and season (not shown). Overall lower mean OH loss occurs due to lower foreground OH concentrations. The two highest contributions change their position. Now most OH is lost due to the depletion of CH_4. In the tagging approach both depend only on the foreground and background concentration of OH. Therefore, the change of the background loss rates leads to those different foreground contributions. The background loss rate of CH_4 increases and is highest close to the surface. Since most tracer stay at low altitudes after the O_3 maximum occurred, higher loss rates occur than due to the destruction of CO (CO is fairly constant at low altitudes). Again almost no OH is lost by Reaction R24.

7.3.7. HO_2 Production Rate

Figure 7.16 provides the mean foreground and background HO_2 production rates until the O_3 maximum is reached. More HO_2 is produced in the foreground, which leads to higher foreground concentrations of HO_2 (Figure 7.10). The background production rates during winter are lower, caused by lower background concentrations.

In the foreground most HO_2 is produced to the additional foreground NO (airProdHO21, Reaction R26), whereas in most cases this reaction rate contributes the least to the background HO_2 gain. This is due to the high foreground to background ratio of NO.

After the O_3 maximum is reached, the relative contribution of all three reactions does not differ between foreground and background (not shown). All contributions are independent of emission altitude and season. Most HO_2 is produced due to Reaction R1 (airLossOH2), followed by the destruction of NO (airProdHO21, Reaction R26). The least HO_2 is produced by Reaction R16 (airLossOH1).

7.3.8. HO_2 Loss Rate

Figure 7.17 shows the mean foreground and background HO_2 loss rate for all contributing reactions, until the O_3 maximum occurs. The lowest contribution to the total HO_2 loss is due to Reaction R27 (airLossHO21). This is caused by low background RO_2 and thus low background loss rates. Most HO_2 is lost due to the additional NO (airProdOH3), followed by Reaction R28 (airLossHO22). Reaction R17 (airProdOH2) and R25 (airLossOH5) contribute similarly at high emission altitudes. At lower emission altitudes however, more HO_2 is lost due to Reaction R17.

HO_2 loss by Reaction R28 has a similar altitude behaviour in the foreground and background. In the background the mean production loss of HO_2, increases with decreasing emission altitude. Since this reaction only depends on the background concentration of HO_2, which is constant with emission

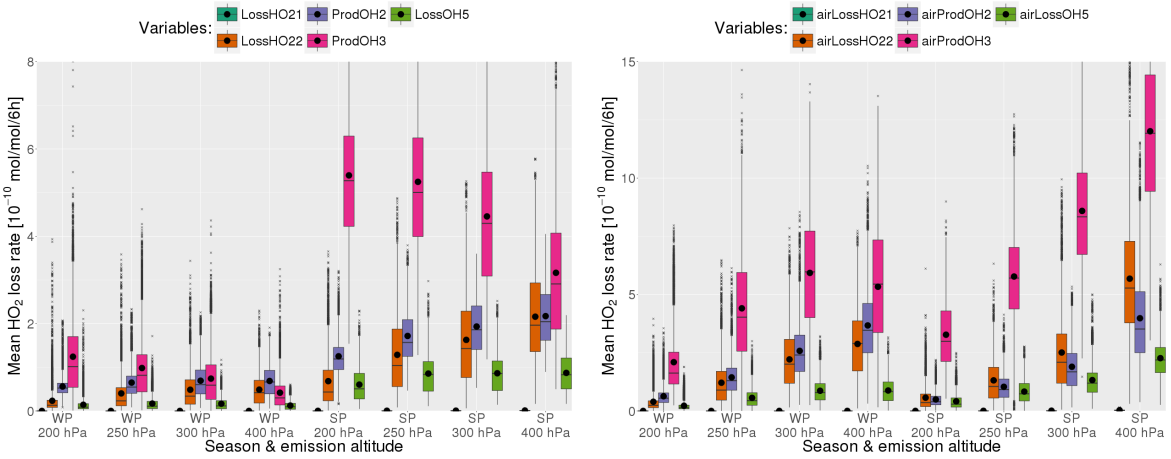

(a) Background (b) Foreground

Figure 7.17: Left: Mean background HO_2 loss rates during the O_3 build-up. Right: Mean foreground HO_2 loss rates during the O_3 build-up. In both figures: different HO_2 loss rates are colour coded.

altitude, this effect can only be caused by an altitude dependency of the reaction rate coefficient. In the foreground higher reaction rates are caused by higher foreground HO_2 concentrations.

After the O_3 maximum is reached, most foreground HO_2 is lost due to Reaction R28 (not shown). Less HO_2 is lost due to NO, due to lower foreground concentrations. The other loss rates do not change with respect to their relative contribution. Only the magnitude of their reaction rates decreases. Overall all reaction rates become independent of emission altitude. During summer slightly higher reaction rates occur, which are caused by slightly higher background reaction rates.

7.3.9. Discussion

It could be observed that a significant seasonal difference exist for the different background production and loss rates. Those seasonal differences are caused by seasonal difference in the background concentrations of all chemicals involved. During winter those tend to be lower, leading to a lower background production or loss rates, even though the respective reaction rate coefficient is only slightly influenced by season (i.e. generally higher temperatures during summer). A seasonal difference also exist for foreground production and loss rates. Due to lower background production and loss rates during winter one would expect that a similar strong seasonal difference exists in the foreground. However, the seasonal difference in the foreground is lower than for background processes. This is caused by a higher concentration difference between foreground and background concentrations of all chemicals involved. This concentration difference is higher during winter, which compensates the lower background chemical activity.

Seasonal difference in the total CH_4 loss are caused by different OH productions path ways for both seasons, lower background production efficiencies and different foreground OH concentrations. The highest seasonal difference is given for the OH production by H_2O, which is mainly caused by lower background H_2O concentrations during winter. Fuglestvedt et al. (1999) and Hoor et al. (2009) suggest that the specific humidity controls the OH production and thus the total CH_4 loss. This becomes most evident after the O_3 maximum is reached, since most air parcel stay at a lower altitudes, where H_2O concentrations tend to be higher.

Stevenson et al. (2004) demonstrated that in the first month after emission most OH is produced due to NO, the second most due to H_2O and the least due to HO_2. This relative contribution changes in the second month. Here, most OH is produced due to H_2O and almost non is produced by the other reactions. Those results are based on an actual aviation emissions during January. It is assumed that the O_3 build-up and the O_3 destruction occurs in the first and second month respectively. Thus the results from Stevenson et al. (2004) differ to the findings of this thesis. In this thesis, the OH production due to H_2O contributes the least during the O_3 build-up. Since Stevenson et al. (2004) used a perturbation method, it is expected that those differences are caused by non-linear compensation effects in the atmospheric chemistry and different emission altitudes used. Additionally, the emissions

occurred in both hemispheres. Due to different chemical compositions in the SH, different production pathways might occur which can not be assessed, by using REACT4C results.

Gilmore et al. (2013) identified that the O_3 production efficiency due to aviation attributed NO_x emissions is about 40% higher during summer and about 30% lower during winter, if compared to the annular mean. Similar results have been found by Stevenson et al. (2004). Therefore, the tendency obtained within this thesis, agree with the results of those two studies. However, the O_3 production efficiency difference between the foreground and background is lower during winter than during summer. Still, less O_3 is produced during winter, based on a lower background production efficiency.

In Section 7.2 it became evident that significant altitude differences in the foreground concentration exist. The same altitude difference can be observed for the production and loss rates. This leads to the conclusion, that those altitude differences are due to varying chemical activities. Those are mainly caused by different background concentrations, were the decreasing background NO_x and O_3 concentrations with altitude have the highest impact.

The highest emission altitude during summer behaves different than all other emission locations. This becomes evident by lower CH_4 depletion rates in the foreground than in the background. For all other emission locations the foreground loss of CH_4 is always higher than the background loss. This is ultimately caused by the fact that the foreground OH concentration is lower in the foreground than in the background, which is caused by overall lower OH production rates at this emission altitude. This effect is caused since the emitted NO_x is lower than the background concentration of NO_x. A higher NO_x emission in each air parcel would have caused a different behaviour and a higher total CH_4 loss at this emission altitude.

While analysing the loss of OH and HO_2 it became evident that in each case one chemical reaction did not contribute much to the total loss rate (Reaction R24 and R26). Computational time and storage space are always limited. Due to their insignificant contribution, both reaction show potential to be neglected in future studies. It is hard to assess if this low contribution is caused due to the model set-up used. A study performed by Hornbrook et al. (2011) compared simulations of Reaction R26 with real flight measurements. They found that their model underestimated the RO_2 concentration, and thus the HO_2 production of this reaction. They suggested that this is most likely caused by other sources of RO_2, which are not taken into account in their modelling approach. No complete list of all reactions taken into account by Hornbrook et al. (2011) could be obtained. Therefore, it is hard to estimate if the model set-up used by REACT4C suffers from the same underestimation of RO_2 concentrations. For future studies it should be investigated, if this is the case. If the model set-up does not suffer from this underestimation, future studies could neglect those reaction path ways to improve computational efficiency.

7.4. Relation Between O_3 and CH_4

The prior analysis of the production and loss rates, as well as the theoretical analysis given in Section 4 showed that the tropospheric chemistry of O_3 and CH_4 is highly linked. A correlation between the short-lived O_3 and the long-lived CH_4 climate impact is expected. This section analyses the correlation between both chemicals.

7.4.1. Maximum O_3 Concentration vs. Total CH_4 Loss

Figure 7.18a shows the total CH_4 loss in relation to the maximum O_3 concentration. The Spearman rank coefficient (0.66) indicates a strong correlation. The mean and the variability increase with increasing maximum O_3 concentration (heteroskedastic behaviour). The minimum total CH_4 loss increases with increasing maximum O_3 concentration. At low O_3 maxima, the total CH_4 loss can only reach a certain concentration. This effect is base on the foreground OH production. In Section 7.3.5 it became clear that OH is either produced due to the emitted NO_x or the foreground O_3. Even if no OH is produced by NO, a certain O_3 concentration leads to minimum foreground OH concentration, leading to a depletion of CH_4. During the O_3 build-up the biggest source of OH is NO. This allows for a higher total CH_4 loss, even if the maximum O_3 is lower. If O_3 would be the only source of OH, the variability at higher O_3 maxima would be lower. This becomes evident in Figure 7.18b, which gives the relative OH produced by NO in relation to the fraction of the total CH_4 loss and the maximum O_3 concentration. If most OH is produced by NO, the total CH_4 loss is below one indicating that the total CH_4 loss is lower than the maximum O_3 concentration. If however most OH is produced due to O_3 the total CH_4 loss is higher

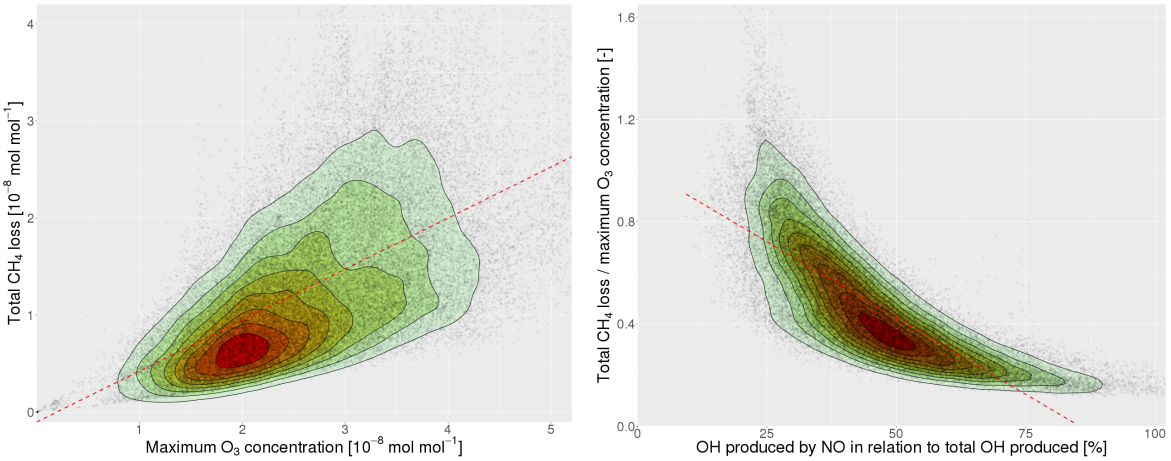

(a) Maximum O_3 concentration vs. total CH_4 loss

(b) OH produced by NO

Figure 7.18: Left: Maximum O_3 concentration in relation to the total CH_4 loss. ($R_{sp} = 0.66$, $R_{pe} = 0.62$) Right: Relative contribution of NO to the total OH production in relation to the ratio of the total CH_4 loss and the maximum O_3 concentration ($R_{sp} = -0.85$, $R_{pe} = -0.75$). Each scatter plot includes a density approximation of the number of points per location. Here, red indicates a high density, whereas a low densities are indicated by green.

than the maximum O_3 concentration. Therefore, the different contribution of NO to the foreground OH causes the variability between O_3 and CH_4. Furthermore, variability of all other OH loss reactions leads to a higher variability between O_3 and CH_4.

From Figure 7.14b it becomes evident that the highest relative contribution of NO to the total OH production occurs at the highest emission altitude. This indicates that air parcels originating from higher altitudes have a weaker O_3 to CH_4 relation because less OH is produced by the foreground O_3. This higher contribution of NO to OH in the foreground is due to a higher contribution in the background (see Figure 7.14a). This higher contributions are caused by higher NO background concentrations.

7.4.2. Discussion

Comparing those findings to other studies is complicated, since most studies concentrate on RF values. Holmes et al. (2011) performed an analysis of the relation between the RF of O_3 and CH_4 due to aviation attributed NO_x emissions. In this analysis, 21 different simulation results are compared with each other. For better comparison, all results are scaled to 1 Tg(N)yr^{-1}, since most simulation used different NO_x emissions. A strong anticorrelation between the short-lived O_3 and the long-lived CH_4 RF, across all considered models is observed ($R^2 = 0.79$). This relation indicates that the higher the short-lived O_3 RF, the higher the cooling effect of CH_4 is going to be. A similar relation could be identified in this study. Here, each concentration change of O_3 leads to a minimum CH_4 loss.

Some of the simulations (namely those from Hoor et al. (2009) and Myhre et al. (2011)) considered by Holmes et al. (2011) use a simplified version of the CH_4 RF calculation used by REACT4C (Section 5.5.2). This indicates that the variation in Holmes et al. (2011) in the O_3 to CH_4 relation is not caused by the using the same IPCC formula. It became evident that in the REACT4C model, the variability of the O_3 to CH_4 relation is caused by different contributions of NO to the OH production. It also became evident that this contribution is location dependent due to different background concentrations of NO. The different studies compared by Holmes et al. (2011) used different emission locations and emission altitudes. The background NO concentration most likely differs for each emission location used. This leads to different contributions of NO to the OH production and thus different CH_4 losses. It is therefore expected that the variability in the results found by Holmes et al. (2011) is influenced by comparing local to global emissions at different emission locations.

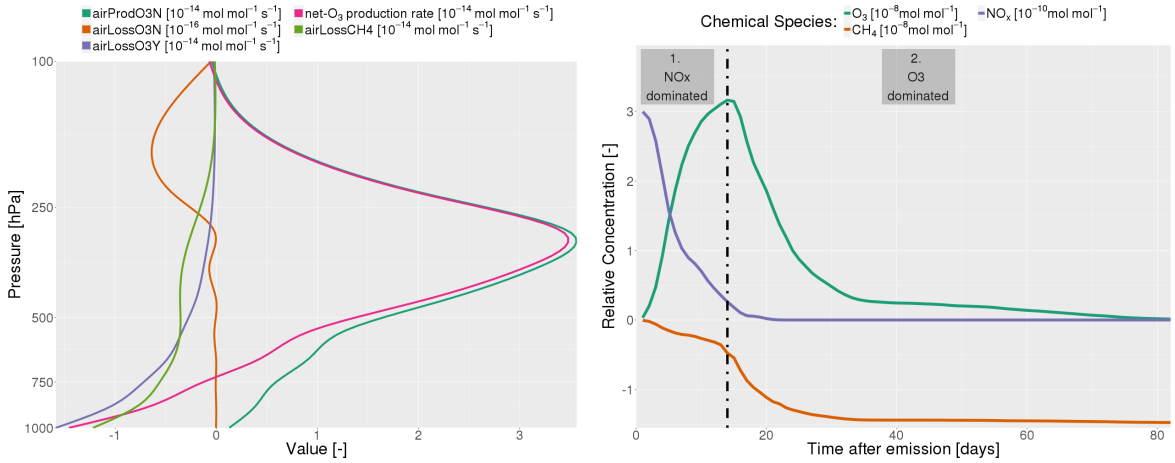

(a) Vertical profile (b) Temporal development

Figure 7.19: Left: Vertical profile of all production and loss rates related to O_3, the net-O_3 production rate and the CH_4 loss rate. Profile is based on the mean vertical profile of all winter pattern. Right: Temporal development of the emitted NO_x concentration and the resulting concentration changes of O_3 and CH_4, given for one emission occurring during winter (WP1, 200 hPa, 0°W, 40°N).

7.5. Results Summary

Based on the results obtained in this chapter, many important insides are obtained on the tropospheric NO_x chemistry as well as the temporal development of O_3 and CH_4. This section provides a comprised summary of the most important findings. In a first step, the vertical profile of the net-O_3 production and the CH_4 depletion are elaborated. In a second step, the temporal concentration changes of O_3 and CH_4 (due to the emitted NO_x), are discussed.

7.5.1. Vertical Profile of the Net-O_3 Production and the CH_4 Depletion

Figure 7.19a gives the mean vertical profile of the O_3 production and depletion rates and the CH_4 loss rate during winter. Each production and loss rate is discussed separately.

The O_3 production rate due to the emitted NO_x is highest, close to the emission altitude. This is caused by higher background production rates at higher altitudes. Additionally, the foreground NO_x concentration is highest in the early phase (i.e. early after emission). Above the tropopause, the foreground O_3 production decreases, which is caused by higher background NO_x concentrations. This leads to lower O_3 production rates, even though the background production rate is high. When air parcel are transported to lower altitude, the foreground concentration of NO_x decreases (due to the production of O_3), which leads to a low foreground production rate.

The depletion of O_3, due to NO_2 is highest in the stratosphere. The high background concentration of NO_x, leads to high background production rates. However, the significantly higher background than foreground concentration of NO_x, limits the O_3 depletion in the upper stratosphere.

The depletion of O_3 by all non-NO_x reactions is low in the upper and high in the lower troposphere. Most O_3 is depleted while reacting with H_2O. H_2O is generally highest close to the surface but very low close to the tropopause. Additionally, the foreground O_3 concentration tends to be higher at lower altitudes, since air parcels are transported to lower altitudes during the O_3 depletion. Overall the net-O_3 production rate (due to NO_x emissions in the upper troposphere), is high in the upper troposphere. The depletion of O_3 dominates at lower altitude.

The highest CH_4 loss rate is given close to the surface, which is caused by high O_3 depletions by reacting with H_2O. This forms OH which than reacts with CH_4, leading to a depletion of CH_4. Close to the emission altitudes a CH_4 loss rate is given. This is based on a OH production by NO at those altitudes (due to higher foreground NO concentrations). This formed OH leads to a depletion of CH_4.

These findings illustrate that emission location as well as seasonal differences in resulting concentration changes of O_3 and CH_4 (due to NO_x emissions), are related to varying background concentrations of all chemicals involved.

7.5.2. Temporal Development of O_3 and CH_4

Figure 7.19b gives the temporal concentration development of the emitted NO_x and the resulting concentration changes of O_3 and CH_4 for an emission during winter. Due to the different chemical processes during the O_3 build-up and the O_3 depletion, this section analyses both parts of the temporal development separately.

During the O_3 build-up, the O_3 and the OH chemistry are dominated by reactions including NO_x. At the time of emission the foreground NO_x concentration is highest and continuously decreases while the O_3 concentration increases. At the same time the high foreground NO_x concentration leads to a production of OH which leads to a depletion of CH_4. The non-NO_x loss rates of O_3 increase with decreasing NO_x concentration. After fourteen days the O_3 maximum is reached. At this point about 10% of the emitted NO_x are still present. Up to this point about 28% of the final total CH_4 loss are lost.

When the O_3 depletion dominates (after the O_3 maximum), the tropospheric O_3 and OH chemistry is dominated by reactions including O_3. NO_x still produces O_3 and OH. However, due to the relative low foreground NO_x concentration (less than 10% of the emitted concentration), this contribution is very low. After the O_3 maximum, the air parcel is at a low altitude, where most O_3 is depleted by reacting with H_2O. This leads to an increase in OH and thus a depletion of CH_4. After 35 days, this specific air parcel is transported to high altitudes, where the depletion of O_3 by reacting with H_2O is very low. This leads to the fact that the total CH_4 loss is reached after 37 days, even though their is still O_3 present. The rest foreground O_3 is depleted at high altitude, by reacting with NO_2. No OH is produced by this reaction, which leads to no further depletion of CH_4. In general, most (in this example about 72%) CH_4 is depleted based on reactions producing OH and depleting O_3.

8

Weather Influences on the Temporal Development of O_3 and CH_4

This chapter elaborates on the weather influences on the temporal development of O_3 and CH_4. Throughout Chapter 7 it became evident that most production and loss rates depend on the tracer location. The transport processes are therefore analysed in a first step. In a second step, the cause of those transport is identified (Section 8.2). Section 8.3 analysis the influence of temperature on the different production and loss rates. The influence of the background concentration of NO_x and HO_2 are analysed in Section 8.4 and 8.5. The last weather influence analysed for all emissions, is specific humidity (Section 8.6). The cause of specific tracer behaviours (identified in Section 6.4.1), are discussed in Section 8.7 and 8.8. From literature some weather influences (e.g. lightning) could be identified. Within this thesis not all of those influences had an impact on the temporal development of O_3 and CH_4. The reason why each of this factors has no impact is discussed in Section 8.9. Up to this point in the analysis, only season difference are analysed. The a last step, the inter-seasonal variability is assessed (Section 8.10). Finally, an overall summary of the most important results is provided (Section 8.11).

8.1. Transport Processes

While analysing the location of the O_3 maximum (Section 7.1.3 and 7.1.4), it became evident that all air parcels are transport to lower altitude, to reach their O_3 maximum. Additionally, most weather factors are location dependent. Therefore, this section focuses on analysing the atmospheric transport in relation to the time of the O_3 maxima. Atmospheric transport occurs in three dimensions, vertical transport, meridional transport and zonal transport. Each of the three dimensions is analysed separately. Air parcel originating from the same emission altitude have their O_3 maximum at similar altitudes. This suggests that air parcel with a late O_3 maxima stay at higher altitudes before the O_3 maxima occurs. Since the first maxima occur around the seventh day after emission, focus will be on the transport within those first seven days. This allows for better comparison, since the transport shortly after emission, seems to influence the time when the O_3 maximum occurs.

8.1.1. Vertical Transport

Figure 8.1a shows the mean vertical wind velocity of the first seven days after emission. Based on this figure it is identified, that the vertical transport within the first seven days impacts the time when the O_3 maximum occurs. The mean of the vertical wind velocity is highest if the O_3 maximum occurs within in first nine days. It is about $-6 \cdot 10^{-3}$ ms^{-1} (winter) and -4.10^{-3} ms^{-1} (summer). The mean vertical velocity decreases the later the O_3 maximum occurs. During winter the mean even becomes negative, if the O_3 maximum is reached after 28 days. Generally, the mean value is higher during winter than during summer. During summer the mean reaches almost zero after 33 days. This shows that upward motion is more common during winter than during summer.

In general, the mean vertical wind velocity is similar for each emission altitude (not shown). During summer this value is different for the lowest emission altitude. If the O_3 maximum occurs after the 21st

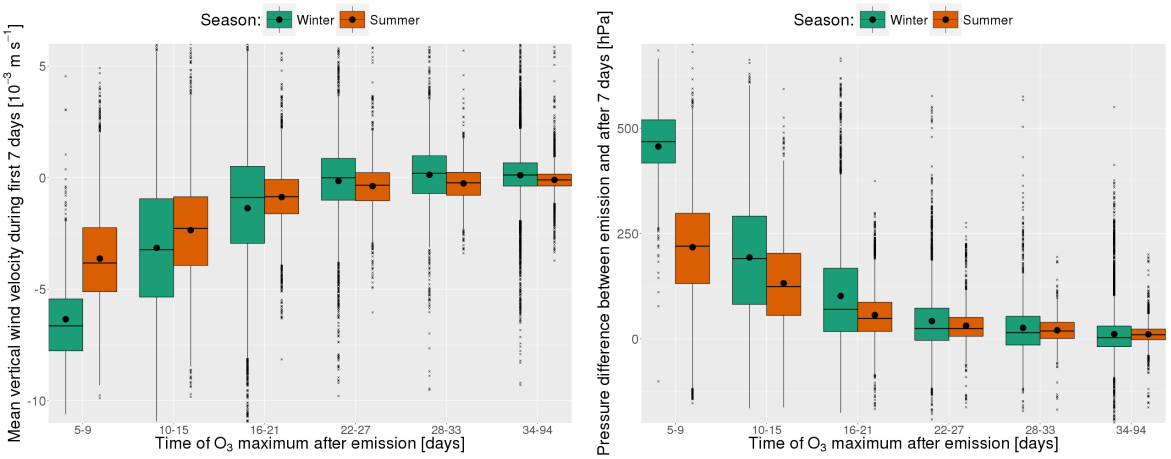

(a) Mean Vertical Wind Velocity

(b) Pressure Difference

Figure 8.1: Left: Mean vertical wind velocity of the first seven days after emission. Right: Pressure difference between the time of emission and after seven days. In both figures the season is colour coded.

day, the mean vertical velocity is positive. For the three higher emission altitudes, the mean value is negative. This indicates that during summer, air parcel with an O_3 maximum after the 21st day are transported upwards if the emission occurs at 400 hPa.

Figure 8.1b represent the pressure difference between emission and after seven days. Here, a similar observation is made. The earlier the O_3 maximum occurs, the lower the tracer is located after seven days. The higher mean vertical velocity during winter also results in a lower altitude. No influence of the emission altitude can be identified (not shown).

8.1.2. Meridional Transport

Figure 8.2a shows the mean meridional wind velocity during the first seven days after emission. Compared to the vertical transport, the variability is higher. If the O_3 maximum is reached within the first 21 days, the variability is lower. During winter, early O_3 maximum have a mean meridional wind velocity which is northwards. A seasonal difference exist for O_3 maxima after the 21st day. During winter the mean is negative, indicating an overall transport towards the equator. In summer the mean is positive. This means that those air parcels are transported polewards to higher latitudes.

The trend is the same for all five lower emission latitudes (not shown). Only the highest emission latitude (80°N) has a negative mean, which is about 3 m/s higher than all other emission latitudes. Therefore, tracer emitted close to the poles are transported fast to lower latitudes. The same observation is made if the latitude difference between the time of emission and after seven days is compared (Figure 8.2b). If the latitudinal difference is analysed between emission and the time of the O_3 maximum (not shown), it can be noted that if the O_3 maximum occurs late during the simulation, tracers emitted at a low latitude are transported towards higher latitudes. The mean indicates that most air parcel having an O_3 maximum towards the end of the simulation, are transported to higher latitudes (above 75°N).

No clear emission altitude difference is observed (not shown).

8.1.3. Zonal Transport

The zonal transport with respect to the time of emission, did not show any statistically significant trend. The only observation made is that tracer emitted at lower latitudes have higher zonal wind velocities. This is true for every tracer, independent of the time after emission when the O_3 maximum occurs. Additionally, no influence on the maximum O_3 concentration and total CH_4 loss, is identified.

8.1.4. Discussion

Based on the analysis performed, it can be concluded that the time of the O_3 maximum depends on the vertical transport in the atmosphere. The faster an air parcel is transported towards lower altitudes,

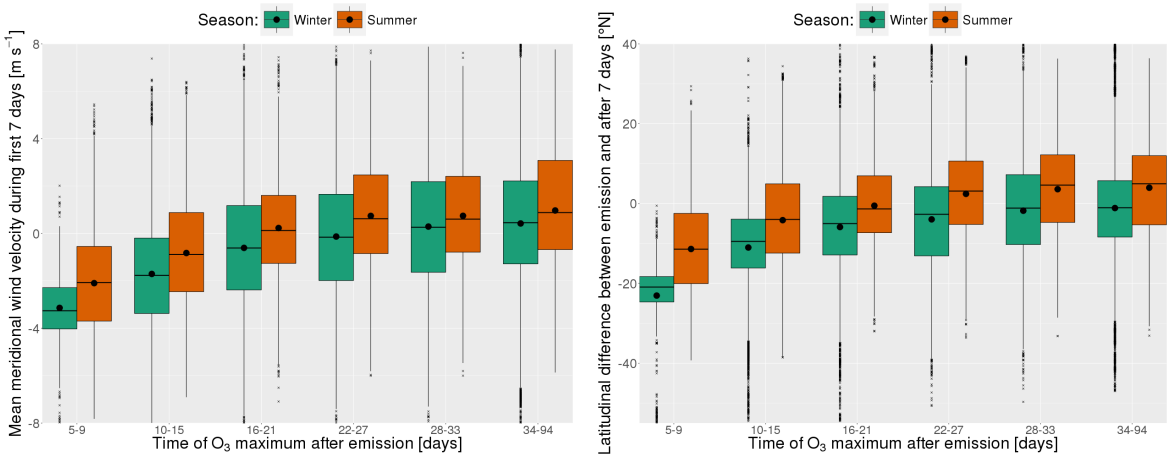

(a) Mean meridional wind velocity

(b) Latitude difference

Figure 8.2: Left: Mean Meridional Wind Velocity during the first seven days. Right: Latitude difference between emission and after seven days. In both figures the season is colour coded.

the earlier the O_3 maximum occurs. If the air parcel stays close to the emission altitude or is even transported to higher altitudes, the O_3 maximum occurs late.

The transport processes itself do not influence the production and loss rates. Therefore, transport processes are not the cause why an air parcel has an earlier O_3 maximum, if a fast transport to lower altitudes and latitudes occurs. It is rather expected that air parcel with an early O_3 maximum are transported to an area with a higher chemical activity. Due to this higher chemical activity, the air parcels O_3 maximum occurs earlier.

In Section 3.3 it became evident that subsidence occurs in high pressure systems. Air parcel with an early O_3 maximum have a high downward motion, which is most likely caused by subsidence inside a high pressure system. Tracer are transported to higher altitudes due to the absence of subsidence in a low pressure system. Much uncertainty remains on the meridional transport due to a high variability within the data set.

Based on those observations made, two main areas of interest arise. First, it is necessary to identify the cause of the downward and upward motion. It became evident that this transport is most likely caused by different pressure systems (Section 8.2). Secondly, it needs to be understood why an air parcel transported to lower altitudes experience a higher chemical activity (Section 8.3).

8.2. Geopotential and Geopotential Height

This section analysis the geopotential. First, the concept of geopotential is explained and how it can be used to identify certain weather situation. Afterwards, multiple different weather analysis techniques are applied to characterise the weather situation that an air parcel experiences.

8.2.1. Definition: Geopotential

All definitions and information related to geopotential are based on Ahrens (2012). The geopotential gives the work necessary to lift a unit mass from sea-level to a certain pressure height against gravitation. It is given by:

$$\Phi(h) = \int_0^h g(\phi, z)dz \tag{8.1}$$

Here, $g(\phi, z)$ is the gravitational acceleration which depends on altitude (z) and latitude (ϕ). The geopotential is often expressed as geopotential height. The geopotential increases with altitude and is generally higher at lower latitudes. Geopotential height is an approximation of the actual height of a pressure surface above the mean sea-level. It is calculated by dividing the geopotential by the Earth's standard gravitation (g_0):

$$Z(h) = \frac{\Phi(h)}{g_0} \tag{8.2}$$

In weather analysis and forecasting the geopotential height is analysed by using three different methods. First, the geopotential height anomaly is calculated by comparing the value at a certain pressure altitude with average values. Normally monthly averages are considered. From the ideal gas law it is known that temperature influences the volume of an air parcel. The geopotential height at a given pressure altitude is an approximation of the altitude above sea-level for this specific pressure level. Therefore, geopotential height is influenced by temperature. By analysing the geopotential height anomaly, one can therefore identify regions that are warmer or colder than usual.

In the second method, the geopotential at 500 hPa is analysed. By using this method, cyclones and anticyclones can be identified. Not all pressure or frontal systems reach to the surface. By analysing the surface pressure, not every cyclone and anticyclone would be identified. Analysing the 500 hPa layer eliminates this uncertainty. If 500 hPa geopotential charts would be analysed, one could even differentiate between high pressure systems or high pressure ridges. Analysing weather maps for each tracer is not applicable, due to the high number of emissions.

The last method uses the geopotential height to estimate the thickness of a certain layer. This is simply performed by calculating the difference of the geopotential height of two pressure levels. The 1000-500 hPa layer thickness is calculated by:

$$dH_{1000-500hPa} = Z(500hPa) - Z(1000hPa) \tag{8.3}$$

The layer thickness is proportional to the mean virtual temperature of the layer. Virtual temperature indicates the temperature of a moist air parcel, a theoretical dry air parcel would have, if it would have the same density and pressure as the moist air parcel. Therefore, the layer thickness is a function of the layer temperature and moisture content. A higher thickness corresponds to a higher mean virtual temperature and therefore to a higher temperature and moisture content. Typical layer analysed are 1000-500 hPa, 850-500 hPa or 850-250 hPa.

To overcome latitudinal biases, result are also presented by calculating the latitudinal anomaly. This is done by adjusting each value to the mean at the given latitude (method two, see Section 6.6.7).

8.2.2. Seasonal and Monthly Geopotential Anomaly

The geopotential anomaly was calculated in relation to monthly and seasonal mean values. Further, multiple pressure levels (850, 500 and 250 hPa) were analysed. However, the analysis of the monthly and seasonal data were inconclusive. No clear influence on the time after emission when the O_3 maximum occurs, the maximum O_3 concentration, the total CH_4 loss nor on the different production and loss rates, could be identified. This is most likely linked to the fact that the monthly mean is based on a one year simulation, only. Since weather systems can exist for longer time spans, the mean value of the same month is to similar. In daily weather analysis and forecasting, the monthly mean is based on multiple years (Ahrens, 2012). Therefore, the mean is less biased towards a particular weather situation during a particular year.

8.2.3. Geopotential at 500 hPa

Figure 8.3a shows the mean geopotential at 500 hPa during the O_3 build-up. A seasonal difference exist. Overall, the values tend to be higher during summer. This is caused by higher mean temperatures during summer. The variability is higher during winter. Figure 5.1 shows the geopotential at 250 hPa for each weather pattern at the time of emission. Those representations already suggest that each winter pattern has a higher variability in the geopotential than each summer pattern has. Since this variability exist at 250 hPa, it also exists at 500 hPa.

For both seasons the mean geopotential at 500 hPa is higher if the O_3 maximum occurs earlier. This trend is more evident during winter which relates to the general higher variability. During winter the greatest difference between the means is 3700 $m^2\,s^{-2}$, while during summer the difference is only 1700 $m^2\,s^{-2}$.

Figure 8.3b shows the geopotential latitudinal anomaly during the O_3 build-up. A positive value indicates that the geopotential is higher than the mean value at the specific latitude. A negative anomaly indicates a lower geopotential. Seasonal differences are eliminated, by analysing seasonal latitudinal

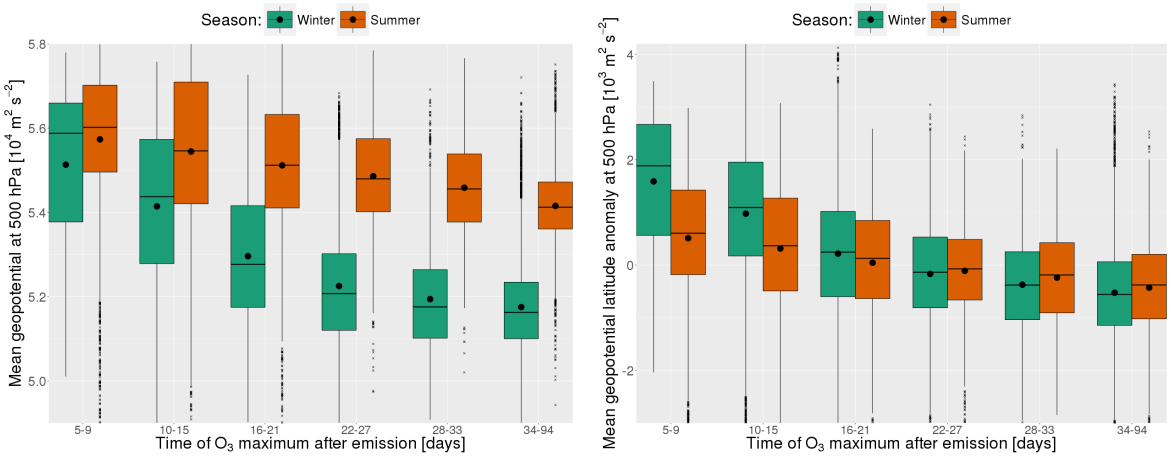

(a) Geopotential (b) Geopotetial latitude anomaly

Figure 8.3: Left: Mean geopotential at 500 hPa during the O_3 build-up. Right: Mean geopotential latitude anomaly at 500 hPa during the O_3 build-up. Latitude anomalies are calculated by using method two (described in Section 6.6.7). To calculate the latitudinal anomaly, seasonal values are used. In both figures the season is colour coded.

means. The mean value is positive if the O_3 maximum occurs before the 22nd (winter) and the sixteenth (summer) day after emission. Therefore, early O_3 maxim occur if the geopotential is higher than the latitudinal mean. If the O_3 maximum occurs after this day, the mean geopotential is negative (lower than the latitudinal mean).

If the 500 hPa geopotential is analysed at the time of emission (not shown), the identified relation is not observed. Only air parcel that have an O_3 maximum within the first ten days, have a higher mean geopotential and geopotential latitude anomaly at 500 hPa. While comparing the latitudinal anomaly for air parcels with an O_3 maximum after the 22nd day after emission, the performed Tukey HSD test indicates that the null hypothesis can not be rejected. This indicates that those populations are very similar. If however, the 500 hPa geopotential and geopotential latitude anomaly is analysed for the first seven days (not shown), the same trend is observed.

8.2.4. Thickness Analysis

Sometimes it is not possible to obtain the geopotential height at an pressure altitude of 1000 hPa (in some cases it is below the surface). Therefore, many data are missing if the most common layer thickness of 1000-500 hPa is analysed. This would lead to a biased analysis towards certain air parcel. Therefore, the 850 hPa pressure level is the lowest layer analysed. There are still locations that have a lower surface pressure. This mainly occurs in the Antarctic. Since almost no air parcel reaches the Antarctic until its O_3 maximum, this influence is neglected. In total, two different layer thicknesses are analysed, namely 850-500 hPa and 850-250 hPa. From both analysis the same observation are made (not shown). Therefore, only results for the 850-250 hPa layer thickness are presented.

Figure 8.4a shows the mean 850-250 hPa layer thickness until the O_3 maximum. Values are generally higher during summer (similar to the geopotential at 500 hPa). Since the thickness is an indication of the mean layer virtual temperature, this seasonal difference is again linked to higher temperatures during summer. The variability of the thickness is similar for both seasons. Overall the mean thickness is higher if the O_3 maximum occurs early and decreases the later the O_3 maximum occurs.

The same trend is observed if the layer thickness is adjusted to the latitudinal mean (Figure 8.4b). Independent of latitude, air parcel with an early O_3 maximum are in an atmospheric column were the 850-250 hPa layer thickness is higher than the latitudinal mean. That holds for air parcel with an O_3 maximum before the 22nd (winter) and the sixteenth (summer) day after emission. Only if the O_3 maximum occurs before the tenth day after emission, the mean thickness might be lower than the latitudinal mean (first quartile is negative).

The identified layer thickness trend can not be observed if only the time of emission is taken into account (not shown). This is similar to the geopotential and geopotential anomaly at 500 hPa. Only

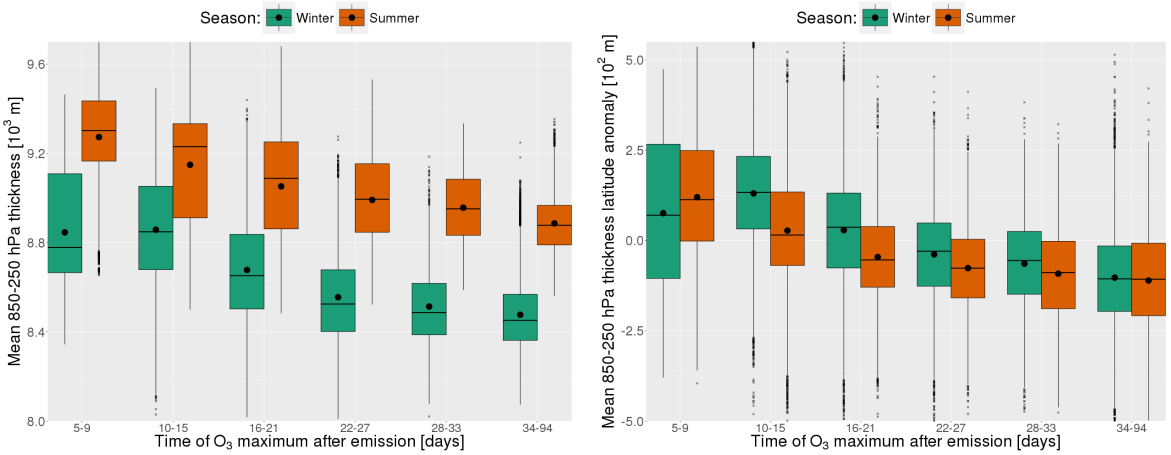

(a) Mean thickness

(b) Mean thickness latitude anomaly

Figure 8.4: Left: Mean 850-250 hPa layer thickness during O_3 build-up. Right: Mean 850-250 hPa layer thickness anomaly during O_3 build-up. Latitude anomalies are calculated by using method two (described in Section 6.6.7). To calculate the latitudinal anomaly, seasonal values are used. In both figures seasons are colour coded.

higher mean values for air parcel with an O_3 maximum within the first ten days exist. If the first seven days after emission are however analysed, the same trend is observed (both not shown).

8.2.5. Discussion

The geopotential itself is an approximation of the altitude above sea-level. A higher geopotential at a given pressure level indicates a higher height above sea-level. High pressure areas are associated with higher temperatures. An air parcel increases its volume with increasing temperature, the same column of air will have a higher height if the temperature is higher. Therefore, the altitude above sea-level at a constant pressure altitude would be higher for an area with higher temperatures. This leads to the fact that a higher geopotential at a constant pressure altitude, indicates an area of higher pressure. Additionally, a higher layer thickness indicate a higher mean temperature within the layer, which is an indication of a higher pressure.

Both analyses performed showed that the 850-250 hPa layer thickness as well as the 500 hPa geopotential is higher the earlier the O_3 maximum occurs. This means that air parcel, with an early O_3 maximum spends more time within a high pressure system until the O_3 maximum occurred. A higher 500 hPa geopotential in a certain area is associated with the core of the pressure system. In this analysis, the higher the determined geopotential or the geopotential latitudinal anomaly, the higher the pressure deviates from seasonal mean values. Higher deviations dominate if the O_3 maximum occurs within the first ten days. Those air parcel stay most likely within the centre of a strong high pressure system. Air parcel with an O_3 maximum between the tenth and the fifteenth day, do not stay inside the core of a pressure system. They most likely stay within an area of high pressure. This could be located in a less strong pressure system or in an area close to the core of a strong high pressure system (e.g. a location west of a high pressure ridge). Tracer with an O_3 maximum between the sixteenth and the 21st day after emission stay in a neutral area. The rest of the tracer spend most of their time in a low pressure area.

The fact that those relations are weak for the time of emission but strong for the first seven days, indicates that a tracer does not necessarily need to be emitted, within a high pressure area or high pressure ridge, as long as the air parcel is transported into high pressure areas, within the first days (about seven). Tracer with an O_3 maximum within the first nine days have a higher mean geopotential at 500 hPa at the time of emission (not shown). This indicates that those tracer are emitted within a high pressure system. This further shows that those tracer are most likely emitted in the core of a high pressure system (e.g. a high pressure ridge).

In Section 8.1.1 it became evident that subsidence is higher during winter. Within this section a similar observation is made for the strength of the pressure system in which the tracer are located.

During summer the latitudinal anomaly seems to be lower, indicating a lower pressure difference than usual. This indicates that the pressure difference between a high pressure system and the surrounding is lower. This lower pressure difference leads to a lower pressure gradient force and therefore a lower divergence towards the centre of high pressure. This lower divergence leads to a lower subsidence (in magnitude). Therefore, lower subsidence during summer is relate to lower pressure anomalies.

The methods used within this analysis introduced some uncertainties. Those are mainly caused by approximating the geopotential at a all three pressure levels (250, 500 and 850 hPa) as well as using six hour mean values. Those approximations are then used to approximate the thickness of multiple layers, which introduces additional uncertainties. Still a clear trend in the mean values is observed. Due to the variability and uncertainties, it might be the case that not only high pressure systems cause subsidence within the atmosphere. However, from the REACT4C data set, no other influence could be obtained.

Frömming et al. (2017) assessed the influence of a high pressure ridge on the O_3 production, based on the REACT4C data. In this analysis subsets of specific emission locations across the different winter pattern are compared. The two subsets which are of most interest for this study are associated with emission locations inside a high pressure ridge (HPR) and emission locations just west of the analysed HPR. The later one are outside the high pressure area. In this study they found that emissions occurring inside the HPR have an earlier peak O_3 gain, occurring at a lower altitude and latitude compared to the emission west of the HPR.

The relation found by Frömming et al. (2017) can be generalised based on the findings in this thesis. It has been shown that the relation is not only valid for emissions within a HPR, but also for all air parcel that stay within a high pressure anomaly. Additionally, it could be demonstrated that this relation does not only hold for air parcel originating from a HPR. Instead it could be shown that as soon as the air parcel is transported (in an early stage after emission) towards an area of high pressure, this specific air parcel experience an early O_3 maximum.

8.3. Dry Air Temperature

Prior to this section, the cause of the downward motion was identified. However, no explanation is found why the downward motion correlates with a higher chemical production rate of O_3. It has been shown that air parcel with an earlier O_3 maximum, also experience a higher 850-250 hPa layer thickness and thus a higher mean layer temperature. Additionally, literature suggests that a high chemical reaction rate might be caused by higher temperatures (see Section 4.4.1). This section elaborates on how temperature influences the temporal development of O_3. First, the temperature influence on the production and loss terms is discussed, followed by the relation between temperature and the time after emission when the O_3 maximum occurs.

8.3.1. Definition: Dry Air Temperature

Dry air temperature gives the absolute temperature of an air parcel, if it is not influenced by radiation and if no moisture is present. It indicates the amount of heat within the air parcel and is therefore proportional to the kinetic energy. Within the troposphere the temperature decreases with increasing altitude and tends to be higher at low latitudes (Ahrens, 2012).

8.3.2. Influence on Production and Loss Rates

Reaction rates are mainly influenced by the reaction rate coefficient and the concentrations of each chemical species involved (see Section 4.4). In Section 4.4.1 the influence of temperature on the reaction rate coefficient was discussed. In addition the temperature may influence the concentrations of certain chemical species (due to temperature influences on their production and loss rates). This section therefore discusses the influence of temperature on the most important reactions. Focus is on the influence during the O_3 build-up. Within the troposphere, high temperatures are only reached close to the surface. During the O_3 build-up, almost no air parcel reaches the surface (see Section 7.1.3). Therefore, the highest temperature taken into account is 280 K.

Most chemical species involved in the tropospheric NO_x chemistry are location dependent (see Chapter 7.2). To eliminate the location influence of those chemicals on the reaction rate, methods one (explained in Section 6.6.7) is applied. This means that a latitude and altitude grid is designed. By assuming that the background concentrations of all chemicals involved depend only on temperature

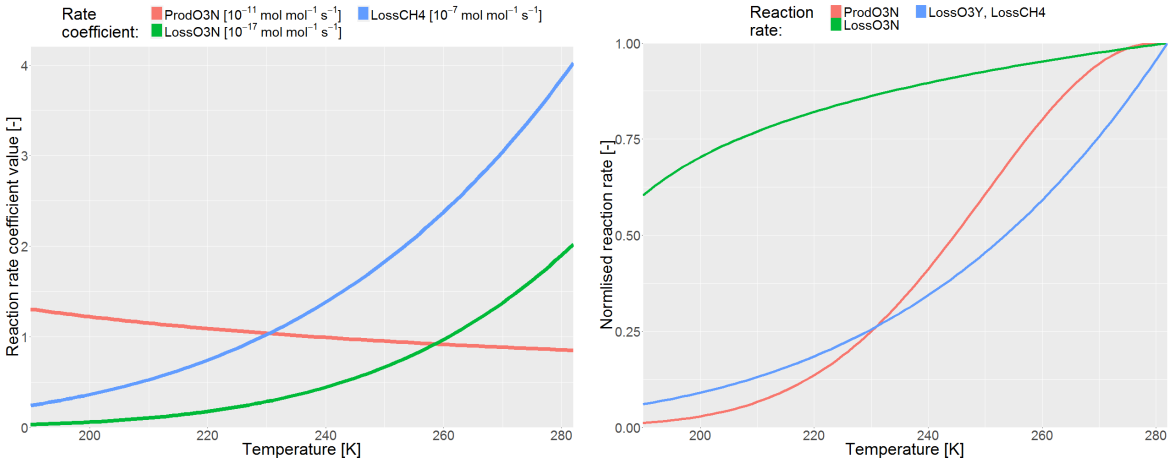

(a) Reaction rate coefficient (b) Reaction rate

Figure 8.5: Left: Temperature influence on the reaction rate coefficient of O_3 production and depletion by NO_x as well as CH_4 depletion. Each reaction rate coefficient is calculated by Equation 8.4, where each coefficient is given in Table 8.1. Right: Temperature influence on the reaction rates. Each reaction rate is based on Equation 4.1. All values are normalised, due to varying magnitudes in each grid box (for more details see text).

(within a grid box), the temperature influence on each reaction rate within each grid box is analysed. Due to the generally different background concentrations, the magnitude of the reaction rates differs. Focus in this analysis is only on identifying general trends of the temperature influence.

The reaction rate coefficient for the O_3 production, the O_3 loss due to NO_2 and the depletion of CH_4 are given by Equation 8.4. Here, temperature is represented by T. For each reaction rate coefficient, the coefficients A, B and C are given in Table 8.1.

$$k = A \cdot \exp\left(B \cdot \log(T) + \frac{C}{T}\right) \tag{8.4}$$

No reaction rate coefficient is given for the non-NO_x depletion rate of O_3. This is due to the fact that this reaction group is including too many different reactions (see Table A.1). Figure 8.5a provides a graphical representation of the temperature influence on each reaction rate coefficient.

The reaction rate is calculated based on Reaction 4.1. Figure 8.5b gives a graphical representation of an approximation of the temperature influence on the reaction rates. In this case all reaction rates have been normalised to the highest value of each reaction rate, due to varying magnitudes for different grid boxes.

The production rate of O_3 due to the reaction of NO with HO_2 (Reaction R3, airProdO3N) is influenced in a different manner by temperature than its reaction rate coefficient (Figure 8.5). The reaction rate increases, whereas the reaction rate coefficient decreases with temperature. This different influence of temperature is caused by different HO_2 concentrations at different temperatures. The HO_2 concentration is low at low temperature, which limits the O_3 production rate. At very high temperature the HO_2 concentration is high. This is caused by the fact that all HO_2 production rates tend to be

Table 8.1: Coefficient A, B and C for each reaction rate coefficient represented by Equation 8.4. For each reaction rate coefficient the respective source is given. All sources are obtained from the supplement of Sander et al. (2005).

Prod/Loss Term	A	B	C	Source
ProdO3N	$3.50 \cdot 10^{-12}$	0	250	(Sander et al., 2003)
LossO3N	$1.20 \cdot 10^{-13}$	0	-2450	(Sander et al., 2003)
LossCH4	$1.55 \cdot 10^{-12}$	2.83	-987	(Atkinson, 2003)

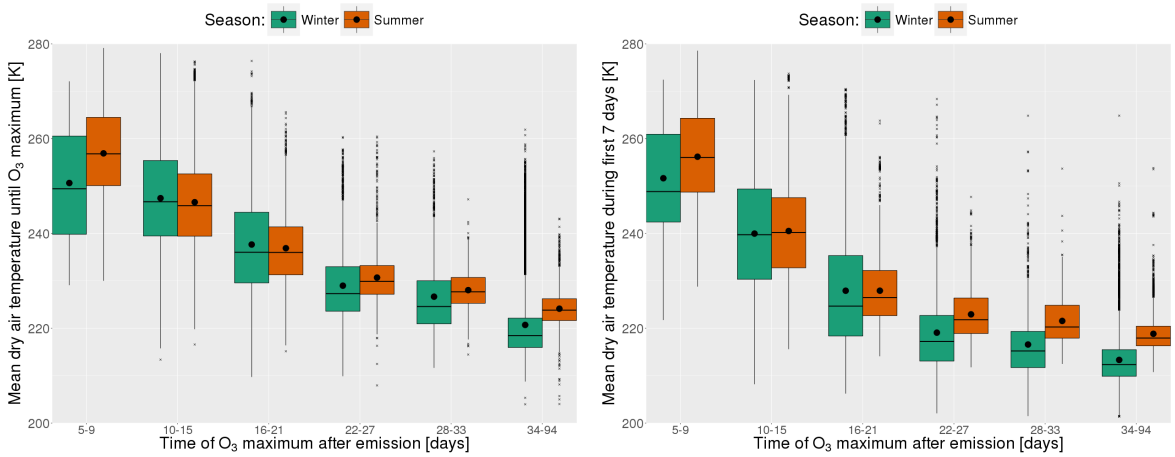

(a) Till O_3 maximum

(b) During first seven days

Figure 8.6: Left: Mean dry air temperature from the time of emission until the O_3 maximum is reached. Right: Mean dry air temperature during the first seven days after emission. Both in relation to the time after emission, when the O_3 maximum occurs. In both figures seasons are colour coded.

higher at higher temperatures (not shown). At very high temperatures the HO_2 concentration becomes constant, which slightly limits the production of O_3.

The depletion rate of CH_4 is also influenced by temperature. The higher the temperature, the more CH_4 is lost. This is due to the increasing reaction rate coefficient with temperature. Additionally, the OH concentration tends to be higher at high temperatures, which further increases the CH_4 loss. The higher OH concentration is based on higher OH production rates at higher temperatures (not shown). Those higher OH reaction rates are related to higher H_2O concentrations at higher temperatures (influences Reaction R19).

The depletion of O_3 by all non-NO_x reactions is influenced by temperature in the same manner as the depletion of CH_4. This is linked to the same reason. Most O_3 is depleted by reacting with H_2O. Since higher H_2O concentrations are possible at high temperatures, more O_3 is depleted at higher temperatures.

The depletion rate of O_3 by NO_2 increases with increasing temperature, which is mainly linked to the higher reaction rate coefficient at higher temperatures. At higher temperatures, most O_3 is however lost by all non-O_3 reactions. This reduces the O_3 concentration and also limits the depletion of O_3 by NO_2. In general, this reaction dominates in the stratosphere, were temperatures tend to be lower.

8.3.3. Temperature in Relation to the Time of the O_3 Maximum

Figure 8.6a shows the mean dry air temperature along the air parcel trajectory until the O_3 maximum occurs. The mean dry air temperature is higher for early O_3 maxima. In general, the variability is higher during summer. Additional, in most cases the summer mean is slightly higher than the winter mean. This can be related to generally higher temperature in the NH during summer. The same trend can be observed for the mean dry air temperature for the first seven days (Figure 8.6b). This figure is also shown to better compare the mean dry air temperature to the transport processes discussed in Section 8.1.

For both cases there is no emission altitude difference within the mean dry air temperature, if the O_3 maximum is occurring before the 22nd day after emission. This can be related to the fact that air parcel with an early O_3 maximum are transported to lower altitudes, independent of the emission altitude. If during winter the O_3 maximum occurs later, the mean value of the lowest emission altitude is about 10 K higher than the mean of the three higher emission altitudes. This effect is caused by the generally higher temperature at lower altitudes and the low vertical transport for those air parcels. During summer air parcel with a late O_3 maximum originating from the lowest emission altitude, are all transported to higher altitudes. Therefore, the difference between the different emission altitudes in the mean dry air temperature vanishes.

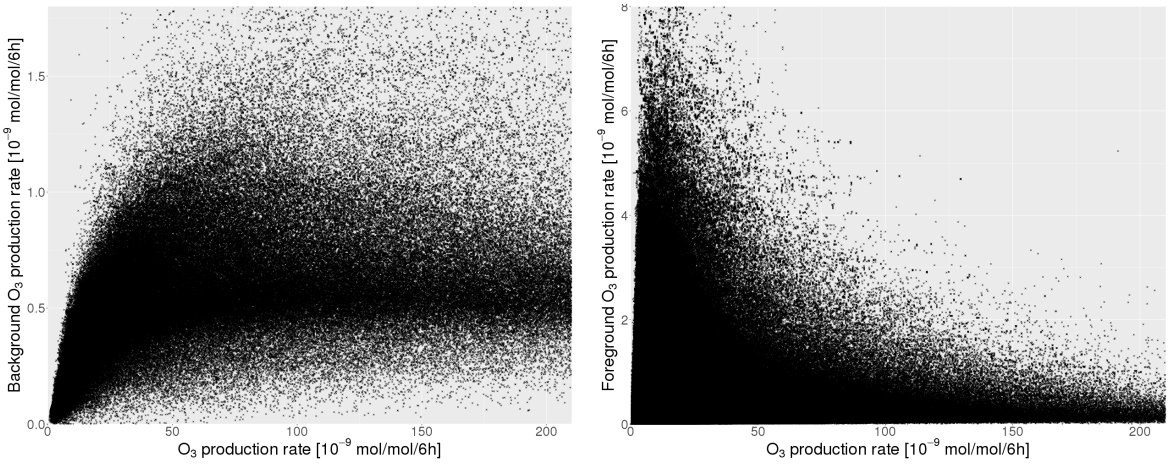

(a) Background (b) Foreground

Figure 8.7: Background and foreground O_3 production rate in relation to the background NO_x concentration. Valid for both seasons. No density plot is provided, since the density in the black area is very similar.

8.3.4. Discussion

During the analysis of the influence of dry air temperature on chemical processes, it became evident that the most important reaction rates are temperature dependent. Either because the reaction rate coefficient or the chemical species involved are influenced by temperature. The mean dry air temperature is higher for air parcel with an early O_3 maximum. This is caused by two factors. Due to the higher subsidence, these air parcels are transported to lower altitudes, where the dry air temperatures is generally higher. Additionally, air parcel with an early O_3 maximum have a higher 850-250 hPa layer thickness and a positive layer thickness latitudinal anomaly. Since a higher layer thickness indicates a higher mean layer temperature, those air parcels are transported downwards to an area in which the temperature is higher than the latitudinal mean temperature.

The production rate of O_3 due to NO_x increases with increasing temperatures which leads to higher O_3 production rates. Due to decreasing foreground NO_x and increasing O_3 loss rates, an earlier O_3 maximum occurs. At the same time the higher temperature leads to a higher loss rate of O_3 by all non-NO_x reactions. Therefore, earlier maxima are caused by a higher chemical activity, which is caused by a higher mean temperature.

The analysis performed shows, that only at higher temperature the O_3 loss rates become higher than the production rates. Therefore, an air parcel needs to be transported to lower altitudes to reach its O_3 maximum. This explains why the O_3 maximum always occurs below the emission altitude (Section 7.1.3). The generally lower mean temperature during winter also explains why O_3 maxima occur later and at lower altitudes, during winter. The lower temperature leads to slightly lower production and loss rates. Therefore, more time is needed to reduce the emitted NO_x.

8.4. Background Concentration of NO_x

Previous studies showed that the background NO_x concentration impacts the net-O_3 production rate. This section analysis the impact of the background NO_x concentration on the production and loss of O_3 and CH_4. Afterwards the impact of the background NO_x concentration on the maximum concentration of O_3 and the total loss of CH_4 is analysed. For better comparability to other studies, the impact of the NO_x concentration at the time of emission is also analysed.

8.4.1. Impact on Production and Loss Rates

All prior sections demonstrated that all production and loss reaction are influenced by many other factors (i.e. foreground and background concentrations, temperature and location). Therefore, this analysis focus on the values were the density is highest (indicated by dark the black area in Figure 8.7).

Figure 8.7a gives a scatter plot of the background production rate of O_3. At very low concentrations of NO_x the production rate is low, due to the missing background NO. If the background concentration

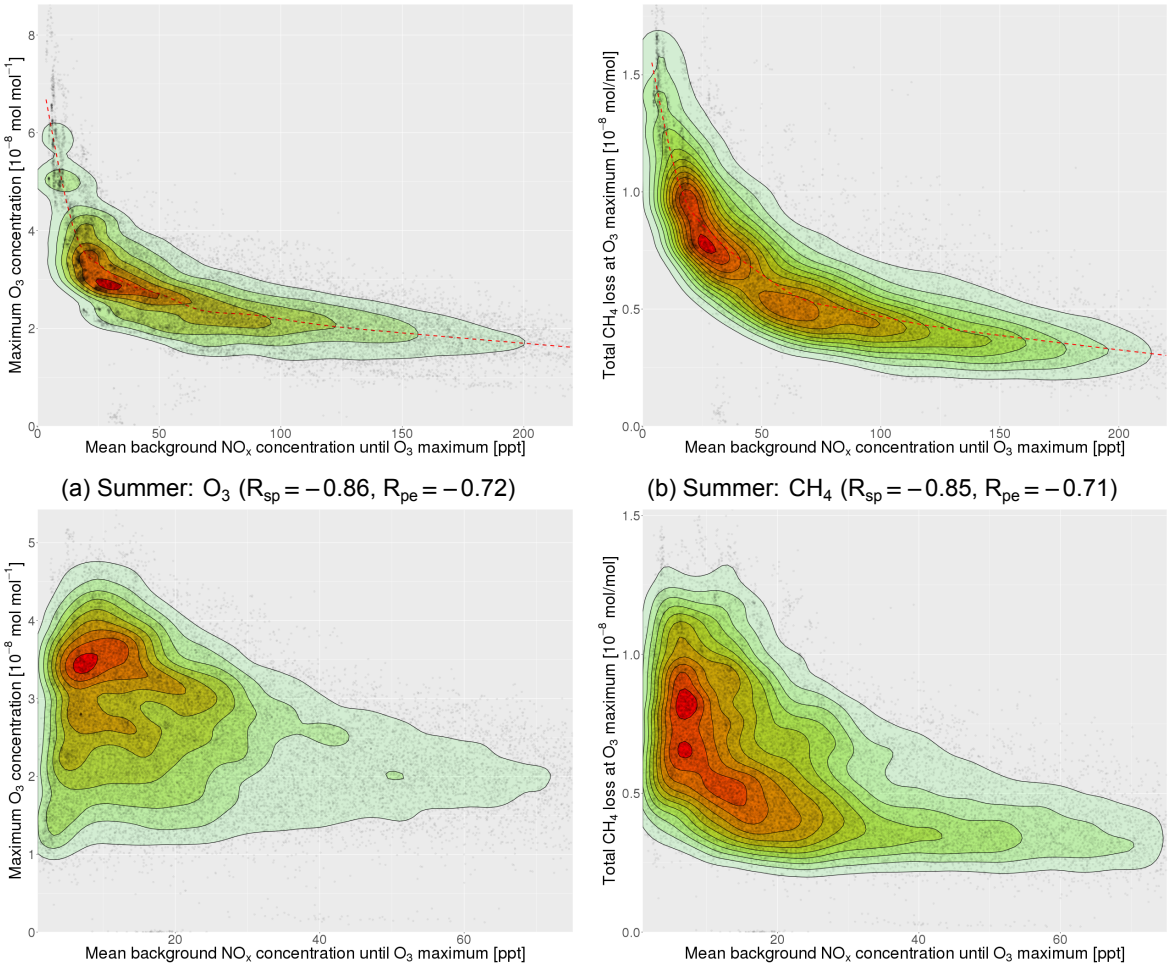

(a) Summer: O_3 ($R_{sp} = -0.86$, $R_{pe} = -0.72$)

(b) Summer: CH_4 ($R_{sp} = -0.85$, $R_{pe} = -0.71$)

(c) Winter: O_3 ($R_{sp} = -0.60$, $R_{pe} = -0.51$)

(d) Winter: CH_4 ($R_{sp} = -0.36$, $R_{pe} = -0.40$)

Figure 8.8: Left: Maximum O_3 concentration in relation to the mean background NO_x concentration during the O_3 build-up. Right: Total CH_4 loss in relation to the mean background NO_x concentration until the O_3 maximum occurred. For both seasons, separate plots are provided. The Spearman rank coefficient (R_{sp}) and the Pearson correlation coefficient (R_{pe}) are given in parenthesis. Each scatter plot includes a density approximation of the number of points per location. Here, red indicates a high density, whereas a low densities are indicated by green.

of NO_x increases, the O_3 production rate increase as well. The O_3 reaction rate reaches a maximum at a background NO_x concentration of about 50 ppt. If the background concentration of NO_x increases further, the O_3 production is limited by lower HO_2 concentrations, leading to lower production rates.

Figure 8.7b provides a scatter plot of the O_3 foreground production rate. The foreground production rate of O_3 behaves different than the background production rate. At very low background concentration of NO_x, the foreground O_3 production rate is highest. If the background production rate and the foreground NO_x concentration are constant, a low background NO_x concentration results in a high foreground production, whereas a low foreground production rate is caused by a high background concentration. This effect compensate low background O_3 production rates, resulting in higher foreground production rates. If the background NO_x concentration increases, the foreground O_3 production rate decreases, even though the background O_3 production rate increases. The higher background concentration of NO_x limits higher foreground O_3 production rates.

8.4.2. Impact of the Mean Background NO_x Concentration

Since the background NO_x concentration influences the O_3 production, it is most likely that the maximum O_3 concentration is also influenced by the background concentration of NO_x. Figure 8.8 gives

scatter density plots for the maximum O_3 concentration and the total loss of CH_4 in relation to the mean background NO_x concentration during the O_3 build-up. Due to the seasonal difference, each season is discussed separately.

During summer the maximum O_3 concentration is highest for low mean background NO_x concentrations. The O_3 concentration decreases exponentially with increasing background NO_x concentration. This can be related to higher possible foreground O_3 production rates at lower background NO_x. If the mean background concentration increases, the mean foreground O_3 production rate decreases, resulting in a lower O_3 maximum. The total CH_4 loss is also higher at low background concentrations of NO_x and decreases if the background NO_x concentration increases. Since O_3 is an important source of OH, the total CH_4 loss increases if more O_3 is produced. Additionally, HO_2 is an important source of OH. The HO_2 concentration is higher at low background NO_x concentration and low at higher concentrations. The low background HO_2 concentration further limits the depletion of CH_4 at low background NO_x concentrations.

During winter the mean background NO_x concentration has a lower impact on the maximum O_3 concentration as well as on the total CH_4 loss. For the total CH_4 loss, the Spearman rank coefficient is only -0.36 (compared to -0.85 during summer) which indicates a very weak correlation. During winter the range of the mean background NO_x is only up to 70 ppt compared to 220 ppt during summer.

For CH_4 similar results are obtained, if the mean background NO_x concentration until the total CH_4 loss is reached, are taken into account (not shown).

8.4.3. Impact of the Background NO_x Concentration at Time of Emission

Stevenson and Derwent (2009) performed a perturbation study and found a relation between the climate impact of NO_x and the background concentration of NO_x at the time of emission. Their simulation set-up differed from the one used by REACT4C. Additional NO_x was released at 111 different locations in the Northern and Southern Hemisphere. Most emissions occur in the Northern Hemisphere at an altitude between 200-300 hPa. All emissions occurred during July. Stevenson and Derwent (2009) used a higher perturbation pulse size than used in REACT4C (Grewe et al., 2014a). Stevenson and Derwent (2009) assessed the climate impact by using a Time-Integrated Radiative Forcing (IRF) based on a time horizon of 100 years. Due to the perturbation method non-linear compensation effects in the atmospheric chemistry might occur.

Figure 8.9 gives the maximum O_3 concentration and the total CH_4 loss in relation to the background NO_x concentration at time of emission. In Section 7.1.2, it became evident that a higher O_3 concentration most likely leads to a higher instantaneous RF. Within this analysis it is thus assumed that a higher O_3 concentration change also leads to a higher IRF. For better comparability the range is limited to the same range provided by Stevenson and Derwent (2009). At higher background NO_x concentrations, only small maximum O_3 concentration and low total CH_4 losses are reached.

During summer the overall shape of the maximum O_3 concentration in relation to the background NO_x compares well with the findings from Stevenson and Derwent (2009). Values above 200 ppt are only reached at an emission altitude of 200 hPa. Here the correspondent O_3 maximum is low. It becomes evident that the lowest NO_x concentration only occurs at an emission altitude of 400 hPa. This emission altitude is not taken into account by Stevenson and Derwent (2009). Those very low background NO_x concentrations at 200-300 hPa, are most like reached in the SH, where the overall background NO_x concentration is lower. This indicates that the relation found in this thesis might be valid for both hemispheres, even though emissions only occurred in the NH. Due to the downward transport, air parcels are transported to areas were the background NO_x concentration is lower. This results into a low mean background NO_x concentration which causes a higher production of O_3.

The CH_4 results obtained in this study do not compare well, with the findings presented by Stevenson and Derwent (2009). The overall variability of the data is higher. Still the highest CH_4 loss occurs at a low background NO_x concentration. Additionally, at very low background NO_x concentration the total CH_4 loss is highest.

For winter, both the O_3 and CH_4 results do not compare well with the findings of Stevenson and Derwent (2009). The shape of both scatter plots is very similar to the findings of Section 8.4.2. However, the overall mean background NO_x concentration is lower than the background concentration of NO_x at emission. This is most likely caused by the downward transport into areas were lower NO_x concentration dominate. The highest O_3 concentration and the highest total CH_4 loss still occur at a very low background NO_x concentration. Both maximum values decrease with increasing background

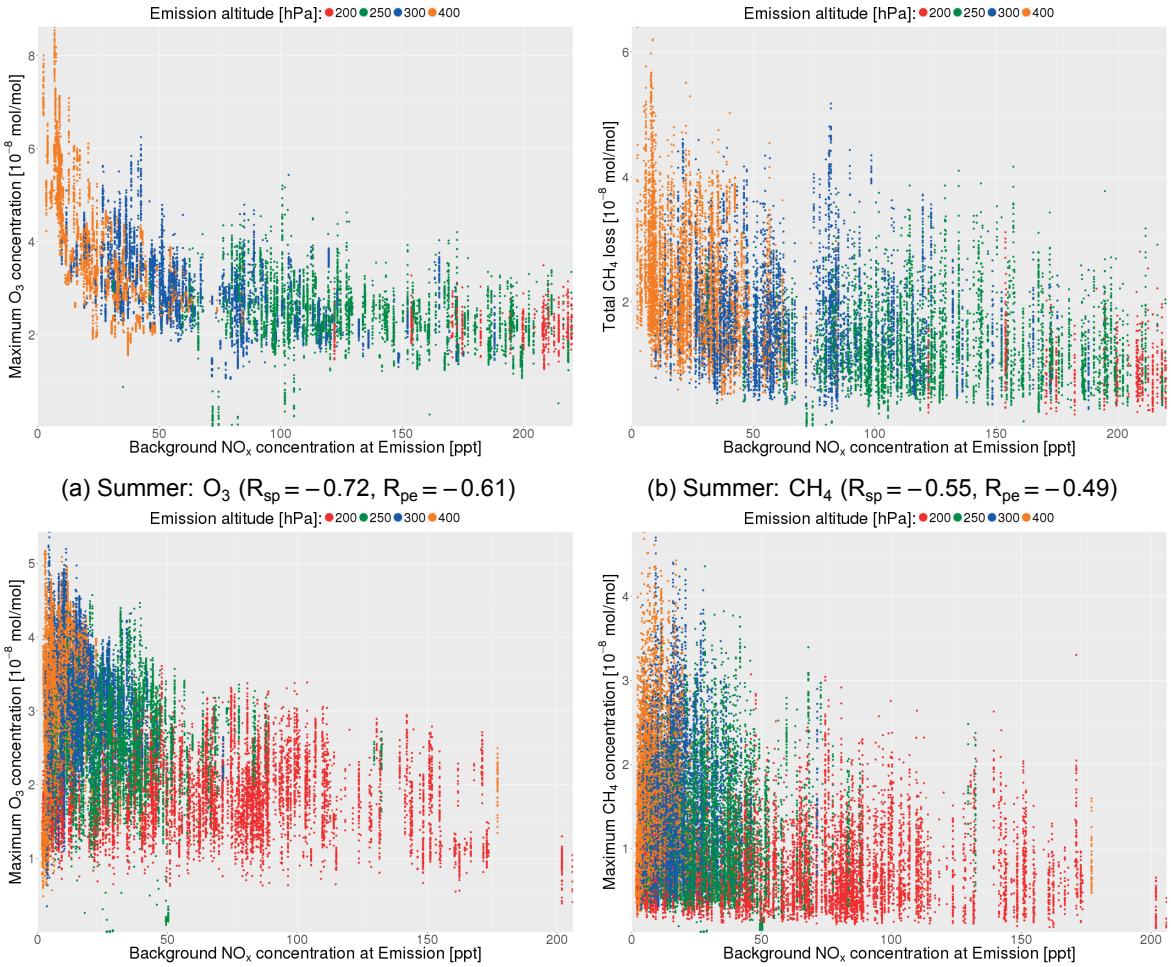

(a) Summer: O_3 ($R_{sp} = -0.72$, $R_{pe} = -0.61$)

(b) Summer: CH_4 ($R_{sp} = -0.55$, $R_{pe} = -0.49$)

(c) Winter: O_3 ($R_{sp} = -0.31$, $R_{pe} = -0.38$)

(d) Winter: CH_4 ($R_{sp} = -0.22$, $R_{pe} = -0.24$)

Figure 8.9: Left: Maximum O_3 concentration in relation to the background NO_x concentration at time of emission. Right: Total CH_4 loss in relation to the background NO_x concentration at time of emission. For both seasons, separate plots are provided. The Spearman rank coefficient (R_{sp}) and the Pearson correlation coefficient (R_{pe}) are given in parenthesis. In all figures, emission altitudes are colour coded.

NO_x concentration. At very low background NO_x concentrations also low O_3 maxima and low total CH_4 losses are possible. Based on those differences the applicability of the findings from Stevenson and Derwent (2009) during winter and in the NH are doubtful. This indicates that those findings are only valid in they specific domain used. However, Stevenson and Derwent (2009) specifically state that their findings are only valid during July.

8.4.4. Discussion

The foreground O_3 production rate, in relation to the background NO_x concentration, compares well to previous literature (see Section 4.4.4) presented by Ehhalt and Rohrer (1995), Brasseur et al. (1998) and Grewe et al. (2012). In all cases the findings are valid for the Northern Hemisphere at mid-latitudes, only. The results obtained in this thesis are valid for all latitudes. All three studies performed the analysis on the net-O_3 production. Those findings showed that at very high background NO_x concentrations, the net-O_3 production becomes negative. This is due to lower HO_2 concentrations and higher loss rates of O_3, by Reaction R15 (Grewe et al., 2012). Such an impact could not be identified in this thesis (not shown). Those high background NO_x concentrations only occur in the lower stratosphere. Air parcels only reach this area soon after emission, when the foreground NO_x concentration is high. In Section 7.3.2 it became evident that the highest O_3 loss due to additional NO_2 is three orders of magnitude lower than the mean O_3 production during the O_3 build-up. Due to the high foreground NO_x

concentration, the production rate of O_3 is still higher, even when the O_3 loss due to additional NO_2 is highest. The foreground O_3 production rate is always higher than the loss rate at higher background NO_x concentrations and no negative net-O_3 production occurs.

In Section 7.2.7 it became evident that the background NO_x concentration decreases with decreasing altitude. For air parcel with an early O_3 maximum, the faster downward transport leads to lower background NO_x concentration and thus higher foreground O_3 production rates. Due to generally lower background NO_x concentrations for air parcels with a lower emission altitude, those air parcels tend to have higher O_3 maxima (Figure 7.6b). Air parcels with a late O_3 maxima stay at higher altitudes were the background NO_x concentrations are higher, which results in lower O_3 maximum concentrations, caused by lower foreground production rates (see Figure 7.8a). This explains altitude differences of the maximum O_3 concentration (see Figure 7.6b). Those relations hold for summer only. It has been shown that during winter the background NO_x concentration has a lower influence on the O_3 concentration. Therefore, another factor influences the maximum attainable O_3 concentration during winter, which needs to be identified (Section 8.5).

During summer the mean background NO_x concentration correlates well with the maximum O_3 concentration. A slightly less stronger correlation can be found, if the background NO_x concentration at the time of emission is taken into account. The still strong correlation is linked to the fact that if the emission occurs at a location with low background NO_x concentrations, it is likely that those air parcel stay in an area of lower background NO_x concentrations (due to the possible downward transport). The correlation would be weaker, if the adjusted RF would be analysed. This is caused by the altitude adjustment of the RF (Section 5.5.1). The adjusted RF for the highest emission altitude (where the background NO_x concentration is highest), would be higher than for the same maximum O_3 concentration at 250 hPa. Further, the instantaneous RF at 200 hPa would be higher for the same concentration change of O_3, since the same concentration change of O_3 lead to higher instantaneous RF at higher altitudes in the troposphere (Section 7.1.2 and Lacis et al. (1990)). Therefore, the highest emission altitude would have a higher adjusted RF at a higher background NO_x concentration.

8.5. Background Concentration of HO_2

In Section 7.3.1 the influence of the background HO_2 concentration on the O_3 production was demonstrated. This influence suggests that the background concentration of HO_2 will influence the maximum O_3 concentration. This section analysis the influence of the background HO_2 concentration on the maximum O_3 concentration and the total CH_4 loss.

8.5.1. Relation Between Background HO_2 and NO_x Concentrations

The HO_2 and NO_x chemistry are linked (see Section 4, 7.2 and 7.3). The correlation between both chemical species depends on the season. During summer both chemicals have a rather strong correlation ($R_{sp} = 0.67$, $R_{pe} = 0.57$), whereas during winter this correlation is very weak ($R_{sp} = 0.09$, $R_{pe} = -0.04$).

This strong seasonal difference is caused by seasonal difference of the production and loss of HO_2 due to NO_x (see Section 7.3.7 and 7.3.8). During summer by far most background HO_2 is produced and lost by reactions including NO. During winter the production of HO_2 due to NO also contributes the most to the background HO_2 concentration but the relative contribution, compared to all other production rates of HO_2, is smaller. The contribution of reactions including NO to the total HO_2 loss is lower during winter. At the lowest emission altitude this reaction is not dominating the HO_2 loss, compared to all other emission altitudes during winter. This seasonal difference in the production and loss of HO_2 by NO causes seasonal differences in the correlations of NO_x and HO_2.

8.5.2. Mean Background HO_2 Concentration

Figure 8.10a gives the density scatter plot of the mean background HO_2 concentration until the O_3 maximum is reached in relation to the maximum O_3 concentration. Overall, the background concentration of HO_2 has a stronger correlation ($R_{sp} = 0.76$, $R_{pe} = 0.59$) during winter than with the background concentration of NO_x ($R_{sp} = -0.60$, $R_{pe} = -0.51$). Low mean background HO_2 concentrations result in relatively low maximum O_3 concentrations. With increasing mean HO_2 background concentration the maximum O_3 concentration increases. At high background HO_2 concentrations (above $2.0 \cdot 10^{-12}\,\mathrm{mol\,mol^{-1}}$), the maximum O_3 concentration levels of and reaches a constant value. Those high background HO_2 concentrations occur if the background NO_x concentration is lower. This lower

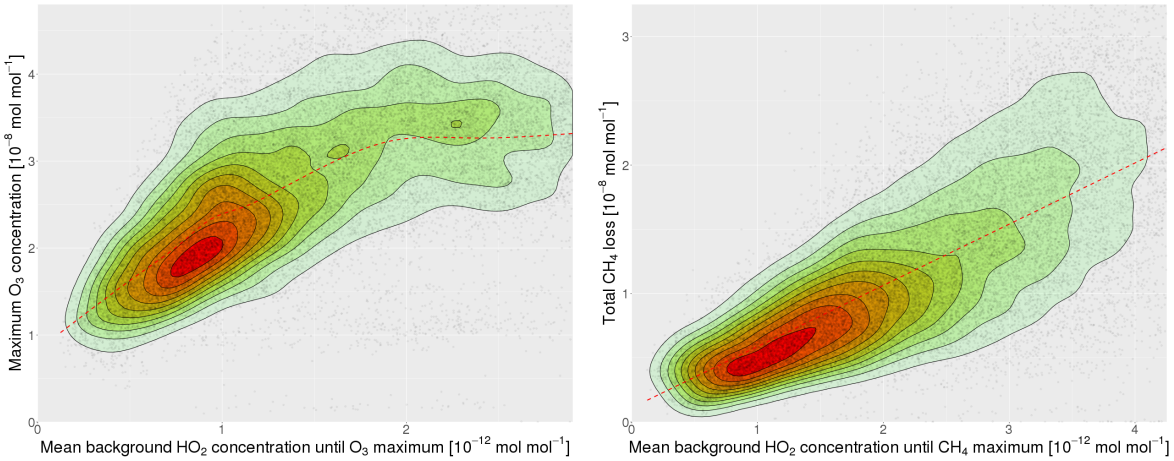

(a) Winter: O_3 ($R_{sp} = 0.76$, $R_{pe} = 0.59$)

(b) Winter: CH_4 ($R_{sp} = 0.78$, $R_{pe} = 0.76$)

Figure 8.10: Left: Maximum O_3 concentration in relation to the mean background HO_2 concentration during the O_3 build-up. Right: Total CH_4 loss in relation to the mean background HO_2 concentration until the total CH_4 loss is reached. Both scatter plots are valid during winter. The Spearman rank coefficient (R_{sp}) and the Pearson correlation coefficient (R_{pe}) are given in parenthesis. Each scatter plot includes a density approximation of the number of points per location. Here, red indicates a high density, whereas a low densities are indicated by green.

NO_x concentration limits the O_3 production.

During summer the correlation between the maximum O_3 concentration and the mean background HO_2 concentration is weak ($R_{sp} = 0.31$, $R_{pe} = 0.26$) (not shown). This indicates that the background NO_x concentration mainly limits the maximum O_3 concentration. This is caused by the generally higher background HO_2 concentration during summer.

The total CH_4 loss also correlates with the mean background HO_2 concentration during winter (Figure 8.10b). The Spearman rank coefficient is 0.78 indicating a strong correlation. This correlation is thus far stronger than the total CH_4 loss in relation to the mean background NO_x concentration ($R_{sp} = -0.36$).

The CH_4 loss depends on the OH concentration. During winter HO_2 and OH concentrations correlate well ($R_{sp} = 0.66$, $R_{pe} = 0.56$). Thus a higher HO_2 concentration leads to a higher OH concentration, which results in a higher CH_4 depletion. During summer the correlation between the total CH_4 loss and the mean background HO_2 concentration is weak ($R_{sp} = 0.50$, $R_{pe} = 0.46$) (not shown).

8.5.3. Discussion

During winter the maximum foreground O_3 concentration depends on the mean background HO_2 concentration. In Figure 8.7b it became evident that a low background NO_x concentration can result in high foreground O_3 production rates, even if the background O_3 production is low. Due to generally lower background NO_x concentrations during winter, one would expect that more O_3 is produced in the foreground, which would result in higher maximum O_3 concentrations. However, since the background HO_2 concentration during winter is not linked to the background NO_x concentration, this foreground O_3 production rate is limited by the background HO_2 concentration. Only if the background HO_2 concentration is high, more O_3 is produced in the background, which results in higher foreground O_3 production rates.

The relation between the mean HO_2 concentration and the total CH_4 loss during winter is caused by two factors. First HO_2 is a major source of OH. A higher background HO_2 results in higher background OH production rates which favour a higher foreground OH production rate. This higher foreground OH concentration, results in higher CH_4 depletion rate. Secondly, higher background HO_2 concentrations result in higher foreground O_3 concentrations. Since foreground O_3 is a major source of OH (especially during the O_3 destruction), more foreground OH is produced, which ultimately results in a higher CH_4 loss.

By comparing the results obtained in this section and Section 8.4, it becomes clear that during

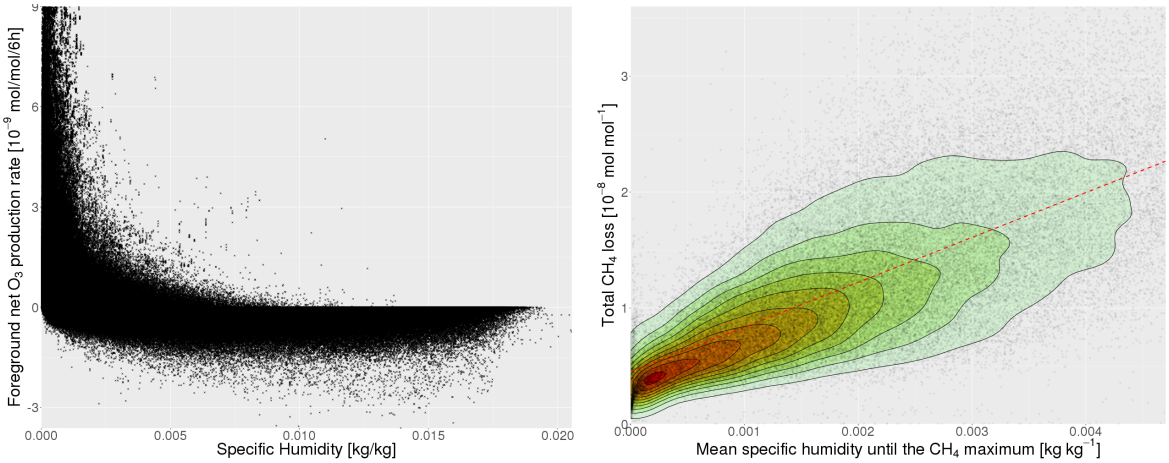

(a) Net-O_3 production

(b) Total CH_4 loss ($R_{sp} = 0.78$, $R_{pe} = 0.75$)

Figure 8.11: Left: Net-O_3 production in relation to the background specific humidity. Right: Total CH_4 loss in relation to the mean specific humidity from emission until the total CH_4 loss is reached. This scatter plot includes a density approximation of the number of points per location. Here, red indicates a high density, whereas a low densities are indicated by green. Both valid for winter and summer.

summer the NO_x concentration limits the foreground O_3 production, whereas during winter lower HO_2 concentrations limit the O_3 production.

8.6. Specific Humidity

Based on literature it is expected that specific humidity might influence the production and depletion of O_3 and CH_4. This expectation is based on the fact that the OH, HO_2 and H_2O chemistry are closely related (see Section 4).

8.6.1. Definition: Specific Humidity

Specific humidity in a moist air parcel is the ratio of the water vapour mass to the total mass of the air parcel. It is calculated using the following equation, were r_v is the mixing ratio of the total air mass and the mass of water vapour (Ahrens, 2012):

$$q = \frac{r_v}{1 + r_v} \tag{8.5}$$

8.6.2. Influence on the Net-O_3 Production

Figure 8.11a gives the net-O_3 production in relation to the background specific humidity. It shows that high net-O_3 production rate only occur if the specific humidity is low. If the specific humidity is high, almost no O_3 is produced. The H_2O mass depends on altitude. In general, H_2O concentrations are higher at low altitudes and decreases with increasing altitude. Therefore, the specific humidity is also highly influenced by altitude. To eliminate altitude dependencies, the first method explained in Section 6.6.7 is applied (not shown). From this analysis it became evident that the mean net-O_3 production rate in relation to the specific humidity is independent of altitude, except at low specific humidities. The maximum net-O_3 production rate (always occurs at low specific humidities) is higher at high altitudes and low close to the surface. In addition, no correlation to the different production and loss rates of OH and HO_2 as well as scavenging processes could be identified.

8.6.3. Influence on the Total CH_4 Loss

Figure 8.11b gives the total CH_4 loss in relation to the mean specific humidity until the total CH_4 loss is reached. Due to the high Spearman rank coefficient of 0.78, the correlation is strong. The higher the mean specific humidity, the more CH_4 is lost. At low mean specific humidities, the variability is low but with increasing specific humidity, the mean and the variability increase (heteroskedastic behaviour). If

the mean specific humidity is very low, CH_4 is still lost.

The specific humidity is a measure of the amount of water within a mass of air. Since H_2O concentrations depend on altitude and latitude, the influence on the loss rate of CH_4 was investigated by using the first method as discussed in Section 6.6.7. It turned out that the production rate dependency of the specific humidity is independent of altitude and latitude (not shown).

The physical explanation of this relation is based on the production of OH due to H_2O and $O(^1D)$ (Reaction R19). In Section 7.3.5 it was discussed that the OH production due to this reaction contributes the least to the foreground OH concentration during the O_3 build-up. If the correlation between the mean specific humidity and the total CH_4 loss is analysed only up to the time of the O_3 maximum, the Spearman rank coefficient reduces to 0.51. This weaker correlation is caused by the higher OH production due to other reactions (including NO). However, after the O_3 maximum is reached, most OH is produced due to Reaction R19. Due to this relation, the specific humidity has a high influence on the foreground OH production and therefore the foreground CH_4 loss.

The relative contribution of H_2O to the total OH production increases with decreasing emission altitude, which is caused by higher specific humidity values at lower altitudes. This partially explains why the total CH_4 loss increases with decreasing emission altitude. However, it is important to keep in mind that the overall production of OH, due to the other two reactions also increases with decreasing emission altitude. Thus the higher specific humidity is not the only cause for higher CH_4 losses at lower altitudes. During summer, the relative contribution of the foreground OH production due to H_2O is higher than during winter. Therefore, the lower specific humidity during winter is one cause of the overall lower CH_4 loss during winter.

8.6.4. Influence on the O_3 Loss due to All Non-NO_x Reactions

The CH_4 loss and O_3 loss due to all non-NO_x reactions, correlates well. This is caused by the fact that most O_3 is lost due to Reaction R19 after the O_3 maximum is reached. Therefore, a similar correlation between the specific humidity and the O_3 loss due to all non-NO_x reactions is identified. Since the same explanation is valid (as discussed in Section 8.6.3), no further analysis and discussion is presented.

8.6.5. Discussion

Based on the analysis performed, it is concluded that the specific humidity does not influence the O_3 production, since no physical explanation could be identified. Further, no causality could be found from literature. Köhler et al. (2008) showed that the net-O_3 production is positive at high altitudes, whereas at low altitudes the O_3 loss dominates (also identified in Figure 7.19a). Since the specific humidity increases with decreasing altitude, the O_3 loss at high specific humidities indicates lower altitudes. It is considered that the correlation between both factors is caused by similar location dependencies of the processes involved. The production rate of O_3 is therefore not influenced by the specific humidity.

The total CH_4 loss is influenced by specific humidity, since one important OH production rate is linked to H_2O. A higher foreground OH concentration leads to a higher CH_4 loss. The variability in this relation is linked to the maximum O_3 concentration. If the specific humidity is high but the maximum O_3 concentration is low, less OH can be produced, which leads to lower total CH_4 losses. The opposite occurs if the maximum O_3 concentration is high. In this case more OH is produced due to H_2O, which leads to a higher total CH_4 loss. Since the production of O_3 is independent of specific humidity, a high specific humidity does not guarantee a high CH_4 loss. At low specific humidities CH_4 is still lost. The production of OH by NO is independent of specific humidity. This OH (produced by NO) leads to a CH_4 depletion, even if no CH_4 is depleted by O_3.

Fuglestvedt et al. (1999) identified that the specific humidity controls the OH concentration. Hoor et al. (2009) also found that the OH production is influenced by solar irradiance and specific humidity. Therefore, both studies agree with the identified correlation (in this thesis) of specific humidity and the total CH_4 loss.

8.7. Tracer Characteristic: O_3 Maximum at the End of Simulation

To identify the cause of some air parcels having their O_3 maximum at the end of simulation, a systematic analysis is performed. This analysis is based on the emission and mean location, as well as the variability of the most important production and loss terms.

Table 8.2: Mean production and loss terms for all important reactions. Mean values are calculated based on all values until the O_3 maximum is reached. Values are given for each tracer characteristic. The mean value for all data points is given as a reference. Mean values are based on both seasons. The unit for each reaction rate is: [mol mol^{-1} 6 h^{-1}]

Prod/Loss Term	All data points	O_3 maximum at end	Constant O_3 concentration
airProdO3N	1.01×10^{-9}	2.49×10^{-10}	3.54×10^{-12}
airLossCH4	1.37×10^{-10}	1.79×10^{-11}	1.21×10^{-12}
airLossO3N	6.44×10^{-13}	1.27×10^{-12}	3.96×10^{-15}
airLossO3Y	7.66×10^{-11}	8.52×10^{-12}	2.82×10^{-15}

8.7.1. Emission Location

Figure 8.12 shows the number of air parcels that have their O_3 maximum at the end of simulation for each weather pattern. A seasonal difference exists. During winter the number of air parcels is higher than during summer. This suggests that the reason why those air parcels have their O_3 maximum at the end of simulation is caused by a weather factor which differs with season. Most air parcel originate from the highest emission altitude. Only during winter a few air parcels also originate from the second highest emission altitude.

During winter the air parcel may originate from any emission latitude. Here, the highest and the lowest emission latitude contribute the least air parcel. It is important to keep in mind that for the highest emission latitude the number of air parcels is lower at the second highest emission altitude (due to missing data, see Section 6.2). During summer the air parcels of interest originate mainly from the highest four emission latitudes.

8.7.2. Mean location

From Section 8.1.1 it became clear that those air parcel experience only little vertical transport. On average those air parcels stay at an altitude between 200 and 300 hPa. No air parcel has a mean altitude below 400 hPa. Only little seasonal and inter-seasonal variation exist. SP3 has a lower variability compared to the other two summer pattern.

A seasonal difference for the mean latitude is observed. During summer air parcel spends most of their time at higher latitudes, whereas during winter the air parcel can also have a mean latitudinal location close to 30°N. This means that during summer air parcel need to be transported or stay at higher latitudes to have an O_3 maximum at the end of simulation.

8.7.3. Production and Loss Terms

Table 8.2 gives the mean production an loss rates of O_3 and CH_4. The mean O_3 production rate is one order smaller if compared to all data points. The same is true for the loss of CH_4 and the O_3 loss by all non-NO_x reactions. The mean loss rate of O_3 due to Reaction R15 is one order higher. The crucial question now is what favours those lower O_3 production and higher loss rate. It is known that the O_3 loss due to Reaction R15 increases in the stratosphere. This is based on the fact that higher background concentrations of O_3 as well as NO_2 are present above the tropopause. The same observation is made for the foreground O_3 loss (see Figure 7.12b).

8.7.4. Time within the Stratosphere

Most air parcel of interest stay at a high altitude and latitude (Section 8.7.2). Combining this information with the low production and loss rates (Section 8.7.3), it becomes evident that the air parcel with a late O_3 maximum spend time within the stratosphere.

At the time of emission about 82% of the air parcel, with an O_3 maximum at the end of simulation, are emitted at an altitude that is above the tropopause. Therefore, most tracer of interest are emitted within the stratosphere. All tracer that are emitted below the tropopause are transported upwards and reach the stratosphere within eight days. On average each air parcel stays 53 days of the 90 days in the stratosphere. Therefore, air parcel with a late O_3 maximum stay more time above the tropoause then below. This explains why the O_3 production rate is reduced and the O_3 loss rate by Reaction R15 is increased.

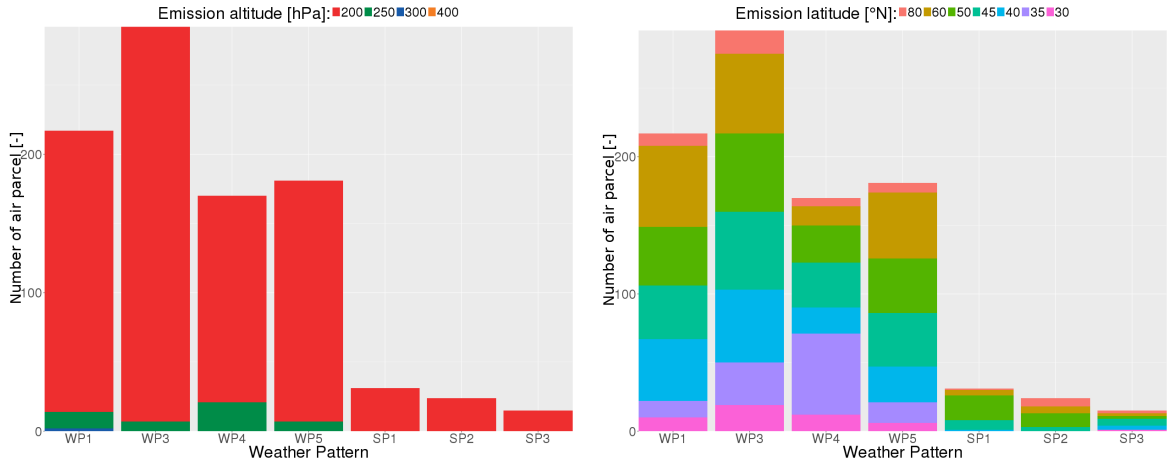

(a) Separated by emission altitude

(b) Separated by emission latitude

Figure 8.12: Number of air parcels that have their O_3 maximum at the end of simulation for each of the seven weather pattern taken into account. The emission altitude and latitude are colour coded.

8.7.5. Discussion

Based on the location and the reaction rates analysed, the following conclusion can be made. If a tracer is emitted and stays within the stratosphere, the O_3 maximum is most likely reached at the end of simulation. The late O_3 maximum is based on lower production rate of O_3 above the tropopause.

The seasonal variation of the tropopause altitude also explains the seasonal differences of the number of air parcels reaching their O_3 maximum at the end of simulation. During summer the tropopause altitude tends to be higher due to higher mean temperatures. The chance that a tracer is emitted within the stratosphere is therefore lower during summer. Due to lower temperatures at high latitudes, the tropopause altitude tends to be lower. This explains that almost all air parcel during summer originate from higher latitudes. Here, the tropoause tends to be lower. The single tracer emitted at 30°N in SP3 is not emitted within the stratosphere but is transported to it within eight days.

In Section 3.5 it was elaborated that an air mass needs up to two years to be transported from the stratosphere towards the troposphere. In this thesis, the time scale of vertical exchange between both parts of the atmosphere acts on shorter time scales. This can be explained by the fact that emitted tracer located in the stratosphere stay very close to the tropopause and are not transported to higher parts of the stratosphere. Therefore transport from the stratosphere towards the troposphere is more likely. The average values discussed in Section 3.5 also considers air masses that originate from higher parts of the stratosphere. Comparisons with values from this thesis are therefore limited.

Grewe et al. (2017) compared simulations from EMAC (resolution of 2.8° x 2.8°) and simulation results form the small-scale model Consortium of Small-scale MOdels (COSMO) (resolution of 0.44° x 0.44°) to atmospheric measurements of O_3 and NO_x. It turned out that EMAC regularly estimated lower tropopause pressure altitude (i.e. a higher altitude above sea-level), which influenced the background concentrations of chemical species in the upper troposphere. It is most likely that in a different model set-up, due to a lower tropopause, more emissions would have occurred within the stratosphere. This would lead to more air parcels with an O_3 maximum at the end of simulation.

8.8. Tracer Characteristic: Constant O_3 Concentration for 4 Days

A constant concentration of O_3 for four days can be caused by two factors. First, a meteorological influence could cause a very low chemical activity. Secondly, a constant O_3 concentration could result from equal production and loss rates of O_3. In a first step the different production and loss terms are analysed, to identify which of the two possible causes leads to the constant concentration. Afterwards, the location of all tracer with a constant concentration of O_3 four four days are analysed. In a final step, a short sensitivity study is performed to identify if the same findings are valid if a constant concentration of O_3 for less than four days occurs.

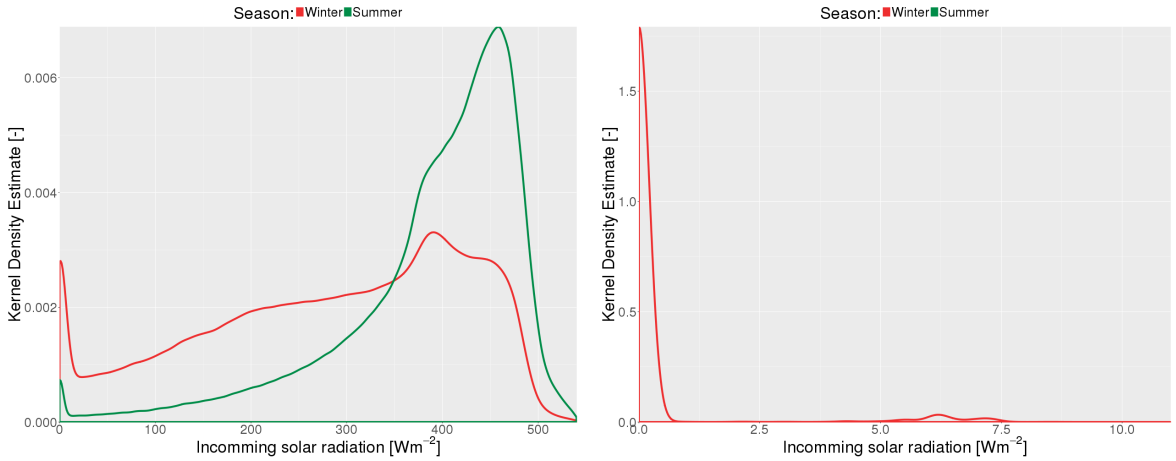

(a) All Tracer

(b) Tracer with a constant O_3 concentration

Figure 8.13: KDE of the incoming solar radiation at the top of the atmosphere. Left: All tracer taken into account. Right: All tracer with a constant O_3 concentration for four days. The season is colour coded in both figures.

8.8.1. Production and Loss Terms

Table 8.2 gives the mean production and loss rates of O_3 and CH_4 associated with certain tracer characteristics. All four production and loss terms are significant lower, if compared to the case were all tracers are taken into account. The mean O_3 production is three orders of magnitude smaller. The O_3 loss rate by all non-NO_x reactions, is even four orders of magnitude smaller. Based on those observation it is concluded, that the constant O_3 concentration is based on the fact that the overall chemical activity is significantly. It is not caused by the fact that the production and loss term of O_3 have the same magnitude.

8.8.2. Location Analysis

Air parcel with a constant O_3 concentration of four days during the O_3 build-up originate from all emission latitudes and altitudes. No clear trend towards a certain emission location can be observed. A seasonal difference exists. During summer no air parcel exist that has a constant O_3 concentration for four days. During winter each weather pattern taken into account has a similar number of air parcel that have a constant O_3 concentration for four days.

All air parcel are transported at some point during the 90 days to higher latitudes. If only the time is analysed were the O_3 concentration is constant, it can be observed that all air parcel are at a latitude higher than 67°N. During winter the polar circle extends to about 66°N. Therefore, all air parcel with a constant O_3 concentration are above the polar circle and experience polar night conditions, where incoming solar radiation is by definition absent.

8.8.3. Incoming Solar Radiation

Based on the fact that all constant O_3 concentration occur above the polar circle, the absence of incoming solar radiation is most likely the cause. Figure 8.13a show the kernel density estimate (KDE) for the incoming solar radiation at the top of the atmosphere if all data points are taken into account. The top of the atmosphere is analysed to eliminate absorption and scattering processes within the atmosphere. In this case the KDE is distributed between 0 and 520 $W\,m^{-2}$. If the O_3 concentration is constant for multiple days, the incoming solar radiation at the top of the atmosphere has a value of 0 $W\,m^{-2}$ (Figure 8.13b). It never reaches a value above 10 $W\,m^{-2}$. The small density increase at 6.25 $W\,m^{-2}$ is caused by an air parcel that stays at a latitude only slightly above 67°N. Thus a very small incoming solar radiation is still effecting the air parcel. However, the energy provided is to low cause a significant production of O_3.

8.8.4. Sensitivity Study: Number of Days With Constant O_3 Concentration

In the this analysis, a fixed time period of four or more days is used. A small sensitivity analysis is performed to assess if a lower number of days has an influence on the result.

If air parcel with a constant O_3 concentration for three days are taken into account, the same results can be obtained. While the O_3 concentration is constant all air parcel stay above 66°N. By also taking air parcel with a constant O_3 concentration for two days into account the results slightly change. Still the majority of air parcels stay above 66°N while their O_3 concentration is constant. Now their are air parcels which have a constant O_3 concentration during summer. Those air parcel however have a constant O_3 concentration, which is caused by the fact that the O_3 production and loss rate have the same magnitude. Therefore, the constant O_3 concentration is not caused by the absence of incoming solar radiation.

During summer there are two air parcel that are transported to the Southern Hemisphere (SH) and reach a latitude of 70°S. Therefore, they are above the polar circle in the Antarctic. For those air parcel the constant O_3 concentration is also caused by the absence of incoming solar radiation during a polar night in the Antarctic.

8.8.5. Discussion

Based on the results obtained and the sensitivity study performed, it is concluded that a constant O_3 concentration for three or more days can only be caused by the absence of incoming solar radiation during a polar night. The missing incoming solar radiation causes a low chemical efficiency which causes almost no O_3 to be produced or depleted. If a constant O_3 concentration occurs for less than three days, this condition can also be caused by equal O_3 production and loss rates.

Since the emission area is in the Northern Hemisphere (NH), air parcel during winter are more prone to have constant O_3 concentrations for more than three days, due to the polar night in the Arctic. If the emission area would be in the SH it is most likely that air parcel during summer would be more prone to constant O_3 concentrations (polar night in the Antarctic occurs during the NH summer).

Based on this analysis, it can generally be concluded that the lower incoming solar radiation (polar night) is one of the influences that causes the latitudinal difference in O_3 and CH_4 concentrations during winter (as suggested in Section 7.2.12).

8.9. Non-Influencing Weather Factors

This section elaborates on weather factors that do not have an influence on the O_3 or CH_4 concentration change. Here, relations that have been identified from literature but could not be proven within this thesis project, are discussed. Additionally, correlations that have been identified but were no causality could be proven, are shortly elaborated.

8.9.1. Lightning

Lightning has a significant impact on the background concentration of NO_x and is considered to be the major natural source of NO_x in the upper troposphere (Schumann and Huntrieser, 2007). Within this thesis it was found that the background concentration of NO_x, has a significant influence on the O_3 production (Section 8.4).

Earlier studies by Berntsen and Isaksen (1999) investigated the influence of lightning on aviation NO_x climate impacts, by reducing the yearly lightning emissions of NO_x to $5\,\mathrm{Tg(N)yr^{-1}}$ and compared the O_3 production to a reference case with a yearly lightning emission of $12\,\mathrm{Tg(N)yr^{-1}}$. In a sensitivity study, they concluded that overall the O_3 production efficiency in the upper troposphere increased if less lightning occurs. They also concluded that the impact differs with regions. The Arctic is most sensitive to a reduction in lightning. The lowest effect is observed near the NH tropics. This regional difference can be explained by the amount of flashes and the resulting NO_x emission in each region. In the Arctic the number of flashes is low compared to the tropics. If now the amount is even further reduced, the relative change of flashes is higher in the Arctic than in the tropics (Berntsen and Isaksen, 1999).

By using the available data related to lightning processes (see Table 6.2), the impact of lightning events on the tracer was studied. By decreasing the total yearly NO_x emission due to lightning, Berntsen and Isaksen (1999) indirectly reduces the overall NO_x background concentration. In the REACT4C such an approach is not made. Only single lightning events can be studied. Therefore,

comparisons of both studies are bounded by limitations. Figure 8.8 shows that a lower background NO_x concentration results in a higher O_3 concentration and thus a higher instantaneous RF. If the yearly emitted NO_x concentration due to lightning would be reduced in EMAC, the overall foreground production of O_3 would be higher, leading to higher O_3 maxima. In the REACT4C simulation a single lightning event leads to a background NO_x increase of less than 0.001%. This means that a single lightning event would have only little influence on the maximum O_3 concentration (see Figure 8.8). Therefore, non influence of lightning on the production of O_3 is identified.

Additionally, the approach of reducing the lightning NO_x emissions (done by Berntsen and Isaksen (1999)) does not represent future lightning expectations. The average atmospheric temperature is currently increasing due to climate change. Due to a higher temperature, the atmosphere is capable to take up more water vapour. Stocker et al. (2013) expect that this most likely leads to more precipitation and more lightning events. Therefore, more NO_x emissions due to lightning can be expected in the future, indirectly increasing the background NO_x concentration. Berntsen and Isaksen (1999) however reduced the amount of additional emissions from lightning. Due to the complex relation involved it is hard to estimate if a reversed effect will be observed (of the relation identified by Berntsen and Isaksen (1999)), if the amount of emitted NO_x from lightning is increased.

8.9.2. Turbulent Kinetic Energy

Turbulent Kinetic Energy (TKE) is a measure for the kinetic energy within turbulent flows. An analysis showed that if high kinetic energy is present in the atmosphere, the production and loss terms of O_3 and CH_4 are reduced (not shown). Further it can be concluded that more turbulence within a grid box reduces the chemical efficiency of this specific grid box. However, in this modelling approaches, it is generally assumed that the content of that grid box is well mixed. Thus the TKE should have no influence on the production and loss terms.

The TKE in the atmosphere is location dependent. The planetary boundary layer (PBL) is the lowest layer of the atmosphere spanning from the surface to a hight of about 300-2000 m. Within this layer vertical mixing dominates, which results in a higher TKE. Above this PBL, the TKE tends to be lower due to lower influence of surface drag and less vertical mixing. Therefore, the TKE value indicates if the tracer is inside or outside the PBL.

The tracer only reach the lowest part of the atmosphere, after the O_3 maximum is reached (see Section 7.1.5). Thus the foreground concentration of NO_x is low within the PBL. This low foreground concentration only allows low foreground O_3 production rates. Additionally, in most cases (about 80%) the highest CH_4 concentration change is already reached before the tracer reaches the PBL. Thus the production and loss rates are per definition lower.

This proves that even though a correlation exist between the TKE and the O_3 production and CH_4 loss, no causality is identified. It is more likely that in this case the TKE only indicates that the air parcel is in the PBL.

8.9.3. Convection

Convection processes within the atmosphere mainly refer to atmospheric motions in the vertical direction in the lower part of the troposphere. The Earth's surface is heated up by incoming solar radiation. This rapid increase of temperature warms the overlying air. Due to increasing temperatures air becomes less dense than the surrounding air, which causes warmer air parcel to rise. Due to the decreasing surrounding air, moisture within the air parcel may condense which results in clouds. Most convection processes occur below 500 hPa. Rarely convection processes extend above this layer. Those convection processes are refereed to as deep convection.

No correlation and causality could be found between convection processes and the O_3 and CH_4 temporal development. In Figure 7.1.3 it can be seen that most tracer have an O_3 maximum around 500 hPa. Only during winter way lower altitudes are reached. Therefore, during the O_3 build-up, most air parcel stay above this atmospheric area, where convection processes dominate. Only rarely do convection processes occur at the high altitudes. This explained why no correlation could be found.

Berntsen and Isaksen (1999) found that convection has an impact on the climate impact of O_3. They reduced the number of convection events by 67% and compared the results to a reference scenario. Overall the production efficiency of O_3 in the upper troposphere decreased. The relative change was lowest in the Pacific area and highest in the NH tropics (Berntsen and Isaksen, 1999).

Convection processes are important for the exchange of energy and chemical species between

the lower and the upper troposphere. By reducing the number of convection events inside the atmosphere, this exchange process is reduced. This changes the overall chemistry within the upper atmosphere. Additionally, due to less energy exchange, the overall temperature decreases in the upper atmosphere. In Section 8.3 it became evident that a lower temperature results in a lower O_3 production efficiency. Thus the impact of reducing the convection processes (as done by Berntsen and Isaksen (1999)) causes a global change in the atmospheric chemistry. A single convection event, as analysed in this thesis, does not have such an impact. This explains why this study did not find similar results as Berntsen and Isaksen (1999) did.

As it was with the lightning reduction, the convection reduction does not represent the expected change in convection of future climate change assessments. Stocker et al. (2013) expect that convection events will increase in the future. It is again arguable if the reverse effect of the influence identified by Berntsen and Isaksen (1999) would be observed. This reduces the applicability of the results found by Berntsen and Isaksen (1999).

8.9.4. Clouds

Section 2.2.5 explained that clouds influence incoming solar radiation, since they can reflect incoming solar radiation back into open space. Basically all chemical reactions depend on incoming solar radiation (see Section 4.4.3). One could expect that clouds may influence the production and loss rates, associated with the tropospheric O_3 chemistry.

The analysis to identify influences of clouds is based on the values given in Table 6.2. In this analysis a air parcel is only taken into account, if it is inside or below the cloud. It is expected that no influence can be observed if the air parcel is above a given cloud. However, the performed analysis did not reveal any conclusive correlations (not shown). Even if the cloud cover was high, the production and loss rate were not reduced compared to clear sky conditions. Physically this could be explained by the fact that scattering processes within the atmosphere still cause solar radiation to be present below the cloud, providing enough energy to enable the production of O_3 or other reactions.

A weak correlation between the time after emission when the O_3 maximum occurred and the cloud cover percentage is found. Cloud cover is given as a percentage of the EMAC grid box in which the air parcel is located. It is a 3D-variable (latitude, longitude and time), since the cloud cover is independent of the level in which the air parcel is located. The clear sky condition is given if their is no cloud within the grid box. If the O_3 maximum is reached within the first 21 days after emission, air parcels experience clear sky conditions for about 85% of the time, until the O_3 maximum is reached. If the O_3 maximum is reached after the 21st, the mean time is reduced to only 60%. The lower cloud coverage associated with early O_3 maxima is considered to be caused by the weather condition given in a high pressure system. In Section 3.3 it was explained that due to subsidence within a high pressure system less clouds form. Therefore lower cloud coverage is caused by the high pressure system but does not influence the foreground production and loss terms of O_3 and CH_4.

8.10. Inter-Seasonal Variability

Up to this point only seasons difference were analysed. Within the REACT4C eight different weather situations have been simulated, of which seven are available in this thesis. The most important relations are shortly reviewed in this section, to identify inter-seasonal variabilities. This is done by systematically comparing the Spearman rank coefficient for each relation and weather pattern. Additionally, some relations are visually inspected.

8.10.1. Vertical Transport

Figure 8.14 provides the mean vertical wind velocity during the first seven days in relation to the time when the O_3 maximum is reached. Additionally, Table 8.3 gives the Spearman rank coefficient for each weather pattern. For both seasons the one-way ANOVA test indicates that for air parcels with a late O_3 maximum (after the 34th day), the null hypothesis can not be rejected. This indicates that those populations are very similar. Overall, the same trend (as concluded before) is observed for each weather pattern. The variability of the mean is higher during winter. The same is represented by the Spearman rank coefficients. They tend to be lower and differ more during winter. Still all Spearman rank coefficients indicate strong correlations. It can be concluded that the overall trend that earlier O_3 maxima occur if the tracer is transported faster towards lower altitudes, is true for all weather pattern.

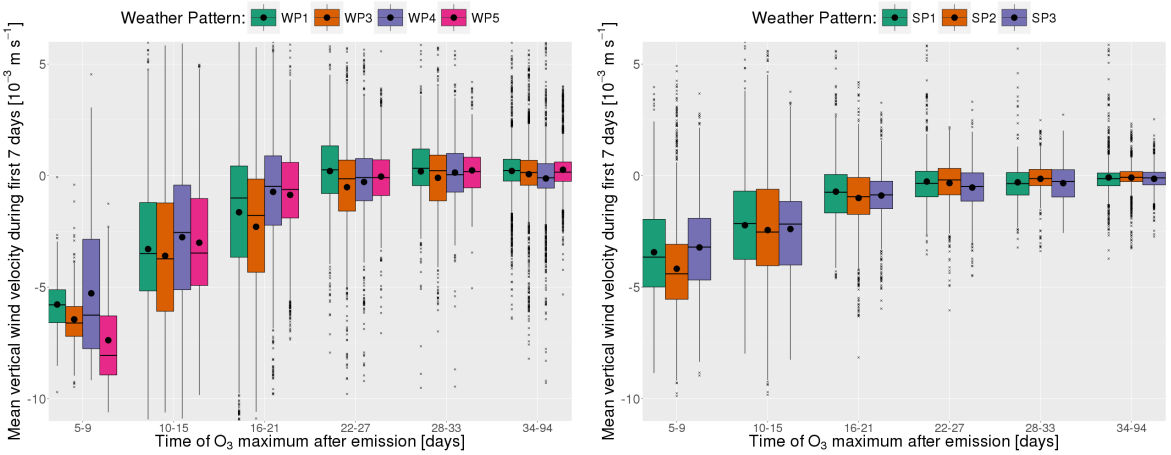

(a) Winter (b) Summer

Figure 8.14: Mean vertical transport during the first seven days, in relation to the time when the O_3 maximum is reached. Different weather pattern are colour coded in both figures.

It is expected that the difference of each individual weather situation (i.e. the number, location and strength of the high pressure systems) causes the inter-seasonal variability.

Table 8.3: Spearman rank coefficient for the correlation between the mean vertical wind velocity during the first seven days and the time of the O_3 maximum. Values are given for all seven weather pattern.

WP1	WP3	WP4	WP5	SP1	SP2	SP3
0.65	0.71	0.66	0.63	0.71	0.74	0.71

8.10.2. Background NO_x Concentration

Figure 8.15a shows a scatter plot of the mean background NO_x concentration during summer, in relation to the maximum O_3 concentration during the O_3 build-up. The Spearman rank coefficient for each weather pattern is given in Table 8.4. It becomes evident that for all three summer pattern, the points are equally distributed. This is also indicated by similar Spearman rank coefficients. This correlation is therefore valid for each summer pattern. The same observation can be made for the total CH_4 loss (not shown).

In Section 8.4.2 it became evident that during winter, the background NO_x concentration does not limit the maximum O_3 concentration. It is instead limited by the background HO_2 concentration. The Spearman rank coefficient for most winter patter indicates a weak correlation. Only WP5 differs. Here, the rank coefficient indicates a moderate correlation. The overall mean background concentration of NO_x is highest for this weather pattern (about 49 ppt). All other winter pattern are below 36 ppt and WP1 has a mean of 20 ppt. This also explains why this weather pattern has the lowest Spearman rank coefficient. It is expected that due to the generally higher background NO_x concentration for WP5, the maximum O_3 concentration is in some cases limited by higher background NO_x concentrations.

Table 8.4: Spearman rank coefficient for the correlation between the mean background NO_x concentration and the maximum O_3 concentration or the total CH_4 loss, during the O_3 build-up. Both given for each weather pattern.

-	WP1	WP3	WP4	WP5	SP1	SP2	SP3
O_3	-0.10	-0.43	-0.44	-0.57	-0.79	-0.79	-0.84
CH_4	-0.16	-0.37	-0.39	-0.39	-0.79	-0.83	-0.84

8.10.3. Background HO_2 Concentration

Figure 8.15b shows a scatter plot of the relation between the mean HO_2 background concentration during winter and the maximum O_3 concentration, during the O_3 build-up. Table 8.5 gives the Spearman

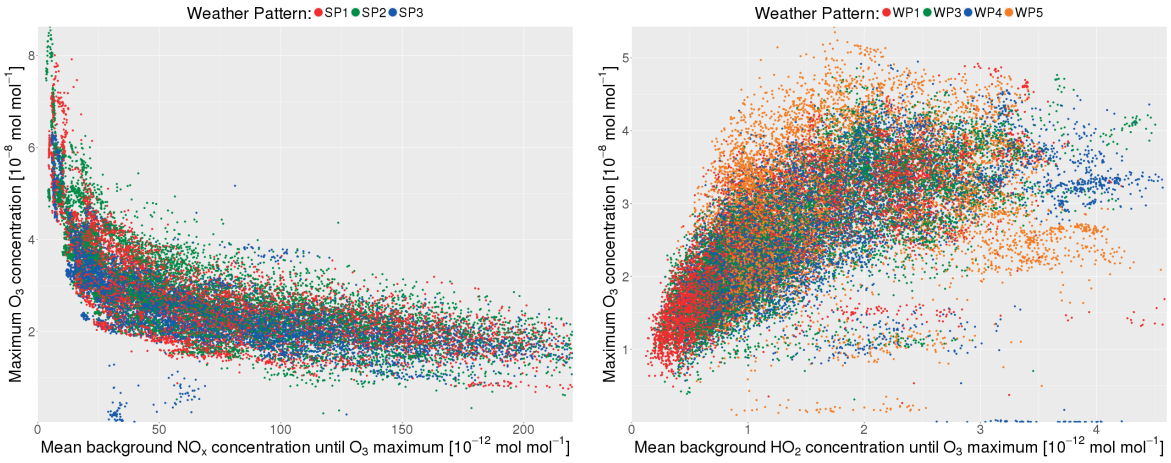

(a) Summer: NO_x (b) Winter: HO_2

Figure 8.15: Left: Mean background NO_x concentration in relation to the maximum O_3 concentration during the O_3 build-up. Valid for summer. Right: Mean HO_2 background concentration in relation to the maximum O_3 concentration during the O_3 build-up. Valid during winter. In both figures different weather pattern are colour coded.

rank coefficients for the same correlation. WP1, WP3 and WP4 represent this correlation in a good manner. Only WP5 behaves different and has a moderate correlation. Due to the higher background NO_x concentration (for this winter pattern), the maximum O_3 concentration is not only limited by the HO_2 concentration. It is rather limited by a combination of the background concentration of NO_x and HO_2. The same observations hold for the total CH_4 loss. During summer only weak correlations are given.

Table 8.5: Spearman rank coefficient for the correlation between the mean background HO_2 concentration and the maximum O_3 concentration or the total CH_4 loss, during the O_3 build-up. Both given for each weather pattern.

-	WP1	WP3	WP4	WP5	SP1	SP2	SP3
O_3	0.81	0.77	0.73	0.51	0.37	0.18	0.39
CH_4	0.87	0.85	0.83	0.61	0.46	0.46	0.47

8.10.4. Specific Humidity

Specific humidity influences the total CH_4 loss due to the influence of H_2O on the OH production. Table 8.6 gives the Spearman rank coefficient for the relation between the mean specific humidity during the CH_4 loss phase and the total CH_4 loss. The rank coefficient indicates that the relation is valid for all weather pattern. Only a slight seasonal difference exist. The correlation tends to be weaker during summer. This is caused by the overall higher H_2O content (and thus specific humidity) in the atmosphere. This causes a higher variability in the specific humidity which leads to a lower rank coefficient.

Table 8.6: Spearman rank coefficient for the correlation between the mean specific humidity and the total CH_4 loss, during the CH_4 loss phase. Values are given for all seven weather pattern.

WP1	WP3	WP4	WP5	SP1	SP2	SP3
0.84	0.87	0.81	0.79	0.73	0.73	0.74

8.10.5. Discussion

Overall it has been demonstrated that (except for WP5) the inter-seasonal difference is little. Therefore, the seasonal relations found in this thesis are generally valid for each weather pattern. For WP5 the

influence of the background NO_x and HO_2 differs. This is mainly due to higher background values for this pattern. However, the question still remains why this specific weather pattern is different. WP5 is the pattern where the emission occurs at the end of winter. The first winter pattern is initialised at the end of December. WP3 and WP4 are initialised in the middle and end of January. WP5 however is initialised on the 26th February. This is more than a month later than the other pattern. The mean background NO_x concentration increases the later the emission occurs. This indicates that the relations found are most likely not valid during spring. Additionally, it is not possible to just separate between winter and summer, to assess the yearly climate impact.

8.11. Results Summary

Based on the analysis performed in this chapter, many important insides on how weather influences the concentration changes of O_3 and CH_4 (due to aviation attributed NO_x emissions), are obtained. This section brings all those influences together by providing separated short summaries for O_3 and CH_4. First, the influence on O_3 is summarised. In a second step the influence on CH_4 is discussed. Each weather influence is illustrated by using a representative weather pattern. In this case, WP3 (as used in Chapter 1) at 300 hPa and SP1 at 300 hPa are used.

8.11.1. Weather Influences on the Temporal Development of O_3

The results obtained in the performed analysis showed that two characteristics of the temporal development of O_3 are influenced by weather. These two characteristics are the time and the magnitude of the O_3 maximum. The time of the O_3 maximum is influenced by the vertical transport in the atmosphere. If an air parcel experiences a fast downward transport an early O_3 maximum occurs. If an air parcel stays long at a high altitude, the O_3 maximum occurs later. It could be identified that air parcels that experience a fast downward motion, stay most of their time (until the O_3 maximum is reached), within an area of a high positive geopotential anomaly. A high geopotential is an indication of a high pressure area which is associated with subsidence. Air parcel with a late maximum spend most of their time in areas of negative geopotential anomalies which are associated with low pressure areas, where no subsidence occurs. Only if an air parcel stays most of its time in a high pressure system, an early O_3 maximum occurs.

Figure 8.16a shows the mean geopotential at 500 hPa until the O_3 maximum occurs (for WP3 at 300 hPa). The contours indicate the geopotential at 500 hPa at the time of emission. Emission locations were the O_3 maximum occurs early or late are indicated. It can be observed that only if the mean geopotential at 500 hPa is high, early O_3 maxima occur. Areas with low mean geopotential at 500 hPa are associated with late O_3 maxima. The figure shows that the emission does not necessary need to occur in a high pressure system (low geopotential at 500 hPa at the time of emission), as long as those air parcels are transported into areas of high pressure. Late O_3 maxima only occur at emission locations where a low pressure system was present at the time of emission (in this case above Greenland).

If a tracer is transported to lower altitudes, the surrounding temperature increases. This higher temperature leads to a higher chemical activity. This causes a faster build-up of O_3 and a faster reduction of the emitted NO_x. At the same time the O_3 depletion increases. At some point the O_3 depletion is higher than the O_3 build-up, leading to an O_3 maximum.

During summer the maximum O_3 concentration is controlled by the background NO_x concentrations. A lower NO_x background concentration leads to higher foreground O_3 production rates and thus a higher O_3 maximum. Figure 8.16b shows the mean background NO_x concentration until the O_3 maximum occurs. Contours indicate the background NO_x concentration at the time of emission. Emission locations with very high and very low maximum O_3 concentrations are indicated. Only a low mean background concentration of NO_x results in a high maximum O_3 concentration. If the mean background concentration of NO_x is high, only low O_3 maxima occur.

During winter the background concentration of NOx is rather low. Therefore, the background NO_x does not limit the foreground O_3 production rate. During winter low background concentration of HO_2 limit the foreground O_3 production rate. A low mean background HO_2 concentration leads to low O_3 maxima.

The relation between the mean HO_2 concentration until the O_3 maximum and the mean of the maximum O_3 concentration is given in Figure 8.16c. The mean HO_2 background concentration is colour coded and emission locations with very high or very low mean O_3 maxima, are indicated. Contours

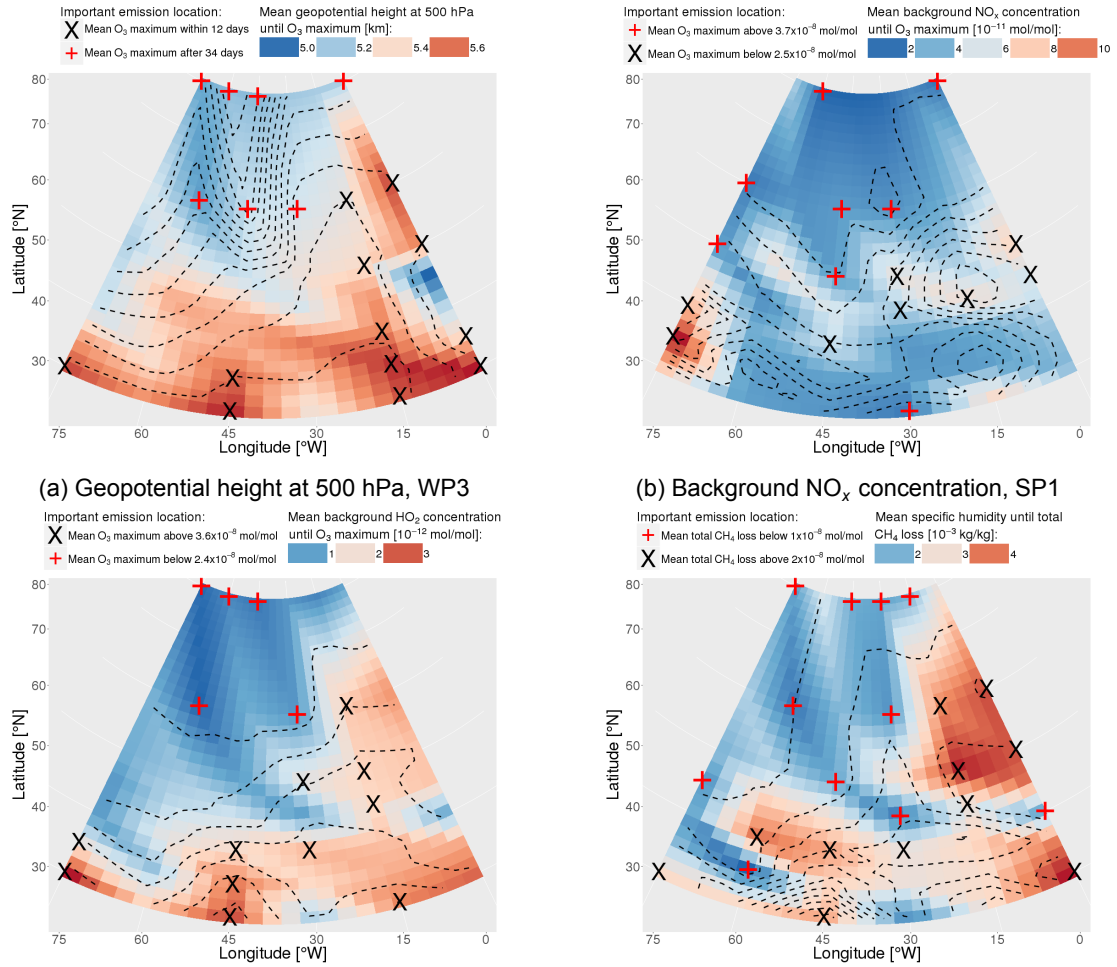

(a) Geopotential height at 500 hPa, WP3

(b) Background NO_x concentration, SP1

(c) Background HO_2 concentration, WP3

(d) Mean specific humidity, WP3

Figure 8.16: (a): Heat map of the mean geopotential height at 500 hPa until the O_3 maximum occurs. Emission locations with a very early and a very late O_3 maximum are indicated. Figure valid for WP3 at 300 hPa. (b) Heat map of the mean background NO_x concentration until the O_3 maximum occurs. Emission locations with a very high and a very low maximum O_3 concentration are indicated. Figure valid for SP1 at 300 hPa. (c): Heat map of the mean background HO_2 concentration until the O_3 maximum occurs. Emission locations with a very high and a very low maximum O_3 concentration are indicated. Figure valid for WP3 at 300 hPa. (d): Heat map of the mean specific humidity until the total CH_4 loss is reached. Emission location with a very high and a very low total CH_4 loss are indicated. Figure valid for WP3 at 300 hPa. (All): Contours indicate the colour coded weather variable at the time of emission. For all figures the mean of all 50 tracer at each emission location is taken.

indicate the background HO_2 concentration at the time of emission. Only if the mean HO_2 concentration is high, a high O_3 maxima occurs. Low background concentrations also lead to low O_3 maxima.

By comparing Figure 8.16a and 8.16c, it can be observed that an early O_3 maximum does not necessary lead to a high O_3 maximum concentration. This is related to the fact that a high pressure system does not necessary have a low background NO_x concentration (during summer) or a high background HO_2 concentration (during winter). However, if the O_3 maximum occurs late, only low O_3 maxima are possible.

8.11.2. Weather Influences on the Temporal Development of CH_4

Compared to the temporal development of O_3, their is only one characteristic which is important for the CH_4 depletion. Only the magnitude of the total CH_4 loss is of interest. This is based on the long perturbation lifetime of CH_4. This perturbation lifetime is so long, that a difference of a couple of days does not lead to a higher RF.

It has been shown that the maximum O_3 concentration has a significant influence on the total CH_4 loss. The higher the maximum O_3 concentration, the higher the total CH_4 loss. This influence is due to the fact that O_3 is a major source of foreground OH. Since CH_4 is lost by reacting with OH, a higher foreground OH (produced by higher O_3 concentrations) leads to higher CH_4 loss rates. Therefore, the total CH_4 loss correlates well with all weather influencing factors of O_3.

The most dominant weather influence of CH_4 is the specific humidity. Only if high amounts of H_2O are present in the background, a higher foreground O_3 depletion occurs, which leads to higher foreground OH concentrations.

Figure 8.16d gives the mean specific humidity until the total CH_4 loss is reached. Contours illustrate the specific humidity at the time of emission. Emission locations with very high and very low total CH_4 losses are indicated. Only a high mean specific humidity leads to a high total CH_4 loss. The opposite holds if the specific humidity is low.

By comparing Figure 8.16c and 8.16d it becomes evident that a high O_3 maximum concentration, does not necessary lead to a high total CH_4 loss. The specific humidity has no direct influence on the foreground production of O_3. Therefore, a high specific humidity does not necessary lead to a high O_3 concentration which is necessary for a high total CH_4 loss.

Figure 8.16 shows that each weather influence, impacting the temporal concentration change of O_3 and CH_4, varies in each weather situation and with each emission location. This explains why the resulting CCF results (for WP3 see Figure 1.1b) also differ with each emission location. By using the findings of this thesis, the varying climate impact of NO_x emission in a particular weather situation can be understood. This show great potential to improve future re-routing mitigation strategies.

8.11.3. Other Weather Influences

Additionally, two other weather factors influence the temporal development of both chemical species. If an air parcel stay most of its time within the lower stratosphere, the O_3 maximum occurs late and the O_3 maximum tends to be lower. Due to this lower foreground O_3 concentration, less CH_4 is lost. The second influencing factor is the polar night. If a tracer is transported above 66°N or 66°S (above the polar circle) during winter and summer respectively, the missing incoming solar radiation causes no O_3 to be produced or deplete.

9 Discussion

In this chapter a systematic discussion of all factors, that are not directly linked to weather influences on the temporal development of O_3 and CH_4, is performed. Therefore, no discussion on the weather influences itself are discussed here. Those discussions were presented in Chapter 7 and 8. In a first step, certain aspects of the REACT4C project will be analysed that influence the results obtained. In Section 9.2, other verification possibilities for the results obtained in this study, are discussed. Afterwards, the relation to previous literature is discussed in Section 9.3. In a last step, a possible application of the obtained results is elaborated.

9.1. The REACT4C Project

This section focuses on the REACT4C project. Only parts that directly influence the results of this thesis, are discussed. Influences of other steps (e.g. the re-routing model SAAM) are neglected. Since most topics discussed are not necessarily linked to each other, each discussion is group in one section.

9.1.1. EMAC Model Set-up

In numerous studies the underlying ECHAM5 model of EMAC has been verified. However, Grewe et al. (2017) demonstrated that regional differences of the tropopause level are underestimated in certain weather situations. This influences the background concentrations of many chemicals. In the specific case analysed by Grewe et al. (2017) the background NO_x concentration was only half of the concentration obtained from real time measurements. Stevenson and Derwent (2009) and this thesis demonstrated that the background NO_x concentration during summer, limits the maximum O_3 concentration. Therefore, uncertainties in the modelling approach can have major impacts on the maximum O_3 concentration (and therefore the resulting climate impact). COSMO (the other model set-up used by Grewe et al. (2017)), is capable of representing local difference in the tropopause altitude in a better manner. However, this model set-up overestimated the background NO_x concentration in certain cases. The magnitude of the overestimation was higher than the underestimation by EMAC. Currently, it is not possible to investigate the magnitude of uncertainties introduced by a wrong estimation of the tropopause altitude, on the temporal development of O_3 and CH_4 due to NO_x emissions.

9.1.2. Weather Pattern Used

It has been demonstrated that mainly seasonal differences exist and that the inter-seasonal variation is little. This is in particular true during summer. During winter only WP5 differs from the other three winter pattern. This indicates that the overall relations hold for both seasons. Still different weather situation lead to different climate impacts (e.g. different location, strength and duration of high pressure systems). It is still necessary to assess multiple weather pattern, to estimate the mitigation possibility of re-routing aircraft to avoid climate sensitive areas.

Irvine et al. (2013) do not indicate if additional weather systems need to be analysed for spring and autumn. The deviation of WP5 from all other winter pattern indicates that additional simulations are most likely need to estimate the yearly climate impact. In the NH, spring starts in the middle of

March. WP5 was initialised at the end of February (26th February 2001), which is at the end of winter. Most likely due to different background NO_x and HO_2 concentrations during spring, the maximum O_3 concentration will be limited by a combination of both chemical species. It is most likely necessary to also include weather pattern during spring in the yearly assessment. The same observation could not be made for autumn, since no summer pattern is initialised at the end of summer. Due to decreasing NO_x and HO_2 concentrations in autumn, it is most likely that those two chemical species influence the maximum O_3 concentration in a similar manner as it is expected for spring. However, further research needs to be conducted to fully assess the influence of spring and autumn.

9.1.3. Geographic Domain

The maximum O_3 concentration is influenced by the background NO_x and HO_2 concentration within the atmosphere. It is known that those two concentrations are higher in the NH. Stevenson and Derwent (2009) and this thesis identified a higher O_3 production efficiency if the background NO_x concentration is low during summer. Gilmore et al. (2013) found that flights originating from the SH introduce a higher O_3 burden. Overall, the geographic domain used in the REACT4C project is limited. In combination with the regional differences identified by Köhler et al. (2013) and Skowron et al. (2015), it can only be stated that the relations identified within this thesis, are valid for the particular area of REACT4C. Further research is necessary to assess if those relations are universally valid in the atmosphere or differ, if the emission occurs in the SH or at a different latitude and longitude in the NH. This is in particular important for regions with a strong increasing aviation activity (i.e. India and China).

9.1.4. Tagging Approach

Compared to a perturbation study, the specific tagging approach used with in REACT4C adds some inaccuracy to the simulation (Grewe et al., 2014a). Non-linear compensation effects in the atmospheric chemistry are eliminated by isolating the foreground processes from the background. This avoids misinterpretation of the results obtained (Grewe et al., 2012). It has been demonstrated that in some cases the foreground concentrations are way higher than the background concentrations of specific chemical compounds (e.g. OH). In addition with the simplified physics for the foreground calculation it is assumed that those assumptions introduce uncertainties. However, for a single tracer this effect is assumed to be small.

9.1.5. The Amount of NO_x Emitted

Expect for the highest emission location during summer, the emitted NO_x concentration is always higher than the background NO_x concentration. This favours higher foreground O_3 and OH production rates. At the highest emission location during summer, the foreground NO_x concentration tends to be lower than the background NO_x concentration. This effects in particular the foreground OH concentration. Less OH is produced which leads to lower CH_4 loss rates in the foreground than in the background during the O_3 build-up. Grewe et al. (2014a) provide no particular reason why they emitted $5 \cdot 10^5$ kg(NO) at each time region point. It is not clear if this effect for the highest emission altitude during summer is intended by Grewe et al. (2014a). A higher emission amount would have enabled a higher foreground production rate of OH and thus a higher CH_4 loss.

9.1.6. Concentration Changes vs. RF

In Section 7.2 it became evident that the maximum O_3 concentration and the total CH_4 loss increase with decreasing altitude. Based on Figure 7.2a it is expected that the instantaneous RF will have the same altitude behaviour as the chemical concentrations of O_3 and CH_4. Still, lower O_3 maxima (at 200 hPa) most likely lead to higher instantaneous RF than the same concentration change at 400 hPa would induce (see Section 7.1.2 and Lacis et al. (1990)). The adjusted RF on the other side is not going to have the same altitude relation. Due to the altitude adjustment it is expected that the adjusted RF is going to decrease with increasing altitude, have its minimum at 250 hPa and increase towards the emission altitude of 200 hPa. The CCF results will also have the same altitude relation.

The altitude adjustment is based on three pressure levels from Fichter (2009) and five pressure levels from Stuber (2003) (see Section 5.5.1). The applied fit has an extreme minimum at 250 hPa (Figure 5.2), which will lead to significant lower adjusted RF at this pressure altitude, compare to the other three altitudes. This might influence the potential re-routing results obtained. Results from Grewe

et al. (2014b) show a re-routing shift to 300 hPa at the highest optimisation. Therefore, this effect of the lower adjusted RF at 250 hPa seems to be negligible.

9.1.7. Different Time of Emission

Within this study emissions from 12:00 UTC were only taken into account (the other two emission times were neglected due to incomplete data sets). It could be shown that the transport within the first seven days is influencing the climate impact of each emission. It is expected that the identified relations are also valid if the emission occurs at a different point in time. If the emission occurred at a different time of the day, the weather situation is different at the emission location. Due to this different weather situation, the tracers might be transported to a different location and will have a different temporal development of O_3 and CH_4 than a tracer emitted at the same location at a different time. The climate impact will differ if the emission occurs at a different point in time. Still the physical processes identified in this thesis remain independent of emission time.

9.2. Verification of the Thesis Results

The results of this thesis have been compared to results of previous research and to theoretical meteorology, to explain each causality. A promising verification possibility, is to test if those relations exist also for different simulations and model set-ups.

9.2.1. WeCare Data

Grewe et al. (2017) presented results of the Utilizing Weather information for Climate efficient and eco efficient future aviation (WeCare) project. This project uses the same methodology as the REACT4C project including some advancements. The most notable ones are an additional day that is simulated, a higher graphical domain and changes in the horizontal and vertical resolution. Instead of a regular grid an adaptive grid is used, to better cover ice-saturated areas in which persistent contrails can form. This data set shows potential to be used to verify the relations found in this thesis. At the time of this thesis, some data of this project were available but it was out of the scope to perform this analysis.

Due to the larger domain, this data set could prove that those relations are also valid for emissions outside the analysed domain. By using this data, it is not possible to assess if those relations hold for the SH, since all emissions occur in the NH (Grewe et al., 2017).

9.2.2. Other Climate Models

The model set-up of WeCare is very similar to the one used by the REACT4C project. Thus model differences, like the influence of the tropopause altitude or the influence of Reaction R24 and R27 can not be assessed. A different model like COSMO (Grewe et al., 2017) could be used to assess those differences.

9.3. Relation to Previous Published Research

The number of published research on weather influences of the temporal development of O_3 and CH_4 due to aviation attributed NO_x is low. Frömming et al. (2017) and Grewe et al. (2017) are the main two previous publications that elaborate on the influence of a high pressure ridge on the time of the main O_3 gain. Both results are based on the same data set used within this thesis. Therefore, errors and uncertainties from the REACT4C project influence those results and those of this thesis, in the same manner.

The influence of the background NO_x concentration on the maximum O_3 concentration agreed well with the findings by Stevenson and Derwent (2009), during summer. Some uncertainty remains since there results represent the IRF, whereas this study only takes concentration changes into account. The highest emission altitude causes the lowest concentration change in O_3 due to the high background NO_x concentrations. However, the adjusted RF will be higher due to the applied altitude correction. Due to this altitude adjustment of the RF, it is expected that the exponential fit applied by Stevenson and Derwent (2009) will be different for the REACT4C data. Especially, the highest emission altitude will differ. It is not expected that the seasonal adjustment of the RF will lead to a higher correlations during winter, since all RF are influenced in a similar way.

9.4. Application Possibility: Predicting Climate Impact by Using Weather Forecasts

It is the ultimate goal to use the insides of the REACT4C approach to be able to forecast the CCFs results on a day-to-day base. Those could than be used fore real time re-routing of the aviation activities over the North Atlantic. Matthes et al. (2016) present the European Air Traffic Management for Environment (ATM4E) project which is intended to assess the feasibility of such a mitigation strategy. In particular so called algorithm based Environmental Change Functions (ECF) are obtained from the CCF results from the REACT4C simulation.

9.4.1. Number of Days Taken Into Account

The algorithm ECFs for NO_x are based on the weather situation at the time of emission (van Manen, 2017). Within this thesis it became evident that most relations identified are weak at the time of emission and strengthen if multiple days are taken into account. Common weather forecasting models are capable of predicting seven to fourteen days, in an acceptable manner (Haiden et al., 2015).

Table 9.1 provides the the Spearman rank coefficients for the most important relations identified within this study. Here, the rank coefficient is provided if the mean is based on multiple days after emission. It becomes evident that the correlation becomes stronger the more days after emission are taken into account. This is in particular true for the relation between the vertical transport and the time of the O_3 maximum. At the time of emission, the Spearman rank coefficient indicates a very weak correlation. The same result can be obtained by visually inspecting this correlation (not shown).

It becomes evident that basing the algorithm ECF on multiple days instead of just the time of emission shows a higher potential that those algorithm represent actual physical relations. Using seven days seems to be a good trade off, since the correlations indicated tends to be strong and weather models are capable of forecasting those time periods.

Table 9.1: Spearman rank coefficient for the most important relations identified in this thesis study in relation to the time period after emission on which the mean is based.

-	At Emission	2 days	3 days	4 days	5 days	6 days	7 days	Till O_3 maximum
Mean vertical transport vs. time of O_3 maximum:								
WP	-0.17	-0.33	-0.37	-0.41	-0.44	-0.52	-0.64	-0.66
SP	-0.20	-0.26	-0.41	-0.52	-0.57	-0.61	-0.71	-0.72
Mean background NO_x vs. maximum O_3 concentration:								
SP	-0.76	-0.77	-0.78	-0.79	-0.79	-0.79	-0.80	-0.86
Mean background NO_x vs. total CH_4 loss:								
SP	-0.60	-0.62	-0.64	-0.65	-0.66	-0.66	-0.67	-0.85
Mean background HO_2 vs. maximum O_3 concentration:								
WP	0.67	0.69	0.71	0.73	0.74	0.75	0.76	0.76
Mean background HO_2 vs. total CH_4 loss:								
WP	0.49	0.51	0.54	0.55	0.57	0.59	0.60	0.78
Mean specific humidity vs. total CH_4 loss:								
WP & SP	0.48	0.50	0.52	0.54	0.55	0.59	0.61	0.78

9.4.2. A Two Step Approach

Most concentrations increased monotonically with decreasing emission altitude. Due to the altitude RF adjustment for O_3 in REACT4C (Section 5.5.1) and the altitude dependency of the instantaneous RF identified in Section 7.1.2 (Lacis et al., 1990), a two step approach, to obtain the algorithm ECF shows high potential. It is most likely that the algorithms represent real physical relations if in a first step the concentration changes of O_3 and CH_4 are estimated, based on the local weather situation. A second algorithm should than approximate the CCF values, based on those concentration changes. In this second algorithm the altitude adjustment of RF would than be taken into account.

10

Conclusion and Recommendations

10.1. Conclusion

The research question of this thesis was to identify weather influences on the potential climate impact of NO_x emissions via an O_3 increase and a CH_4 depletion, by systematically analysing the temporal development of both chemical species, based on the REACT4C data set. Due to some missing data, the analysis neglected one winter pattern (WP2). The research objective was met by using a two step analysis. First, the different production and loss terms were analysed, to identify influences of different emission locations and seasons. In a second step, the obtained insides were used to systematically identify weather influences on specific characteristics of the temporal development of O_3 and CH_4.

Many important insides could be obtained on the different production and loss terms involved in the atmospheric NO_x chemistry. The location difference of most production and loss terms is caused by different background concentrations of all chemicals involved. In many cases the foreground production differs from the background production. Even though the background production and loss rates differ significantly between both seasons, only small seasonal differences in the foreground exists. This is caused by a higher foreground to background ratio of important chemicals, during winter.

The time when a tracer has its O_3 maximum is defined by the strength of the downward motion within the first week after emission. Air parcel that experience a fast downward motion tend to have earlier O_3 maxima compared to air parcel that stay long at a high altitude. By analysing the geopotential and geopotential height at 500 hPa as well as the 850-250 hPa layer thickness, it could be demonstrated that air parcels with a high mean downward motion are mainly located within high pressure systems. Not all of those tracers are also emitted in a high pressure system. Air parcel that are transported towards higher pressures in an early stage after emission, also have early O_3 maxima.

The reason why faster downward transport cause an early O_3 maximum is based on higher chemical efficiencies at lower altitudes. Lower altitudes favour higher temperatures which cause an increase in the production and loss rates. However, those higher chemical efficiencies do not necessary mean that higher O_3 concentrations are reached. The magnitude of the O_3 concentration is limited by the background concentration of NO_x (during summer) and HO_2 (during winter). During summer a lower background NO_x concentration leads to higher O_3 concentrations, whereas during winter only high background HO_2 concentrations lead to high O_3 maxima.

The CH_4 temporal development is influenced by multiple factors. First, O_3 is a major source of OH. Thus the more O_3 is gained, the higher the potential CH_4 depletion is going to be. Additionally, higher specific humilities lead to higher CH_4 loss rates and thus higher total CH_4 losses. Since specific humidity is a measure of the H_2O concentration within the air, specific humidity can be seen as a measure of the OH produced by H_2O reacting with O_3.

By analysing the inter-seasonal variability, it could be shown that most relations identified hold for all weather patterns within each season. Therefore, the climate impact of each weather pattern is caused by varying background concentrations as well as the overall weather situation (i.e. number, location, strength and lifetime of high pressure systems). Only WP5 differs to some extend, which might be caused by the emission taking place at the end of winter. This also illustrates that the specific relations identified for a season (influence of NO_x and HO_2) are most likely not valid for spring or autumn.

The insides obtained within this study on the influences on the temporal development show potential to improve the level of scientific understanding (LOSU) as well as future climate assessments of aviation attributed NO_x. It was demonstrated that future algorithm ECF could be improved by using multiple days. If multiple days are used, it is more likely to predict the climate impact based on actual physical processes.

This study also demonstrated that much uncertainty still remains. However, it still shows that by improving the understanding of physical processes in the atmosphere (that influence aviation attributed NO_x emissions), variations in the local climate impact are better understood. This will improve future mitigation strategies to reduce the climate impact of aviation.

10.2. Recommendations

The findings in this thesis lead to multiple recommendations. These are divided into recommendation for future simulations and future climate assessments.

10.2.1. Recommendations: Future Simulations

- Investigate the influence of the underestimation of the tropopause by EMAC on the temporal development of O_3 and CH_4 due to NO_x emission.
- Use a higher resolution of the background model to resolve local weather influences (e.g. tropopause altitude).
- Reassess the RF altitude adjustment for O_3, with a main focus on 250 hPa.
- Reassess the IPCC CH_4 RF approximation and its influence on the CH_4 CCF results.
- Reassess the amount of NO_x emitted on each tracer.
- Consider to apply a simple scaling to account for SWV (Stratospheric Water Vapour).
- Investigate the possibility to neglect Reaction R24 and R26 due to their low contribution to the total OH and HO_2 loss rates, to improve computation efficiency and storage space needed for future studies.

10.2.2. Recommendations: Climate Assessments

- Verify relations identified within this thesis by using the WeCare data.
- Investigate the influence of spring and autumn on the relations identified, by simulating additional weather pattern for those seasons.
- Investigate region difference by expanding the geographical domain to other important areas of aviation (e.g. Asia).
- Investigate the possibility to base the algorithm ECF of the ATM4E project on multiple days.
- Investigate the potential of a multi step approach for the algorithm ECF of ATM4E. A suggested approach based on the results obtained in this study is given by: (1) obtain concentration changes of O_3 and CH_4 from local weather, (2) estimate ECF from concentration changes taking the altitude adjustment of the O_3 RF into account.
- Investigate the influence of the identified wrong tracer initialisation on the obtained REACT4C results (i.e. Grewe et al. (2014b), Frömming et al. (2017) and Grewe et al. (2017)).

Bibliography

Ahrens, C. D.: Meteorology today: an introduction to weather, climate, and the environment, Cengage Learning, 2012.

Appleman, H.: The formation of exhaust condensation trails by jet aircraft, Bulletin of the American Meteorological Society, 34, 14–20, 1953.

Archer, D.: Fate of fossil fuel CO_2 in geologic time, Journal of Geophysical Research: Oceans, 110, n/a–n/a, 2005.

Arrhenius, S.: Über die Dissociationswärme und den Einfluss der Temperatur auf den Dissociationsgrad der Elektrolyte, Wilhelm Engelmann, 1889.

Atkinson, R.: Kinetics of the gas-phase reactions of OH radicals with alkanes and cycloalkanes, Atmospheric Chemistry and Physics, 3, 2233–2307, 2003.

Berntsen, T. K. and Isaksen, I. S. A.: Effects of lightning and convection on changes in tropospheric ozone due to NOx emissions from aircraft, Tellus B, 51, 766–788, 1999.

Brasseur, G. P., Cox, R. A., Hauglustaine, D., Isaksen, I., Lelieveld, J., Lister, D. H., Sausen, R., Schumann, U., Wahner, A., and Wiesen, P.: European scientific assessment of the atmospheric effects of aircraft emissions, Atmospheric Environment, 32, 2329–2418, 1998.

Burkhardt, U. and Kärcher, B.: Global radiative forcing from contrail cirrus, Nature climate change, 1, 54–58, 2011.

Connors, K. A.: Chemical kinetics: the study of reaction rates in solution, John Wiley & Sons, 1990.

Cook, J., Nuccitelli, D., Green, S. A., Richardson, M., Winkler, B., Painting, R., Way, R., Jacobs, P., and Skuce, A.: Quantifying the consensus on anthropogenic global warming in the scientific literature, Environmental research letters, 8, 024 024, 2013.

Dahlmann, K.: Eine Methode zur effizienten Bewertung von Maßnahmen zur Klimaoptimierung des Luftverkehrs, phdthesis, Ludwig Maximilians Universität, 2012.

Dahlmann, K., Grewe, V., Frömming, C., and Burkhardt, U.: Can we reliably assess climate mitigation options for air traffic scenarios despite large uncertainties in atmospheric processes?, Transportation Research Part D: Transport and Environment, 46, 40–55, 2016.

Ehhalt, D. and Rohrer, F.: The impact of commercial aircraft on tropospheric ozone, Special Publication-Royal Society of Chemistry, 170, 105–120, 1995.

Ehhalt, D., Prather, M., Dentener, F., Derwent, R., Dlugokencky, E., Holland, E., Isaksen, I., Katima, J., Kirchhoff, V., Matson, P., et al.: Atmospheric chemistry and greenhouse gases, in: Climate Change 2001: impacts, adaptation and vulnerability, pp. 241–287, Cambridge University Press, 2001.

Esch, M., Giorgetta, M., Schlese, U., and Schulzweida, U.: The atmospheric general circulation model ECHAM-4: model description and simulation of present-day climate, DKRZ-Report No, 218, n/a–n/a, 1996.

Fichter, C.: Climate impact of air traffic emissions in dependency of the emission location and altitude, phdthesis, Manchester Metropolitan University, 2009.

Forster, P., Ramaswamy, V., Artaxo, P., Berntsen, T., Betts, R., Fahey, D. W., Haywood, J., Lean, J., Lowe, D. C., Myhre, G., et al.: 2007: Changes in Atmospheric Constituents and in Radiative Forcing, in: Climate Change 2007: The Physical Science Basis. Contricution of Working Group I on the Fourth Assessment Report of the Intergovernmental Panel on Climate Change, Cambridge University Press, 2007.

Frömming, C., Grewe, V., Jöckel, P., Brinkop, S., Dietmüller, S., Garny, H., Ponater, M., Tsati, E., and Matthes, S.: Climate cost functions as a basis for climate optimized flight trajectories, in: Tenth USA/Europe Air Traffic Management Research and Development Seminar, vol. 2013, 2013.

Frömming, C., Grewe, V., Matthes, S., Brinkop, S., Haslerund, A. S., Irvine, E. A., van Manen, J., and Rosanka, S.: Influence of weather situation on aviation emission effects: The REACT4C Climate Chnage Functions, Atmospheric Environment, in progress, 2017.

Fuglestvedt, J. S., Berntsen, T. K., Isaksen, I. S., Mao, H., Liang, X.-Z., and Wang, W.-C.: Climatic forcing of nitrogen oxides through changes in tropospheric ozone and methane; global 3D model studies, Atmospheric Environment, 33, 961–977, 1999.

Fuglestvedt, J. S., Shine, K. P., Berntsen, T., Cook, J., Lee, D. S., Stenke, A., Skeie, R. B., Velders, G. J. M., and Waitz, I. A.: Transport impacts on atmosphere and climate: Metrics, Atmospheric Environment, 44, 4648–4677, 2010.

Gierens, K. M., Lim, L., and Eleftheratos, K.: A review of various strategies for contrail avoidance, Open Atmospheric Science Journal, 2, 1–7, 2008.

Gilmore, C. K., Barrett, S. R. H., Koo, J., and Wang, Q.: Temporal and spatial variability in the aviation NO_x-related O_3 impact, Environmental Research Letters, 8, 034 027, 2013.

Grewe, V. and Stenke, A.: AirClim: an efficient climate impact assessment tool, Atmospheric Chemistry and Physics, 8, 4621–4639, 2008.

Grewe, V., Tsati, E., and Hoor, P.: On the attribution of contributions of atmospheric trace gases to emissions in atmospheric model applications, Geoscientific Model Development, 3, 487–499, 2010.

Grewe, V., Dahlmann, K., Matthes, S., and Steinbrecht, W.: Attributing ozone to NOx emissions: Implications for climate mitigation measures, 59, 102–107, 2012.

Grewe, V., Frömming, C., Matthes, S., Brinkop, S., Ponater, M., Dietmüller, S., Jöckel, P., Garny, H., Tsati, E., Dahlmann, K., Søvde, O. A., Fuglestvedt, J., Berntsen, T. K., Shine, K. P., Irvine, E. A., Champougny, T., and Hullah, P.: Aircraft routing with minimal climate impact: the REACT4C climate cost function modelling approach (V1.0), Geoscientific Model Development, 7, 175–201, 2014a.

Grewe, V., Champougny, T., Matthes, S., Frömming, C., Brinkop, S., Søvde, O. A., Irvine, E. A., and Halscheidt, L.: Reduction of the air traffic's contribution to climate change: A REACT4C case study, Atmospheric Environment, 94, 616–625, 2014b.

Grewe, V., Dahlmann, K., Flink, J., Frömming, C., Ghosh, R., Gierens, K., Heller, R., Hendricks, J., Jöckel, P., Kaufmann, S., Kölker, K., Linke, F., Luchkova, T., Lührs, B., Van Manen, J., Matthes, S., Minikin, A., Niklaß, M., Plohr, M., Righi, M., Rosanka, S., Schmitt, A., Schumann, U., Terekhov, I., Unterstrasser, S., Vázquez-Navarro, M., Voigt, C., Wicke, K., Yamashita, H., Zahn, A., and Ziereis, H.: Mitigating the Climate Impact from Aviation: Achievements and Results of the DLR WeCare Project, Aerospace, 4, 2017.

Haiden, T., Janousek, M., Bauer, P., Bidlot, J., Dahoui, M., Ferranti, L., Prates, F., Richardson, D., and Vitart, F.: Evaluation of ECMWF forecasts, including 2014-2015 upgrades, 2015.

Hansen, J., Fung, I., Lacis, A., Rind, D., Lebedeff, S., Ruedy, R., Russell, G., and Stone, P.: Global climate changes as forecast by Goddard Institute for Space Studies three-dimensional model, Journal of Geophysical Research: Atmospheres, 93, 9341–9364, 1988.

Hansen, J., Sato, M., and Ruedy, R.: Radiative forcing and climate response, Journal of Geophysical Research: Atmospheres, 102, 6831–6864, 1997.

Holmes, C. D., Tang, Q., and Prather, M. J.: Uncertainties in climate assessment for the case of aviation NO, Proceedings of the National Academy of Sciences, 108, 10 997–11 002, 2011.

Hoor, P., Borken-Kleefeld, J., Caro, D., Dessens, O., Endresen, O., Gauss, M., Grewe, V., Hauglustaine, D., Isaksen, I. S. A., Jöckel, P., Lelieveld, J., Myhre, G., Meijer, E., Olivie, D., Prather, M., Schnadt Poberaj, C., Shine, K. P., Staehelin, J., Tang, Q., van Aardenne, J., van Velthoven, P., and Sausen, R.: The impact of traffic emissions on atmospheric ozone and OH: results from QUANTIFY, Atmospheric Chemistry and Physics, 9, 3113–3136, 2009.

Hornbrook, R., Crawford, J., Edwards, G., Goyea, O., Mauldin Iii, R., Olson, J., and Cantrell, C.: Measurements of tropospheric HO_2 and RO_2 by oxygen dilution modulation and chemical ionization mass spectrometry, Atmospheric Measurement Techniques, 4, 735, 2011.

Irvine, E. A., Hoskins, B. J., Shine, K. P., Lunnon, R. W., and Froemming, C.: Characterizing North Atlantic weather patterns for climate-optimal aircraft routing, Meteorological Applications, 20, 80–93, 2013.

Isaksen, I. and Dalsøren, S.: Getting a better estimate of an atmospheric radical, Science, 331, 38–39, 2011.

Jacob, D.: Introduction to atmospheric chemistry, Princeton University Press, 1999.

Jöckel, P., Tost, H., Pozzer, A., Brühl, C., Buchholz, J., Ganzeveld, L., Hoor, P., Kerkweg, A., Lawrence, M. G., Sander, R., Steil, B., Stiller, G., Tanarhte, M., Taraborrelli, D., Van Aardenne, J., and Lelieveld, J.: The atmospheric chemistry general circulation model ECHAM5/MESSy1: consistent simulation of ozone from the surface to the mesosphere, Atmospheric Chemistry and Physics Discussions, 6, 6957–7050, 2006.

Jöckel, P., Kerkweg, A., Pozzer, A., Sander, R., Tost, H., Riede, H., Baumgaertner, A., Gromov, S., and Kern, B.: Development cycle 2 of the Modular Earth Submodel System (MESSy2), Geoscientific Model Development, 3, 717–752, 2010.

Köhler, M. O., Rädel, G., Dessens, O., Shine, K. P., Rogers, H. L., Wild, O., and Pyle, J. A.: Impact of perturbations to nitrogen oxide emissions from global aviation, Journal of Geophysical Research: Atmospheres, 113, n/a–n/a, 2008.

Köhler, M. O., Rädel, G., Shine, K. P., Rogers, H. L., and Pyle, J. A.: Latitudinal variation of the effect of aviation NO_x emissions on atmospheric ozone and methane and related climate metrics, Atmospheric Environment, 64, 1–9, 2013.

Kirkland, E. J.: Bilinear Interpolation, pp. 261–263, Springer US, Boston, MA, 2010.

Kotz, J., Treichel, P., and Townsend, J.: Chemistry and Chemical Reactivity, Available Titles OWL Series, Cengage Learning, 2008.

Lacis, A. A., Wuebbles, D. J., and Logan, J. A.: Radiative forcing of climate by changes in the vertical distribution of ozone, Journal of Geophysical Research: Atmospheres, 95, 9971–9981, 1990.

Lee, D. S., Fahey, D. W., Forster, P. M., Newton, P. J., Wit, R. C. N., Lim, L. L., Owen, B., and Sausen, R.: Aviation and global climate change in the 21st century, Atmospheric Environment, 43, 3520–3537, 2009.

Lee, D. S., Pitari, G., Grewe, V., Gierens, K., Penner, J. E., Petzold, A., Prather, M. J., Schumann, U., Bais, A., Berntsen, T., Iachetti, D., Lim, L. L., and Sausen, R.: Transport impacts on atmosphere and climate: Aviation, Atmospheric Environment, 44, 4678–4734, 2010.

Lohmann, U. and Feichter, J.: Global indirect aerosol effects: a review, Atmospheric Chemistry and Physics, 5, 715–737, 2005.

Matthes, S., Schumann, U., Grewe, V., Frömming, C., Dahlmann, K., Koch, A., and Mannstein, H.: Climate Optimized Air Transport, in: Atmospheric Physics, edited by Schumann, U., Research Topics in Aerospace, pp. 727–746, Springer Berlin Heidelberg, 2012.

Matthes, S., Grewe, V., Lee, D. S., Linke, F., Shine, K., and Stromatas, S.: ATM4E: A concept for environmentally-optimized aircraft trajectories, 2016.

Myhre, G., Nilsen, J. S., Gulstad, L., Shine, K. P., Rognerud, B., and Isaksen, I. S.: Radiative forcing due to stratospheric water vapour from CH_4 oxidation, Geophysical Research Letters, 34, n/a–n/a, 2007.

Myhre, G., Shine, K. P., Rädel, G., Gauss, M., Isaksen, I. S. A., Tang, Q., Prather, M. J., Williams, J. E., van Velthoven, P., Dessens, O., Koffi, B., Szopa, S., Hoor, P., Grewe, V., Borken-Kleefeld, J., Berntsen, T. K., and Fuglestvedt, J. S.: Radiative forcing due to changes in ozone and methane caused by the transport sector, 45, 387–394, 2011.

Reithmeier, C. and Sausen, R.: ATTILA: atmospheric tracer transport in a Lagrangian model, Tellus B, 54, 278–299, 2002.

Roeckner, E., Bäuml, G., Bonaventura, L., Brokopf, R., Esch, M., Giorgetta, M., Hagemann, S., Kirchner, I., Kornblueh, L., Manzini, E., Rhodin, A., Schlese, U., Schulzweida, U., and Tompkins, A.: The atmospheric general circulation model ECHAM 5. PART I: Model description, no. 349 in Report / MPI für Meteorologie, Max Planck Institute for Meteorology, 2003.

Sander, R., Kerkweg, A., Jöckel, P., and Lelieveld, J.: Technical note: The new comprehensive atmospheric chemistry module MECCA, Atmospheric Chemistry and Physics, 5, 445–450, 2005.

Sander, S. P., Friedl, R., Golden, D., Kurylo, M., Moortgat, G., Wine, P., Ravishankara, A., Kolb, C., Molina, M., Finlayson-Pitts, B., et al.: Chemical kinetics and photochemical data for use in atmospheric studies, evaluation number 14, Jet Propulsion Laboratory, Pasadena, CA, JPL Publication 02-25, n/a–n/a, 2003.

Schettino, V., Bini, R., Ceppatelli, M., Ciabini, L., and Citroni, M.: Chemical Reactions at Very High Pressure, pp. 105–242, John Wiley & Sons, Inc., 2005.

Schmidt, E.: Die entstehung von eisnebel aus den auspuffgasen von flugmotoren, Schriften der Deutschen Akademie der Luftfahrtforschung, Verlag R. Oldenbourg, München, Heft 44, 5, 1–15, 1941.

Schumann, U.: On conditions for contrail formation from aircraft exhausts, Meteorologische Zeitschrift, 5, 4–23, 1996.

Schumann, U. and Huntrieser, H.: The global lightning-induced nitrogen oxides source, Atmospheric Chemistry and Physics, 7, 3823–3907, 2007.

Seinfeld, J. H. and Pandis, S. N.: Atmospheric chemistry and physics: from air pollution to climate change, John Wiley & Sons, 2016.

Shine, K. P., Derwent, R., Wuebbles, D., and Morcrette, J.: Radiative forcing of climate, in: Climate Change: The IPCC Scientific Assessment (1990), Report prepared for Intergovernmental Panel on Climate Change by Working Group I, edited by Houghton, J. T., Jenkins, G. J., and Ephraums, J. J., chap. 2, pp. 41–68, Cambridge University Press, Cambridge, Great Britain, New York, NY, USA and Melbourne, Australia, 1990.

Skowron, A., Lee, D. S., and De León, R. R.: Variation of radiative forcings and global warming potentials from regional aviation NO_x emissions, Atmospheric Environment, 104, 69–78, 2015.

Stevenson, D. S. and Derwent, R. G.: Does the location of aircraft nitrogen oxide emissions affect their climate impact?, Geophysical Research Letters, 36, n/a–n/a, 2009.

Stevenson, D. S., Doherty, R. M., Sanderson, M. G., Collins, W. J., Johnson, C. E., and Derwent, R. G.: Radiative forcing from aircraft NO_x emissions: Mechanisms and seasonal dependence, Journal of Geophysical Research: Atmospheres, 109, n/a–n/a, 2004.

Stocker, T., Qin, D., Plattner, G., Tignor, M., Allen, S., Boschung, J., Nauels, A., Xia, Y., Bex, B., and Midgley, B.: Climate change 2013: The physical science basis. Contribution of working group I to the fifth assessment report of the intergovernmental panel on climate change, Cambridge University Press, 2013.

Stordal, F., Gauss, M., Myhre, G., Mancini, E., Hauglustaine, D. A., Köhler, M. O., Berntsen, T., Stordal, E. J. G., Iachetti, D., Pitari, G., and Isaksen, I. S. A.: TRADEOFFs in climate effects through aircraft routing: forcing due to radiatively active gases, Atmospheric Chemistry and Physics Discussions, 6, 10 733–10 771, 2006.

Stuber, N.: Ursachen der Variabilität des Klimasensitivitätsparameters für räumlich inhomogene Ozonstörungen, DLR, Bibliotheks-und Informationswesen, 2003.

Stuber, N., Sausen, R., and Ponater, M.: Stratosphere adjusted radiative forcing calculationsin a comprehensive climate model, Theoretical and applied climatology, 68, 125–135, 2001.

Student: The probable error of a mean, Biometrika, pp. 1–25, 1908.

Søvde, O. A., Matthes, S., Skowron, A., Iachetti, D., Lim, L., Owen, B., Øivind Hodnebrog, Genova, G. D., Pitari, G., Lee, D. S., Myhre, G., and Isaksen, I. S.: Aircraft emission mitigation by changing route altitude: A multi-model estimate of aircraft NO_x emission impact on O_3 photochemistry, Atmospheric Environment, 95, 468 – 479, 2014.

Tukey, J. W.: Comparing individual means in the analysis of variance, Biometrics, pp. 99–114, 1949.

van Manen, J.: Aviation H_2O and NO_x climate cost functions based on local weather, Master's thesis, Delft University of Technology, Delft, 2017.

Warneck, P.: Chemistry of the natural atmosphere, vol. 71, Academic press, 1999.

Welch, B.: On the comparison of several mean values: an alternative approach, Biometrika, 38, 330–336, 1951.

Welch, B. L.: The generalization ofstudent's' problem when several different population variances are involved, Biometrika, 34, 28–35, 1947.

Wigley, T.: Relative contributions of different trace gases to the greenhouse effect, Climate Monitor, 16, 14–28, 1987.

Wilcox, L. J., Shine, K. P., and Hoskins, B. J.: Radiative forcing due to aviation water vapour emissions, Atmospheric Environment, 63, 1 – 13, 2012.

Wild, O., Prather, M. J., and Akimoto, H.: Indirect long-term global radiative cooling from NO_x Emissions, Geophysical Research Letters, 28, 1719–1722, 2001.

Woollings, T., Hannachi, A., and Hoskins, B.: Variability of the North Atlantic eddy-driven jet stream, Quarterly Journal of the Royal Meteorological Society, 136, 856–868, 2010.

Wuebbles, D. J. and Hayhoe, K.: Atmospheric methane and global change, Earth-Science Reviews, 57, 177 – 210, 2002.

A

Chemical Reaction

The following Table includes a list of all chemical reaction taken into account for each different production and loss group (list obtained from Christine Frömming, personal communication, October 2016).

Table A.1: All chemical reactions taken into account for each production and loss group (list obtained from Christine Frömming, personal communication, October 2016).

Mecca ID	Reaction
ProdO3N:	
G3201	$NO + HO_2 \longrightarrow NO_2 + OH$
G4104	$CH_3O_2 + NO \longrightarrow HCHO + NO_2 + HO_2$
G4204	$C_2H_5O_2 + NO \longrightarrow CH_3CHO + HO_2 + NO_2$
G4212	$CH_3CO_3 + NO \longrightarrow CH_3O_2 + NO_2$
G4305	$IC_3H_7O_2 + NO \longrightarrow 0.96\,CH_3COCH_3 + 0.96\,HO_2 + 0.96\,NO_2 + 0.04\,IC_3H_7NO_3$
G4309	$LHOC_3H_6O_2 + NO \longrightarrow 0.98\,CH_3CHO + 0.98\,HCHO + 0.98\,HO_2 + 0.98\,NO_2 + 0.02\,LC_4H_9NO_3$
G4313	$CH_3COCH_2O_2 + NO \longrightarrow NO_2 + CH_3CO_3 + HCHO$
G4403	$LC_4H_9O_2 + NO \longrightarrow 0.84\,NO_2 + 0.56\,MEK + 0.56\,HO_2 + 0.28\,C_2H_5O_2 + 0.28\,CH_3CHO + 0.16\,LC_4H_9NO_3$
G4408	$MVKO_2 + NO \longrightarrow NO_2 + 0.25\,CH_3CH_3 + 0.25\,ACETOL + 0.75\,HCHO + 0.25\,CO + 0.75\,HO_2 + 0.5\,MGLYOX$
G4415	$LMEKO_2 + NO \longrightarrow 0.985\,CH_3CHO + 0.985\,CH_3CO_3 + 0.985\,NO_2 + 0.15\,LC_4H_9NO_3$
G4504	$ISO_2 + NO \longrightarrow 0.88\,HO_2 + 0.88\,MVK + 0.88\,HCHO + 0.88\,HO_2 + 0.12\,ISON$
G4504a	$ISO_2 + NO \longrightarrow 0.956\,NO_2 + 0.956\,MVK + 0.956\,HCHO + 0.956\,HO_2 + 0.044\,ISON$
LossO3N:	
G3105	$NO_2 + O(^3P) \longrightarrow NO + O_2$
LossO3Y:	
G1002	$O_3 + O(^1D) \longrightarrow 2\,O_2$
G1003	$O_3 + O(^3P) \longrightarrow 2\,O_2$
G2101	$H + O_3 \longrightarrow OH + O_2$
G2102	$H_2 + O(^1D) \longrightarrow H + OH$
G2103	$OH + O(^3P) \longrightarrow H + O_2$
G2104	$OH + O_3 \longrightarrow HO_2 + O_2$
G2106	$HO_2 + O(^3P) \longrightarrow OH + O_2$
G2107	$HO_2 + O_3 \longrightarrow OH + 2\,O_2$
G2111	$H_2O + O(^1D) \longrightarrow 2\,OH$

G3102a $N_2O + O(^1D) \longrightarrow 2\,NO$

G3102b $N_2O + O(^1D) \longrightarrow N_2 + O_2$

G3204 $NO_3 + HO_2 \longrightarrow NO_2 + OH + O_2$

G3210 $NH_2 + O_3 \longrightarrow NH_2O + O_2$

G3215 $NH_2 + NO_2 \longrightarrow N_2O + H_2O$

G3216 $NH_2 + NO_2 \longrightarrow NH_2O + NO$

G3217 $NH_2O + O_3 \longrightarrow NH_2 + O_2$

G3221 $HNO + NO_2 \longrightarrow HONO + NO$

G4100 $CH_4 + O(^1D) \longrightarrow 0.75\,CH_3O_2 + 0.75\,OH + 0.25\,HCHO + 0.4\,H + 0.05\,H_2$

G4105 $CH_3O_2 + NO_3 \longrightarrow HCHO + HO_2 + NO_2$

G4109 $HCHO + NO_3 \longrightarrow HNO_3 + CO + HO_2$

G4201 $C_2H_4 + O_3 \longrightarrow HCHO + 0.22\,HO_2 + 0.12\,OH + 0.23\,CO + 0.54\,HCOOH + 0.1\,H_2$

G4205 $C_2H_5O_2 + NO_3 \longrightarrow CH_3CHO + HO_2 + NO_2$

G4209 $CH_3CHO + NO_3 \longrightarrow CH_3CO_3 + HNO_3$

G4214 $CH_3CO_3 + NO_3 \longrightarrow CH_3O_2 + HO_2$

G4303 $C_3H_6 + NO_3 \longrightarrow LC_4H_9NO_3$

G4405 $MVK + O_3 \longrightarrow 0.45\,HCOOH + 0.9\,MGLYOX + 0.1\,CH_3CO_2 + 0.19\,OH + 0.22\,CO + 0.32\,HO_2$

G4502 $C_5H_8 + NO_3 \longrightarrow ISON$

G6101 $ClO + O(^3P) \longrightarrow Cl + O_2$

G6102a $ClO + ClO \longrightarrow Cl_2 + O_2$

G6102b $ClO + ClO \longrightarrow 2\,Cl + O_2$

G6102c $ClO + ClO \longrightarrow Cl + OClO$

G6203 $ClO + OH \longrightarrow 0.94\,Cl + 0.94\,HO_2 + 0.06\,HCl + 0.06\,O_2$

G6403 $ClO + CH_3O_2 \longrightarrow HO_2 + Cl + HCHO$

G6405 $CH_3Cl + O(^1D) \longrightarrow OH + Cl\,(+ ...)$

G6407 $CH_3CCl_3 + O(^1D) \longrightarrow OH + 2\,Cl\,(+ ...)$

G7101 $BrO + O(^3P) \longrightarrow Br + O_2$

G7102a $BrO + BrO \longrightarrow 2\,Br + O_2$

G7102b $BrO + BrO \longrightarrow Br_2 + O_2$

G7203 $HOBr + O(^3P) \longrightarrow OH + BrO$

G7402b $BrO + CH_3O_2 \longrightarrow Br + HCHO + HO_2$

G7603a $BrO + ClO \longrightarrow Br + OClO$

G7603b $BrO + ClO \longrightarrow Br + Cl + O_2$

G7603c $BrO + ClO \longrightarrow BrCl + O_2$

G9401 $DMS + NO_3 \longrightarrow CH_3SO_2 + HNO_3 + HCHO\,(-O_3)$

G9404 $CH_3SO_2 + O_3 \longrightarrow CH_3SO_3$

G9701 $DMs + Br \longrightarrow DMSO + Br$

J3103b $NO_3 + hv \longrightarrow NO$

J6100 $Cl_2O_2 + hv \longrightarrow 2\,Cl$

J6201 $HOCl + hv \longrightarrow OH + Cl$

J7200 $HOBr + hv \longrightarrow Br + OH$

J7301 $BrNO_3 + hv \longrightarrow 0.29\,Br + 0.29\,NO_3 + 0.71\,BrO + 0.71\,NO_2$

HET200 $N_2O_5 + H_2O \longrightarrow 2\,HNO_3$

HET201 $N_2O_5 \longrightarrow 2\,NO_{3mcs} + 2\,H_{pcs}$

HET410 $HOCl + HCl \longrightarrow Cl_2 + H_2O$

HET420 $ClNO_3 + HCl \longrightarrow Cl_2 + HNO_3$

HET422 $N_2O_5 + HCl \longrightarrow ClNO_2 + HNO_3$

HET510 $HOBr + HBr \longrightarrow Br_2 + H_2O$

HET540 $ClNO_3 + HBr \longrightarrow BrCl + HNO_3$

HET541	$BrNO_3 + HCl \longrightarrow BrCl + HNO_3$
HET542	$HOCl + HBr \longrightarrow BrCl + H_2O$
HET543	$HOBr + HCl \longrightarrow BrCl + H_2O$
LossNOx:	
G3202	$NO_2 + OH \longrightarrow HNO_3$
LossHNO3:	
G306	$HNO_3 + OH \longrightarrow H_2O + NO_3$
J3201	$HNO_3 + hv \longrightarrow NO_2 + OH$
ProdOH1:	
G2111	$H_2O + O(^1D) \longrightarrow 2\,OH$
ProdOH2:	
G2107	$HO_2 + O_3 \longrightarrow OH + 2\,O_2$
ProdOH3:	
G3201	$NO + HO_2 \longrightarrow NO_2 + OH$
LossOH1:	
G2104	$OH + O_3 \longrightarrow HO_2 + O_2$
LossOH2:	
G4110	$CO + OH \longrightarrow H + CO_2$
LossOH3:	
G4200	$C_2H_6 + OH \longrightarrow C_2H_5O_2 + H_2O$
G4202	$C_2H_4 + OH + (M) \longrightarrow 0.6666667\,LHOC_3H_6O_2$
G4208	$CH_3CHO + OH \longrightarrow CH_3CO_3 + H_2O$
G4210	$CH_3CO_2H + OH \longrightarrow CH_3O_2$
G4218	$CH_3CO_3H + OH \longrightarrow CH_3CO_3$
G4300	$C_3H_8 + OH \longrightarrow 0.82\,IC_3H_7O_2 + 0.18\,C_2H_5O_2 + H_2O$
G4302	$C_3H_6 + OH + (M) \longrightarrow LHOC_3H_6O_2$
G4311	$CH_3COCH_3 + OH \longrightarrow CH_3COCH_2O_2 + H_2O$
G4400	$NC_4H_{10} + OH \longrightarrow LC_4H_9O_2 + H_2O$
G4501	$C_5H_8 + OH \longrightarrow ISO_2$
G4508	$ISON + OH \longrightarrow ACETOL + NACA$
LossOH4:	
G4101	$CH_4 + OH + O_2 \longrightarrow CH_3O_2 + H_2O$
LossOH5:	
G2109	$HO_2 + OH \longrightarrow H_2O + O_2$
ProdHO21:	
G4104	$CH_3O_2 + NO \longrightarrow HCHO + NO_2 + HO_2$
G4204	$C_2H_5O_2 + NO \longrightarrow CH_3CHO + HO_2 + NO_2$
G4305	$IC_3H_7O_2 + NO \longrightarrow 0.96\,CH_3COCH_3 + 0.96\,HO_2 + 0.96\,NO_2 + 0.04\,IC_3H_7NO_3$
G4309	$LHOC_3H_6O_2 + NO \longrightarrow 0.96\,CH_3COCH_3 + 0.96\,HO_2 + 0.96\,NO_2 + 0.04\,IC_3H_7NO_3$
G4403	$LC_4H_9O_2 + NO \longrightarrow 0.84\,NO_2 + 0.56\,MEK + 0.56\,HO_2 + 0.28\,C_2H_5O_2 + 0.28\,CH_3CHO + 0.16\,LC_4H_9NO_3$
G4408	$MVKO_2 + NO \longrightarrow NO_2 + 0.25\,CH_3CO_3 + 0.25\,ACETOL + 0.75\,HCHO + 0.25\,CO + 0.75\,HO_2 + 0.5\,MGLYOX$
G4504	$ISO_2 + NO \longrightarrow 0.88\,NO_2 + 0.88\,MVK + 0.88\,HCHO + 0.88\,HO_2 + 0.12\,ISON$
LossHO21:	
G4103a	$CH_3O_2 + HO_2 \longrightarrow CH_3OOH$
G4203	$C_2H_5O_2 + HO_2 \longrightarrow C_2H_5OOH$
G4211a	$CH_3CO_3 + HO_2 \longrightarrow CH_3CO_3H$
G4211b	$CH_3CO_3 + HO_2 \longrightarrow CH_3CO_2H + O_3$
G4304	$IC_3H_7O_2 + HO_2 \longrightarrow IC_3H_7OOH$
G4308	$LHOC_3H_6O_2 + HO_2 \longrightarrow LHOC_3H_6OOH$

G4312	$CH_3COCH_2O_2 + HO_2 \longrightarrow$ HYPERACET
G4402	$LC_4H_9O_2 + HO_2 \longrightarrow LC_4H_9OOH$
G4407	$MVKO_2 + HO_2 \longrightarrow$ MVKOOH
G4414	$LMEKO_2 + HO_2 \longrightarrow$ LMEKOOH
G4503	$ISO_2 + HO_2 \longrightarrow$ ISOOH
LossHO22:	
G2110	$HO_2 + HO_2 \longrightarrow H_2O_2$